Hybrid Active/Passive Models
With Frequency Dependent Damping

Margaretha Johanna Lam

Dissertation submitted to the Faculty of the
Virginia Polytechnic Institute and State University
in partial fulfillment of the requirements for the degree of

DOCTOR OF PHILOSOPHY
in
Mechanical Engineering

D. J. Inman, Co-Chairman
W. R. Saunders, Co-Chairman
H. H. Cudney
H. H. Robertshaw
A. L. Wicks

October 27, 1997
Blacksburg, VA

Key words: Active, Passive, Hybrid, Frequency Dependent Damping, Model Reduction, Feedback

Hybrid Active/Passive Models With Frequency Dependent Damping

Margaretha Johanna Lam

(ABSTRACT**)**

To add damping to structures, viscoelastic materials (VEM) are added to structures. In order to enhance the damping effect of the VEM, a constraining layer is attached, creating a passive constrained layer damping treatment (PCLD). When this constraining layer is an active element, the treatment is called active constrained layer damping (ACLD). Recently, the investigation of ACLD treatments has shown it to be an effective method of vibration suppression. In this work, two new hybrid configurations are introduced by separating the passive and active elements. In the first variation, the active and passive element are constrained to the same side of the beam. The other variation allows one of the treatments to be placed on the opposite side of the beam. A comparison will be made with pure active, PCLD, ACLD and a variation which places the active element underneath PCLD. Energy methods and Lagrange's equation are used to obtain equations of motion, which are discretized using assumed modes method. The frequency dependent damping is modeled using the Golla-Hughes-McTavish (GHM) method and the system is analyzed in the time domain. GHM increases the size of the original system by adding fictitious dissipation coordinates that account for the frequency dependent damping. An internally balanced model reduction method is used to reduce the equations of motion to their original size. A linear quadratic regulator and output feedback are used to actively control vibration. The length and placement of treatment is optimized using different criteria. It is shown that placing the active element on the opposite side of the passive element is capable of vibration suppression with lower control effort and more inherent damping. If the opposite surface is not available for treatment, a suitable alternative places the PZT underneath the PCLD. LQR provides the best control, since it assumes all states are available for feedback. Usually only select states are available and output feedback is

used. It is shown that output feedback, while not as effective as full state feedback, is still able to damp vibration.

DEDICATION

I dedicate this dissertation to my parents, Wim and Simone Lam. Through their support, love and understanding, I was able to complete this work. Throughout the years, they always encouraged me to pursue a science education. They gave me the opportunity and the skills to pursue this degree. The fact that my dad did the impossible, obtaining an Bachelors and Masters degree in Mechanical Engineering in three years while my mother raised two young children, gave me the courage to go on when things were not going smoothly.

ACKNOWLEDGEMENTS

I would like to thank my advisor, Dr. Daniel J. Inman, for the opportunity to pursue this graduate degree. Thank you for supporting me through all these years, whether I was near or far.

I would also like to thank the committee members. I would especially like to thank the co-chairman of my committee, Dr. William R. Saunders. I thank him for all the time he spent with me, especially when I was formulating the work.

Everyone in the Mechanical Systems Laboratory, both old and new, deserves thanks for their support. Of the old "MSL gang", I would like to thank Mauro Atalla, Donald Leo, Brett Pokines, and Ralph Rietz for their friendship, especially the year we all spent in Virginia. Thank you also to the "new MSL gang", Greg Agnes, Eric Austin, Clay Carter, Jens Cattarius, Prasad Gade, Deborah Pilkey, and Dino Sciulli for you support and friendship. Even though I was in town a few weeks during the summer and winter, you made me feel like part of the group. I thank everyone for coming to the airport to pick me up. I don't think anyone escaped this duty and I appreciate you making the time in your busy schedules to drive to Roanoke.

Special thanks go out to Eric Austin for the many productive discussions. Thank you for always being there and answering my questions. Your experience and knowledge helped smooth the bumpy road. Also thanks for spending one whole afternoon picking apart the presentation. It made the actual presentation go much more smoothly. Many thanks go out to both Eric and his wife, Liz, for letting me stay at their place so often. I loved spending time with you, Maggie and Ollie. I must have seemed like a permanent guest sometimes.

Debbie Pilkey also deserves special recognition. Thank you so much for letting me use your computer to give my presentation and making sure everything was set up correctly.

Greg Agnes also deserves to be recognized for the many suggestions and help he gave me when I was doing experiments.

The most important support for this work came from my parents, Wim and Simone, my brother André Lam, and my husband, David Anderson. First of all, my parents and brother were there throughout the years, encouraging me to go further than I thought possible. Dad, I can not thank you enough for running so many of my programs, thereby tying up all your computers. You saved me days, if not weeks, of aggravation and made it possible for me to defend on time. Mom, your sacrifices and support throughout the years have guide me. I hope I make both of you proud. David, your support through this trying time has been my guiding light. You always had confidence in me when my own wavered many times. Thank you and I love you.

TABLE OF CONTENTS

LIST OF TABLES

LIST OF FIGURES

LIST OF SYMBOLS

$\mathbf{A}$	= state matrix
$\mathbf{A}_r$	= reduced state matrix
$\mathbf{A}_c$	= output feedback state matrix
A_b, A_c, A_p, A_s	= cross-sectional area of beam, cover plate, PZT and VEM
b	= beam width
$\mathbf{B}$	= state input matrix
$\mathbf{B}_r$	= reduced input matrix
$\mathbf{C}$	= state output matrix
$\mathbf{C}_r$	= reduced state output matrix
C_{11}^D	= Young's modulus of PZT
D	= electrical displacement
d_{31}	= PZT constant
E	= electric field
E_b, E_c, E_s	= Young's modulus of beam, cover plate and shear layer
$f(x,t)$	= external disturbance force
$\mathbf{F}$	= forcing function
G	= relaxation function of VEM
G^*	= complex modulus
G_0	= equilibrium value of complex modulus
G'	= storage modulus
G''	= loss modulus
h_{31}	= piezoelectric constant
$\mathrm{H}(x)$	= Heaviside's function
H_{calib}	= calibration constant
H_{calib}	= error constant
I_b, I_c, I_p, I_s	= moment of inertia of beam, cover plate, PZT and VEM
$\mathbf{I}$	= identity matrix
$J_{passive}$	= passive vibration suppression index

J_{LQR} = LQR cost function

J_{VS} = active vibration suppression index

J_{CE} = control effort index

$\mathbf{K}$ = stiffness matrix

$\overline{\mathbf{K}}_i$ = contribution of the n^{th} modulus to the stiffness matrix

$\mathbf{K}_c$ = control gains for LQR

$\mathbf{K}_o$ = output feedback control gains

L = beam length

$\mathbf{L}_c$ = lower triangular form of controllability grammian

$\mathcal{L}$ = Lagrangian

$\mathbf{M}$ = mass matrix

M_c = mass

Os_{output} = overshoot of the output

$OS_{voltaget}$ = overshoot of the voltage

$\mathbf{P}$ = positive definite solution to active Ricatti equation

$\mathbf{P}_r$ = reduced transformation matrix

Q_θ, Q_ϕ, Q_ξ = forcing functions

$\mathbf{Q}$ = semi positive-definite weighting function on output for active cost function

$\mathbf{q}$ = displacement field

$\dot{\mathbf{q}}$ = velocity

$\mathbf{R}$ = positive definite weighting function on control input

t_b, t_c, t_p, t_s = thickness of beam, cover plate, PZT and VEM

t_{s_y} = settling time of the response

t_{s_v} = settling time of the control force time history

T_b, T_c, T_p, T_s = potential energy of beam, cover plate, PZT and VEM

U_b, U_c, U_p, U_s = kinetic energy of beam, cover plate, PZT and VEM

u_b, u_c, u_p, u_s = axial displacement of beam, cover plate, PZT and VEM

$\mathbf{U}$ = matrix of eigenvectors

$\mathbf{u}$	=	control input vector
$\mathcal{U}$	=	strain energy density
x_1, x_3	=	right and left end of treatment where $x_3 > x_1$
x_2, x_4	=	right and left end of treatment where $x_4 > x_2$
$\mathbf{x}$	=	state vector
$\mathbf{x}_r$	=	reduced state vector
$\mathbf{x}_0$	=	initial displacement
$\dot{\mathbf{x}}_0$	=	initial velocity
$\mathbf{y}$	=	output vector
$\mathbf{y}_a$	=	active response output vector
$\mathbf{y}_p$	=	passive response output vector
V	=	applied voltage
w	=	transverse displacement of beam
$W(x)$, $U(x)$, $\Psi(x)$	=	admissible functions
$\mathbf{W}_c$, $\mathbf{W}_o$	=	controllability and observability grammian
$\mathbf{z}$	=	dissipation coordinates
$\hat{\alpha}$	=	weighting constant on dissipation coordinate
$\hat{\omega}$	=	natural frequency of dissipation coordinate
$\hat{\varsigma}$	=	damping ratio of dissipation coordinate
ω_y	=	natural frequency of response
ζ_y	=	damping ration of response
ω_v	=	natural frequency of control force time history
ζ_v	=	damping ration of control force time history
β	=	shear strain of VEM
β_{33}^S	=	dielectric constant
$\delta(x)$	=	Dirac delta function
$\delta'(x)$	=	doublet function
$\delta\mathbf{W}_f$	=	virtual work done by externally applied forces
$\delta\mathbf{W}_p$	=	virtual work done by applied voltage of PZT

ε	=	strain
λ, μ	=	Lamé's constants
Λ	=	matrix of eigenvalues
ν	=	Poisson's ratio
η	=	loss factor
ψ	=	shear angle of VEM
ρ_b, ρ_c, ρ_p, ρ_s	=	density of beam, cover plate, PZT and VEM, respectively
τ, σ	=	stress
$\theta(t)$, $\phi(t)$, $\xi(t)$	=	generalized coordinates

BACKGROUND

1.1 Introduction

It is becoming increasingly important to add damping to structures in order to control their motion. Most damping falls in two categories: passive damping and active damping. Recently, a new subset of damping was created by combining passive and active damping, thereby producing a hybrid damping treatment. In this chapter, a brief history of passive, active and hybrid damping is given. The following chapters describe new hybrid damping treatments, address modeling issues and discuss numerical results.

1.2 History of Passive Damping Treatments

Many materials, such as steel, aluminum and other metals, used in engineering have very little inherent damping. Damping ratios for such materials are usually around 0.001. Therefore any structure that is built using these materials, has vibration problems when it is excited near harmonic frequencies. The addition of materials, such as viscoelastic materials (VEM), increases the damping in the structure and reduces the vibration amplitudes at resonances [1].

The first application of VEMs was to simply attach a layer of VEM to the base structure. Vibration of the base structure causes the VEM to strain. This strain energy causes the VEM to increase in temperature. The dissipation of heat from the structure removes vibrational or strain energy from the system and is referred to as damping. Damping reduces the magnitude and duration of the vibration. However, in order to have acceptable levels of damping, large amounts of VEM must be used.

In the 1950's it was discovered that adding a constraining layer to the VEM enhanced the damping capabilities by increasing the strain in the VEM. In the case of a beam, if the constrained layer damping (CLD) treatment is the same size as the underlying structure, a sandwich beam is created. This treatment is also referred to as passive constrained layer damping (PCLD). Kerwin [2] first models the damping of flexural waves for a sandwich beam and establishes equations which describe the viscoelastic behavior through the use of a complex modulus. DiTaranto [3] improves the model by assuming a sixth-order, complex, homogeneous differential equation. Mead and Markus [4] show that the solution to the sixth-order differential equation, as described by DiTaranto [3], yields uncoupled complex forced modes. Douglas and Yang [5] improve upon the Mead and Markus model by modeling the beam and viscoelastic as an eighth-order differential equation with complex coefficients. While these advancements greatly facilitate finding solutions for a sandwich beam, solving the differential equation is still very cumbersome. Also, all of the models mentioned depend on a complex shear modulus to account for the damping behavior of the VEM. This allows only steady state solutions, i.e. solutions at single frequencies. A summary of the principle contributions made to the design and analysis of CLD can be found in [6].

Rao [7] finds a complete set of equations of motion and boundary conditions for a sandwich beam using energy methods. An exact solution is obtained, but it is still cumbersome to solve. Ravi et al. [8] apply eigenvalue perturbation to a sandwich beam which is efficient in the estimation of the natural frequencies and damping ratios. Again, a complex shear modulus is used to account for the damping.

One of the major assumptions made when obtaining equations for PCLD is the fact that the transverse displacement remains the same through each layer: beam, VEM and constraining layer. Bai and Sun [9] state the assumption of equal transverse displacement is invalid and assume a nonlinear displacement field of the core in both the longitudinal and

transverse direction. The assumption of equal transverse displacement is not valid in cases where the viscoelastic core is much thicker than the face plates, or where the core (VEM) modulus is low [10]. However, in this work, only thin VEMs are used compared to beam and cover plate thickness, and the assumption of equal transverse displacement is valid.

It is important to know the configuration of the sandwich beam to give optimal damping. Lifshitz and Leibowitz [11] find the optimal configuration by allowing the thickness of the two face plates and the viscoelastic core to vary. Lekszcki and Olhoff [12] find optimal configurations for non-uniform CLD. All CLD treatments discussed so far have assumed a sandwich configuration. It is not necessary, and indeed it is not optimal, to have full coverage. Plunkett and Lee [13] and Kerwin and Smith [14] address the issue of segmented treatments. It is found that damping could be increased by having multiple segments of optimal length or multiple layers of CLD.

Most of the models using viscoelastic materials and constrained layer damping have been beams. Some other configurations are circular plates with CLD [15], and an outlet guide vane with CLD [16]. There have also been papers which address the issue of multiple layers of CLD, e.g. Sun et al. [17], Rao and He [18], and Hetnarski et al. [19]. These are just a few of the results available.

While passive damping treatments can greatly improve damping of the system, there are limitations. In order to provide adequate damping, different VEMs must be chosen which often complicates analysis and design of the system. The damping behavior of VEMs changes significantly with changes in frequency and temperature. While VEMs are easy to apply, the damping is of limited bandwidth.

One of the main contributions of this work is in the area of improved modeling of the VEM. All of the previously mentioned work use the complex modulus approach to

account for the damping in the viscoelastic model. A major drawback is the solution is only valid for steady state models. In this work, the Golla-Hughes-McTavish method [20] is used to model the behavior of the VEM. This model accounts for the damping over a range of frequencies and allows for a transient solution.

1.3 History of Active Damping Treatments

Active damping has become a vital part in the vibration control of structures. In order to control motion of the structure, piezoelectric materials are used. One of the unique features of piezoelectric materials is that they can serve both as a sensor and an actuator. The early application of piezoelectric materials to control vibration was developed by Olson [21]. However, due to the lack of power of the actuators, the control of vibration was limited. Recently, a great deal of interest has developed in the area of active vibration control, as described in a survey paper by Rao and Sunar [22].

The modeling of piezoelectric materials has been of great interest, and much work has been done in the area. Crawley and de Luis [23] provide a detailed model of the use piezoelectric actuators to control vibration in structures. Hagood et al. [24] develop a general model which couples the effects of the piezoelectric elements with the elastic structure. Dosch et al. [25] address the issue of simultaneously sensing and actuating a structure using piezoelectric elements. Cole et al. [26] estimate modal parameters to describe the structure dynamics, which includes a piezoelectric element, using modal analysis.

As with passive damping, it is important to know the optimal configuration of the piezoelectric material in order to minimize cost. Kim and Jones [27] derive a generalized formulation based on Love's equations of motion for a composite structure and use these equations to estimate the optimal thickness of the piezoelectric actuator layers. The composite structure consists of many layers of active (piezoelectric) and non-active

(bonding and structure) materials. Masters and Jones [28] address the optimal location and thickness of twin piezoelectric actuators embedded in a composite structure. They report the use of a thin actuator if it is attached to the surface, or a thick actuator if it is embedded. Devasia et al. [29] find the optimal placement and size of a piezoelectric element on a beam. They use three optimization problems to determine the optimal placement and size: 1) maximize the damping in the modes by assuming pure collocated damping control, 2) minimize the linear quadratic cost function, and 3) maximize the minimum eigenvalue of the controllability grammian.

Active damping greatly improves the performance of structures, but there are some problems. First of all, there is very little inherent damping in piezoelectric materials. Therefore, in case of failure of one of the active components (sensor, actuator or electronic failures), the structure may not have enough damping. Also, in order to adequately control the vibration, especially in a lightly damped structure, the actuator may need large amplifiers and high power.

1.4 History of Active Constrained Layer Damping Treatments

The properties of active and passive damping are combined in order to create a hybrid damping technique. When the constraining layer of a CLD treatment is made active, the treatment is called active constrained layer damping (ACLD). Recently, investigation of ACLD treatments has shown it to be an effective method of vibration suppression.

ACLD treatment has a number of advantages. First, the passive damping is a fail-safe in case of failure of the active controller. Also, active damping of high frequencies can be costly and very difficult. However, passive damping works well at high frequencies by inducing more shear in the VEM. The reverse it true also, which means the active and passive elements complement each other. ACLD will need less power than a purely active system to reduce unwanted vibration due to the inherent damping in the passive element.

This will be shown in chapter 5. If high gains are needed to improve performance, ACLD will be more effective. This is due to the fact that damping is added to all modes in the system, which delays the uncontrollable modes from becoming unstable. This same damping will help keep unmodeled modes stable. Basically, adding damping increases the closed loop gain margin.

Agnes and Napolitano [30] and Baz [31] first combine active and passive treatments to create ACLD as a more effective method of vibration suppression. Stability and controllability of ACLD treatments is addressed by Shen [32]. Baz and Ro [33] provide a survey and overview of the first two years of research in the field of ACLD. They also address the issue of optimal placement and size of ACLD treatment. Comparisons between passive, active and ACLD are made by Baz and Ro [34], Liao and Wang [35], Azvin et al. [36] and Huang et al. [37].

In Agnes and Napolitano [30], a finite element model of a beam with full-coverage ACLD (active sandwich beam configuration) is compared to an analytical model and shown to effectively damp vibration. Baz [31] uses the damping model of Mead and Markus [4] to obtain a sixth-order differential equation for an active sandwich beam configuration. This principle is extended to a beam with partial coverage in Baz and Ro [37]. Finite element analysis is used to obtain equations for a beam with partial ACLD coverage in Baz and Ro [38]. The use of ACLD treatments to control vibration of plates is investigated in Baz and Ro [39].

Shen [40] uses equilibrium to obtain an eighth-order differential equation governing the bending and axial vibrations of a fully covered beam with ACLD. In Shen [41], the principles used in [40] are extended to a plate with ACLD. Shen [42] again uses the equations governing a plate to obtain a model for ACLD. By assuming the width is much smaller than the length, a set of beam equations is obtained. Torsional vibration control of

a shaft through ACLD is described in Shen et al. [43]. Variational methods is used in [44] to obtain equations of motion for a beam with ACLD. Yellin and Shen [45] examine the use of self-sensing actuators to control vibrations of a partially covered beam.

Azvine et al. [35] show that the use of ACLD produces effective levels of damping in a cantilevered beam. Rongong et al. [46] obtain a mathematical based on the Rayleigh Ritz approach. Veley and Roa [47] compare active, passive and hybrid damping. Modal strain energy is used to account for damping of the VEM. Crassidis et al. [48] uses H_∞ control instead of velocity feedback or LQR in order to control ACLD.

The complex modulus is used to model the damping of the viscoelastic material in the papers described above, except [47], which uses modal strain energy. This restricts the solution to steady-state analysis. When using modal strain energy, proportional damping is assumed. This implies that the damping is a linear combination of the mass and stiffness matrices, which does not model the frequency dependence of the shear modulus very well. Van Nostrand [49] and Van Nostrand and Inman [50] were the first to use thermodynamic fields instead of the complex modulus. This approach allows time domain analysis for any disturbance. Saunders et al. [51] develop a pole-zero model for a composite beam with ACLD, thereby circumnavigating the issue of modeling damping parameters. Liao and Wang [52] allow the piezoelectric treatment to run past the VEM layer and introduce edge elements in an attempt to increase the control authority of the active element. Lesieutre and Lee [53] propose segmented ACLD treatments motivated by the success of segmented PCLD treatments. Various time domain models of viscoelastic materials are used. Ray and Baz [54] address the optimal placement of ACLD by maximizing energy dissipation of the treatment and showed an optimally configured ACLD has higher damping than an optimally configured PCLD. Inman and Lam [55] provide an overview of the papers in the field.

1.5 History of Golla-Hughes-McTavish Method

Modeling the frequency effect of damping is important when VEMs are added to a structure. PCLD has been modeled using the complex shear modulus, but this allows only for steady state vibration at a single frequency. Modal strain energy is used to model damping for passive, active and hybrid treatments by Veley and Rao [47]. While this method allows transient analysis, it assumes proportional damping. In other words, damping modeled using modal strain energy does not take into account the frequency dependence of viscoelastic materials. Van Nostrand [49] uses Augmented Thermodynamic Fields (ATF) to account for frequency dependent damping when modeling ACLD. This method adds fictitious modes to the state space model to account for frequency dependent damping. One detraction however is the loss of physical meaning of the states. Another damping method to model VEM is fractional calculus [56]. It models the mechanical properties of VEMs as a function of frequencies raised to fractional powers. Bagley and Torvik [56] demonstrated this model accounts for the frequency dependence by verifying the numerical model experimentally. A major drawback is the size of the final system, which increases quickly. For the simplest possible viscoelastic model, the order of the system is 5! [57].

The Golla-Hughes-McTavish (GHM) method models the damping of viscoelastic properties [20], [58]. The frequency dependent behavior of the VEM is described through the addition of extra coordinates, called dissipation coordinates. The VEM material properties are therefore introduced through the mass, damping and stiffness matrices as additional states. A major advantage of using this method is that symmetry of the mass, damping and stiffness matrices are retained as well as the physical meaning of the states. It is easily incorporated into a finite element model or an assumed modes model.

Lam et al. [59] are the first to propose using the Golla-Hughes-McTavish damping model to account for the damping in the viscoelastic layer for structures with ACLD. Liao and

Wang [60] also use GHM along with energy methods to model the behavior of partial ACLD treatment. GHM is used in this work to model the behavior of the VEM, because it is most compatible with second order systems.

1.6 Research Goals

This work concentrates on developing and modeling hybrid damping treatments. New hybrid treatments allow the active and passive elements to be placed separately on the beam: on the same side or on the opposite side of the beam. A careful comparison is made with pure active, pure passive, active constrained layer damping, and a treatment that places the active element underneath passive constrained layer damping. Chapter two develops the equations of motion for the different configurations. Another contribution is the use of the Golla-Hughes-McTavish model to account for the frequency dependent damping of viscoelastic materials. GHM is described in chapter three, and experimental verification of the mathematical model using a sandwich beam is reported. When using GHM, the physical states are preserved, but fictitious dissipation states are used to account for the frequency dependent damping which increase the size of the system. A model reduction method will be used to reduce the system to its original order. The control law is developed in chapter four and criteria for optimal location of the hybrid active/passive treatments are assigned. Numeric results are reported in chapter 5, along with time histories of the optimal hybrid treatments. Conclusions and future work are reported in chapter six.

In short, the contributions of this dissertation are: (1) the derivation of equations that allow all combinations of viscoelastic and piezoceramic damping treatments, (2) improved modeling of the viscoelastic damping effects allowing the treatment of transient response complete with experimental verification, and (3) the development of model reduction to improve the viscoelastic modeling, thereby rendering it more practical.

DEVELOPMENT OF THE EQUATIONS

2.1 Introduction

Models of beams with different passive and active configurations are derived using energy methods. The different configurations are passive constrained layer damping (PCLD), active damping, active constrained layer damping (ACLD), and three variations of new hybrid damping treatments. The active element is a piezoelectric element. In the first variation of hybrid damping, the active element is separate from the PCLD treatment, but still on the same side of the beam. Next the active element is allowed to be on the other side. One more variation puts the active element underneath the PCLD treatment.

Many authors ([33], [35], [43], [45] to name a few) have used energy methods to obtain the system equations. The energy method approach does not require the forces and/or torques acting on the system to be determined directly. Instead, the equations of motion are determined through the principle of energy conservation. In this work, the equations of motion for a beam with hybrid damping are derived using Lagrange's equation.

In order to facilitate the modeling and solution of the beam with hybrid damping treatments, assumptions about the materials and its properties are made. In this case, the following assumptions are made when deriving the equations:

1) rotational inertia is negligible,
2) shear deformations of the base beam, cover plate and piezoelectric material are negligible,
3) the transverse displacement is assumed to be constant through all the layers,
4) passive damping is added through shear deformation only,
5) the piezoelectric material, viscoelastic material and constraining layers are perfectly bonded to the structure or each other,

6) applied voltage to the piezoelectric material is assumed to be constant along its length, and
7) linear theories are used to describe elasticity, viscoelasticity and piezoelectricity.

Assumption (3) states that the beam behaves as an Euler-Bernoulli beam.

2.2 Kinematic Relationships for a Beam with Constrained Layer Damping

The geometry of a beam with a partial coverage of a constrained layer damping treatment is given in Fig. 2.1. At this time, no assumptions are made about the boundary conditions. The length of the base beam is denoted by L, the width by b, and the thickness by t_b. The constrained layer damping treatment is applied from point x_1 to x_2, and has thicknesses t_s for the viscoelastic (VEM) layer and t_c for the constraining layer. The transverse vibration, assumed to be constant through all the layers, is denoted by $w(x,t)$. The longitudinal vibration of the beam and cover plate are $u_b(x,t)$ and $u_c(x,t)$ respectively. Note the subscripts b, s, and c refer to the base beam, the VEM layer and the constraining layer. The deformation of the beam is shown in Fig. 2.2. The shear strain, β, for a VEM is given by

$$\beta = \frac{\partial w}{\partial x} - \psi \qquad 2.1$$

where ψ is shear angle of the VEM. Assuming perfectly bonded layers, the longitudinal displacement for the VEM and constraining layer can be rewritten in terms of the longitudinal and transverse displacement of the base beam as well as the shear angle:

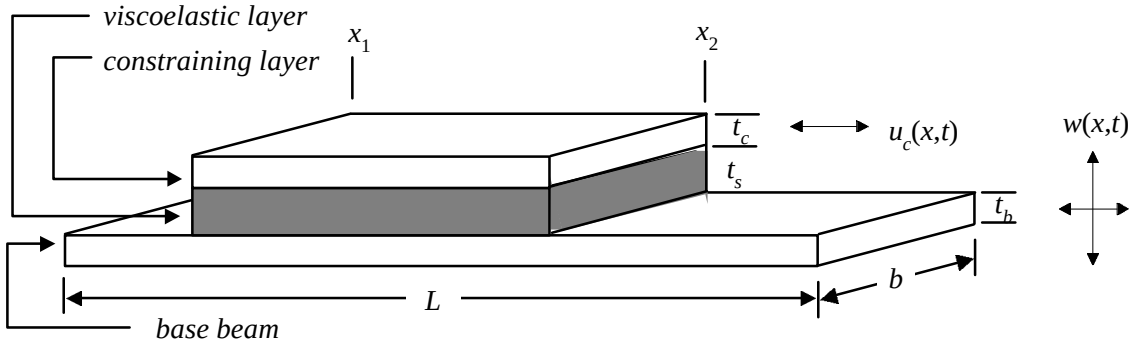

Figure 2. 1 Geometry of Beam with Partial Covering of Constrained Layer Damping

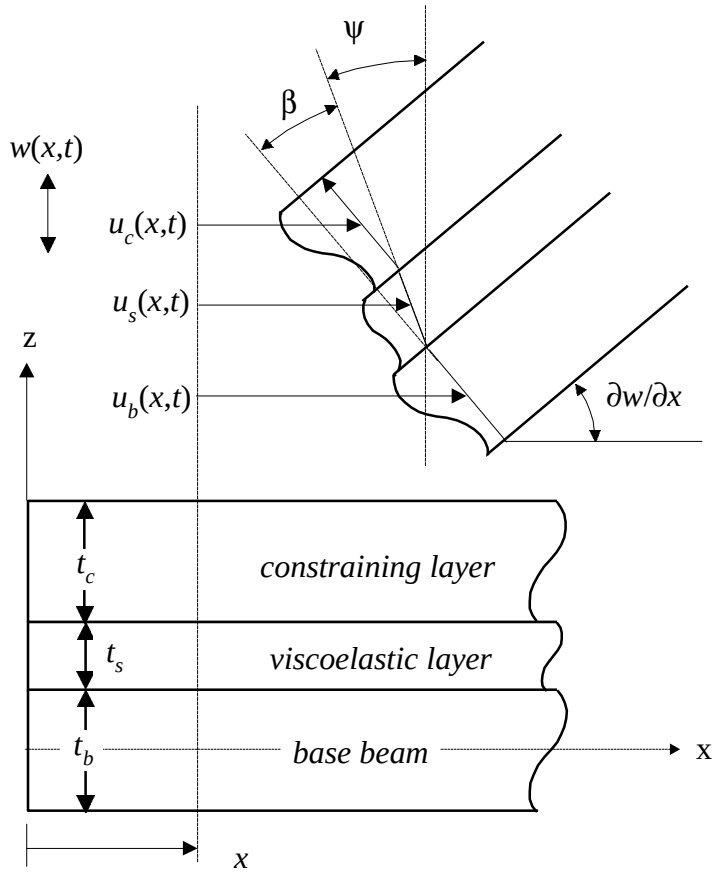

Figure 2. 2 Deformation of Beam with Constrained Layer Damping

$$u_s = u_b - \frac{t_b}{2}\frac{\partial w}{\partial x} - \frac{t_s}{2}\psi \tag{2.2}$$

$$u_c = u_b - \frac{t_b + t_c}{2}\frac{\partial w}{\partial x} - t_s\psi\,. \tag{2.3}$$

2.3 Piezoelectric Equations

The constitutive equation for a piezoelectric element depends on the mechanical stress and strain, τ and ε respectively, as well as the electric field, *E*, and the electrical displacement, *D*. A common form of this equation is the stress and electric field dependent notation, such that

$$\begin{bmatrix} \tau \\ E \end{bmatrix} = \begin{bmatrix} C_{11}^{D} & -h_{31} \\ -h_{31} & \beta_{33}^{s} \end{bmatrix} \begin{bmatrix} \varepsilon \\ D \end{bmatrix} \tag{2.4}$$

where C_{11}^{D} is the elastic stiffness (evaluated at constant electric field), h_{31} is the piezoelectric constant, and β_{33}^{s} is the dielectric constant [59]. For thin piezoelectric layers, *D* is assumed to be constant through the thickness.

2.4 Kinetic and Potential Energy Equations

In this section, the kinetic and potential energy expressions will be formulated for the different layers: base beam, VEM, constraining layer and piezoelectric layer. The expression for kinetic energy, T, for any layer is the following integral over the volume, *V*,

$$\mathrm{T} = \frac{1}{2}\int_V \rho\dot{\mathbf{q}}\cdot\dot{\mathbf{q}}\,dV \tag{2.5}$$

where $\dot{\mathbf{q}}$ is the velocity, and ρ the density of the material. The appropriate subscript will denote which layer is addressed. The potential energy, U, can also be written as an integral over the volume such that

$$\mathrm{U} = \frac{1}{2}\int_{V} E\mathbf{q}\cdot\mathbf{q}\,dV \tag{2.6}$$

where **q** is the displacement field and *E* is the material modulus. Again, the appropriate subscript will identify which layer is being described.

2.4.1 Base Beam

The kinetic and potential energy equations for the base layer are expressed in terms of the transverse, $w(x,t)$, and the longitudinal, $u_b(x,t)$, deflections,

$$\mathrm{T}_b = \frac{\rho_b A_b}{2}\int_0^L \left[\left(\frac{\partial u_b}{\partial t}\right)^2 + \left(\frac{\partial w}{\partial t}\right)^2\right] dx \tag{2.7}$$

$$\mathrm{U}_b = \frac{1}{2}\int_0^L \left[E_b A_b\left(\frac{\partial u_b}{\partial x}\right)^2 + E_b I_b\left(\frac{\partial^2 w}{\partial x^2}\right)^2\right] dx \tag{2.8}$$

where *A* is the cross-sectional area, *I* the moment of inertia about the neutral axis of the layer, and the subscript *b* represents the beam. Again, ρ is the density and *E* Young's modulus of the beam. These equations remain the same for all configurations, regardless of the damping treatment placed on the beam.

2.4.2 Viscoelastic Layer

In the case of the VEM, the kinetic energy can be written in terms of the transverse, $w(x,t)$, and the longitudinal, $u_s(x,t)$, deflections such that

$$T_s = \frac{\rho_s A_s}{2}\int_0^L \left[\left(\frac{\partial u_s}{\partial t}\right)^2 + \left(\frac{\partial w}{\partial t}\right)^2\right]\left[H(x-x_1) - H(x-x_2)\right]dx \qquad 2.9$$

Since the VEM treatment does not have to cover the whole beam, Heaviside's function, $H(x\text{-}x_1)$, is used to integrate over the appropriate length, where

$$\int_{-\infty}^{\infty} f(x)\left[H(x-x_1)\right]dx = \int_{x_1}^{\infty} f(x)dx \qquad 2.10$$

In order to write the potential energy for the VEM, it is necessary to look at the strain density. The strain energy density for a linear isotropic material is

$$\mathcal{U} = \frac{1}{2}\varepsilon_{ij}\tau_{ij} = \frac{1}{2}\lambda\varepsilon_{ii}\varepsilon_{jj} + \mu\varepsilon_{ij}\varepsilon_{ij} \qquad 2.11$$

where λ and μ are Lamé's constants, τ is the stress, ε the strain [60]. Rewriting equation 2.11 in terms of the shear modulus, G, and Poisson's ratio, ν, and expanding on i and j gives

$$\begin{aligned}\mathcal{U} = {} & \frac{G\nu}{1-2\nu}\left(\varepsilon_{xx}^2 + \varepsilon_{yy}^2 + \varepsilon_{zz}^2 + 2\varepsilon_{xx}\varepsilon_{yy} + 2\varepsilon_{xx}\varepsilon_{zz} + 2\varepsilon_{yy}\varepsilon_{zz}\right) \\ & + G\left(\varepsilon_{xx}^2 + \varepsilon_{yy}^2 + \varepsilon_{zz}^2 + 2\varepsilon_{xy}^2 + 2\varepsilon_{xz}^2 + 2\varepsilon_{yz}^2\right)\end{aligned} \qquad 2.12$$

If plane stress is assumed, then τ_{yy}, τ_{xy}, and τ_{xz} are zero, which leads to $\varepsilon_{xy} = \varepsilon_{yz} = 0$ and $\varepsilon_{yy} = -\nu(\varepsilon_{xx} + \varepsilon_{zz})/(1-\nu)$. The strain energy density can then be written as

$$\mathcal{U} = \frac{G}{1-\nu}\left(\varepsilon_{xx}^2 + \varepsilon_{zz}^2 + 2\nu\varepsilon_{xx}\varepsilon_{zz}\right) + 2G\varepsilon_{xz}^2 \tag{2.13}$$

If the z plane is also assumed to be stress free, then $\varepsilon_{zz} = -\nu\varepsilon_{xx}$ and equation 2.13 reduces to

$$\mathcal{U} = G(1+\nu)\varepsilon_{xx}^2 + 2G\varepsilon_{xz}^2 = \frac{1}{2}E_s\varepsilon_{xx}^2 + 2G\varepsilon_{xz}^2 \tag{2.14}$$

At this point, it is necessary to derive expressions for the stress in terms of the displacements of the beam. Referring again to Fig. 2.2 and assuming plane stress, the axial displacement is

$$u_1(x,z) = u_s - z\psi \tag{2.15}$$

where u_s is longitudinal displacement at the center of the VEM, and ψ the shear angle. The displacement field in the transverse direction, u_3, is a function of the transverse displacement, *w*, and axial strains. However, any axial strains will be negligible when compared to the transverse displacement, and the transverse deformation is defined as $u_3 = w$. The strain equations are therefore

$$\begin{bmatrix} \varepsilon_{xx} \\ \varepsilon_{zz} \\ 2\varepsilon_{xz} \end{bmatrix} = \begin{bmatrix} \dfrac{\partial u_1}{\partial x} \\ \dfrac{\partial u_3}{\partial z} \\ \dfrac{\partial u_3}{\partial x} + \dfrac{\partial u_1}{\partial z} \end{bmatrix} = \begin{bmatrix} \dfrac{\partial u_s}{\partial x} - z\dfrac{\partial \psi}{\partial x} \\ 0 \\ \dfrac{\partial w}{\partial x} - \psi \end{bmatrix} \tag{2.16}$$

Substituting equation 2.16 into equation 2.14 gives the following expression for the strain energy density:

$$\mathcal{U} = \frac{1}{2} E_s \left(\frac{\partial u_s}{\partial x} - z \frac{\partial \psi}{\partial x} \right)^2 + \frac{1}{2} G \left(\frac{\partial w}{\partial x} - \psi \right)^2 \tag{2.17}$$

The potential energy is obtained by integrating equation 2.17 over the width and through the thickness, such that

$$\mathrm{U}_s = \frac{1}{2} \int_0^L \left[E_s A_s \left(\frac{\partial u_s}{\partial x} \right)^2 + E_s I_s \left(\frac{\partial \psi}{\partial x} \right)^2 + G A_s \left(\frac{\partial w}{\partial x} - \psi \right)^2 \right] \left[\mathrm{H}(x - x_1) - \mathrm{H}(x - x_2) \right] dx \tag{2.18}$$

This expression fully describes the potential energy of a VEM. Note that Heaviside's function, described in equation 2.10, is used to locate the placement of the VEM on the base beam. Liao and Wang [52] include the shear term as virtual work instead of potential energy. While their model accurately accounts for damping, it is not correct to include shear as virtual work.

2.4.3 Constraining Layer

The kinetic and potential energies of the constraining layer are written as

$$\mathrm{T}_c = \frac{\rho_c A_c}{2} \int_0^L \left[\left(\frac{\partial u_c}{\partial t} \right)^2 + \left(\frac{\partial w}{\partial t} \right)^2 \right] \left[\mathrm{H}(x - x_1) - \mathrm{H}(x - x_2) \right] dx \tag{2.19}$$

and

$$\mathrm{U}_c = \frac{1}{2} \int_0^L \left[E_c A_c \left(\frac{\partial u_c}{\partial x} \right)^2 + E_c I_c \left(\frac{\partial^2 w}{\partial x^2} \right)^2 \right] \left[\mathrm{H}(x - x_1) - \mathrm{H}(x - x_2) \right] dx . \tag{2.20}$$

respectively. Heaviside's function is used to place the constraining layer at the same location as the VEM, creating a PCLD treatment. These equations assume that the constraining layer is not active.

2.4.4 Piezoelectric Layer

The kinetic energy of a piezoelectric layer located between x_1 and x_2 is written as

$$\mathrm{T}_p = \frac{\rho_p A_p}{2}\int_0^L \left[\left(\frac{\partial u_p}{\partial t}\right)^2 + \left(\frac{\partial w}{\partial t}\right)^2\right]\left[\mathrm{H}(x-x_1) - \mathrm{H}(x-x_2)\right]dx\,. \tag{2.21}$$

Using the constitutive equation for a piezoelectric material, equation 2.4, the potential energy can be derived such that

$$\begin{aligned}\mathrm{U}_p &= \frac{1}{2}\int_V (\tau\varepsilon + ED)dV \\ &= \frac{1}{2}\int_0^L \Bigg[C_{11}^D A_p\left(\frac{\partial u_p}{\partial x}\right)^2 + C_{11}^D I_p\left(\frac{\partial^2 w}{\partial x^2}\right)^2 - 2A_p h_{31} D\left(\frac{\partial u_p}{\partial x}\right) \\ &\qquad + A_c \beta_{33}^S D^2\Bigg]\left[\mathrm{H}(x-x_1) - \mathrm{H}(x-x_2)\right]dx\end{aligned} \tag{2.22}$$

However, since the electric displacement, D can be written as $\partial Q/\partial x$, where Q, the charge, is a constant, the last two terms in equation 2.22 will go to zero. This can be shown by looking at the variation of the last two terms.

$$\begin{aligned}-\int_0^L 2A_p h_{31} b\delta\left(\frac{\partial Q}{\partial x}\frac{\partial u_p}{\partial x}\right)dx &= -\int_0^L A_p h_{31} b\left(\frac{\partial(\delta Q)}{\partial x}\frac{\partial u_p}{\partial x} + \frac{\partial Q}{\partial x}\frac{\partial(\delta u_p)}{\partial x}\right)dx \\ &= -A_p h_{31} b\left(\delta Q\frac{\partial u_p}{\partial x}\bigg|_0^L - \int_0^L \frac{\partial^2 u_p}{\partial x^2}\delta Q dx + \delta u_p\frac{\partial Q}{\partial x}\bigg|_0^L - \int_0^L \frac{\partial^2 Q}{\partial x^2}\delta u_p dx\right)\end{aligned}$$

and

$$\int_0^L A_p \beta_{33}^s \frac{\partial Q}{\partial x} \frac{\partial(\delta Q)}{\partial x} dx = A_p \beta_{33}^s \left(\delta Q \frac{\partial Q}{\partial x}\bigg|_0^L - \int_0^L \frac{\partial^2 Q}{\partial x^2} \delta Q dx \right)$$

However, since Q is a constant, the variation with respect to Q is zero, and any derivatives of Q with respect to x are also zero. Therefore, the potential energy for a piezoelectric is given as

$$\mathrm{U}_p = \frac{1}{2} \int_0^L \left[C_{11}^D A_p \left(\frac{\partial u_p}{\partial x} \right)^2 + C_{11}^D I_p \left(\frac{\partial^2 w}{\partial x^2} \right)^2 \right] \left[\mathrm{H}(x - x_1) - \mathrm{H}(x - x_2) \right] dx \tag{2.23}$$

The kinetic and potential energy terms can be used to describe a piezoelectric element bonded directly to the beam, or attached to a VEM. The kinematic relationships (e.g. equations 2.2 and 2.3) describe the correct configuration. At this point, all basic energy equations describing the motion of a beam with different damping treatments are available.

2.5 Virtual Work

There are only two expressions for virtual work necessary. One is for the work done by the piezoelectric material and the other by any external disturbances. The virtual work done by the voltage applied to a piezoelectric material, subscript *p*, is

$$\delta \mathrm{W}_p = \int_0^L \left[A_p d_{31} C_{11}^D V(t) \delta \left(\frac{\partial u_p}{\partial x} \right) \right] \left[\mathrm{H}(x - x_1) - \mathrm{H}(x - x_2) \right] dx \tag{2.24}$$

where d_{31} is a piezoelectric constant and $V(t)$ is the applied voltage. The virtual work done by an external disturbance force, $f(x,t)$, is

$$\delta W_f = \int_0^L f(x,t)\delta w(x,t)dx . \qquad 2.25$$

Here δ denotes the variation and the subscript f denotes the external disturbance force. It is assumed that the disturbance force is applied in the transverse direction only.

2.6 Energy Equations for a Beam with Different Treatments

In this section, the kinetic and potential energy equations of different active and passive damping treatments are expanded using kinematic relationships. The object is to write all energy equations in terms of the transverse displacement, the longitudinal displacement of the beam, and the shear angle of the VEM where applicable. The different treatments are PCLD, active, ACLD, the active element underneath PCLD, and two variation of the active element separate from PCLD. For all the different treatments, the equations for the kinetic and potential energy (equations 2.7 and 2.8) for the base beam are the same and will not be repeated for each treatment.

2.6.1 Passive Constrained Layer Damping Treatment

Figure 2.1 depicts a beam with passive constrained layer damping. Equations 2.9 and 2.19 represent the kinetic energy for the viscoelastic layer and the constraining layer, respectively. Equations 2.18 and 2.20 represent the potential energy for these layers. Using the kinematic relationships given in equations 2.2 and 2.3, the kinetic and potential energy for the VEM and constraining layer are written in terms of the shear angle of the VEM (ψ), and the longitudinal, u_b, and transverse displacement, w, of the beam. The kinetic energy for the VEM and constraining layers become

$$\mathrm{T}_s = \frac{\rho_s A_s}{2}\int_0^L \left[\left(\frac{\partial u_b}{\partial t}\right)^2 - t_b\left(\frac{\partial u_b}{\partial t}\right)\left(\frac{\partial w}{\partial x \partial t}\right) + \frac{t_b^2}{4}\left(\frac{\partial w}{\partial x \partial t}\right)^2 - t_s\left(\frac{\partial u_b}{\partial t}\right)\left(\frac{\partial \psi}{\partial t}\right) + \frac{t_b t_s}{2}\left(\frac{\partial w}{\partial x \partial t}\right)\left(\frac{\partial \psi}{\partial t}\right) + \frac{t_s^2}{4}\left(\frac{\partial \psi}{\partial t}\right)^2 + \left(\frac{\partial w}{\partial t}\right)^2\right]\left[\mathrm{H}(x - x_1) - \mathrm{H}(x - x_2)\right]dx \tag{2.26}$$

and

$$\mathrm{T}_c = \frac{\rho_c A_c}{2}\int_0^L \left[\left(\frac{\partial u_b}{\partial t}\right)^2 - (t_b + t_c)\left(\frac{\partial u_b}{\partial t}\right)\left(\frac{\partial w}{\partial x \partial t}\right) + \frac{(t_b + t_c)^2}{4}\left(\frac{\partial w}{\partial x \partial t}\right)^2 - 2t_s\left(\frac{\partial u_b}{\partial t}\right)\left(\frac{\partial \psi}{\partial t}\right) + (t_b + t_c)t_s\left(\frac{\partial w}{\partial x \partial t}\right)\left(\frac{\partial \psi}{\partial t}\right) + t_s^2\left(\frac{\partial \psi}{\partial t}\right)^2 + \left(\frac{\partial w}{\partial t}\right)^2\right]\left[\mathrm{H}(x - x_1) - \mathrm{H}(x - x_2)\right]dx \tag{2.27}$$

respectively. The potential energy equations for the VEM and constraining layer now become

$$\mathrm{U}_s = \frac{1}{2}\int_0^L \left[E_s A_s\left\{\left(\frac{\partial u_b}{\partial x}\right)^2 - t_b\left(\frac{\partial u_b}{\partial x}\right)\left(\frac{\partial^2 w}{\partial x^2}\right) + \frac{t_b^2}{4}\left(\frac{\partial^2 w}{\partial x^2}\right)^2 - t_s\left(\frac{\partial u_b}{\partial x}\right)\left(\frac{\partial \psi}{\partial x}\right) + \frac{t_s t_b}{2}\left(\frac{\partial^2 w}{\partial x^2}\right)\left(\frac{\partial \psi}{\partial x}\right) + \frac{t_s^2}{4}\left(\frac{\partial \psi}{\partial x}\right)^2\right\} + E_s I_s\left(\frac{\partial \psi}{\partial x}\right)^2 + GA_s\left\{\left(\frac{\partial w}{\partial x}\right)^2 - 2\left(\frac{\partial w}{\partial x}\right)\psi + \psi^2\right\}\right]\left[\mathrm{H}(x - x_1) - \mathrm{H}(x - x_2)\right]dx \tag{2.28}$$

and

$$\mathrm{U}_c = \frac{1}{2}\int_0^L \Bigg[E_c A_c \Bigg\{ \left(\frac{\partial u_b}{\partial x}\right)^2 - \left(t_b + t_c\right)\left(\frac{\partial u_b}{\partial x}\right)\left(\frac{\partial^2 w}{\partial x^2}\right) + \frac{\left(t_b + t_c\right)^2}{4}\left(\frac{\partial^2 w}{\partial x^2}\right)^2 - 2t_s\left(\frac{\partial u_b}{\partial x}\right)\left(\frac{\partial \psi}{\partial x}\right) + t_s\left(t_b + t_c\right)\left(\frac{\partial^2 w}{\partial x^2}\right)\left(\frac{\partial \psi}{\partial x}\right) + t_s^2\left(\frac{\partial \psi}{\partial x}\right)^2 \Bigg\} + E_c I_c\left(\frac{\partial^2 w}{\partial x^2}\right)^2 \Bigg] \left[\mathrm{H}\left(x - x_1\right) - \mathrm{H}\left(x - x_2\right)\right] dx \qquad 2.29$$

Note the use of the shear modulus to account for the damping of the viscoelastic material. Also, Heaviside's function places the passive treatment between x_1 and x_2.

2.6.2 Active Damping

Figure 2.3 shows a beam with an active element, in this case a piezoelectric element. For an active element without the VEM, a variation of the kinematic relation given in equation 2.3 is needed. In this case, it is assumed that the piezoelectric is perfectly bonded to the structure. In other words, the thickness of the shear layer is set to zero, and the kinematic relation becomes

$$u_p = u_b - \frac{t_b + t_p}{2}\frac{\partial w}{\partial x} \qquad 2.30$$

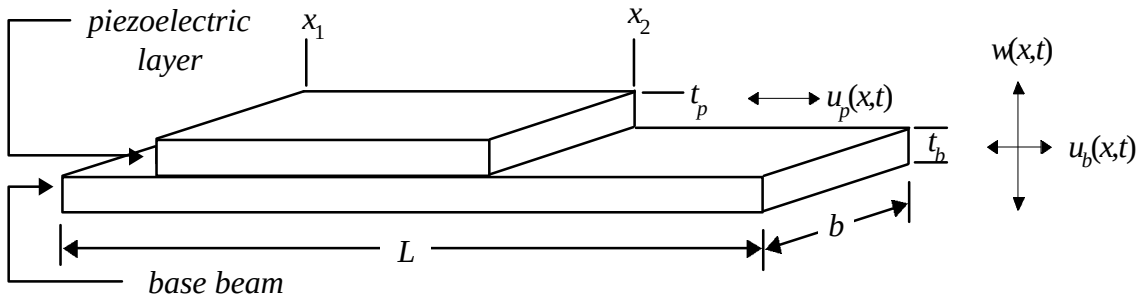

Figure 2. 3 Geometry of a Beam with a Active Damping

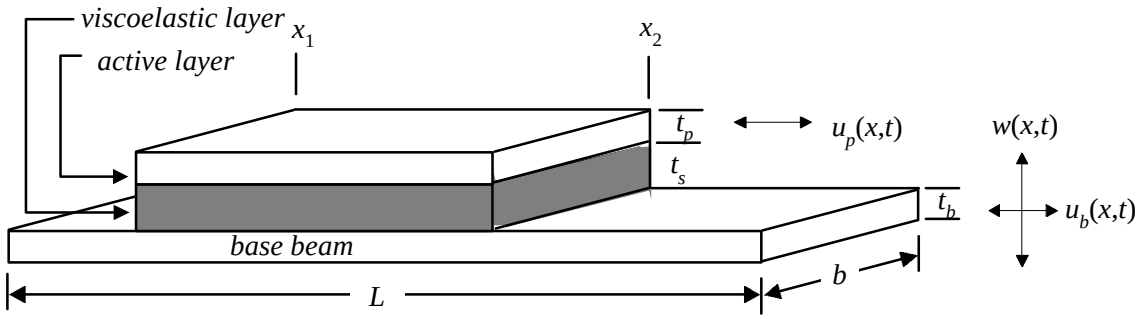

Figure 2. 4 Geometry of a Beam with Active Constrained Layer Damping

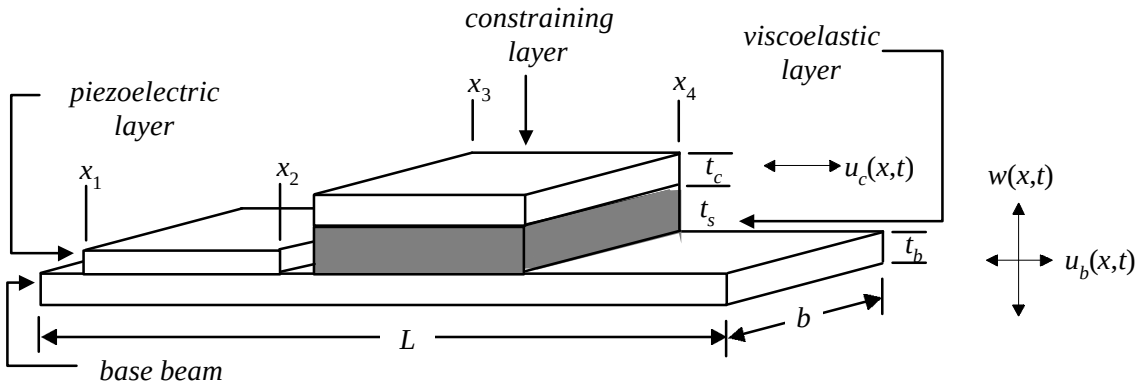

Figure 2. 5 Geometry of a Beam with PCLD and Active Damping, Same Side

Using the above kinematic relationship with equations 2.21 and 2.23, the following expressions for kinetic and potential energy can be derived

$$\mathrm{T}_p = \frac{\rho_p A_p}{2}\int_0^L \left[\left(\frac{\partial u_b}{\partial t}\right)^2 - \left(t_b + t_p\right)\left(\frac{\partial u_b}{\partial t}\right)\left(\frac{\partial^2 w}{\partial t \partial x}\right) + \frac{\left(t_b + t_p\right)^2}{4}\left(\frac{\partial^2 w}{\partial t \partial x}\right)^2 + \left(\frac{\partial w}{\partial t}\right)^2\right]\left[\mathrm{H}\left(x - x_1\right) - \mathrm{H}\left(x - x_2\right)\right]dx \tag{2.31}$$

$$\mathrm{U}_p = \frac{1}{2}\int_0^L \left[C_{11}^D A_p \left\{\left(\frac{\partial u_b}{\partial x}\right)^2 - \left(t_b + t_p\right)\left(\frac{\partial u_b}{\partial x}\right)\left(\frac{\partial^2 w}{\partial x^2}\right) + \frac{\left(t_b + t_p\right)^2}{4}\left(\frac{\partial^2 w}{\partial x^2}\right)^2\right\} + C_{11}^D I_p\left(\frac{\partial^2 w}{\partial x^2}\right)^2\right]\left[\mathrm{H}\left(x - x_1\right) - \mathrm{H}\left(x - x_2\right)\right]dx \tag{2.32}$$

Since the piezoelectric material is most effective at the area of greatest strain, the boundary conditions will dictate the location of the active patch. For example, for a cantilevered beam, the piezoelectric material is usually placed near the cantilevered end. This concept is shown in chapter 5.

2.6.3 Active Constrained Layer Damping

This derivation is just like passive constrained layer damping, but the constraining layer is now a piezoelectric layer (see Fig. 2.4). The kinematic relationships in equations 2.3 and 2.4 are used by substituting the subscript *p*, describing the piezoelectric layer, for *c*, describing the constraining layer. The energy equations are therefore

$$\mathrm{T}_s = \frac{\rho_s A_s}{2}\int_0^L \left[\left(\frac{\partial u_b}{\partial t}\right)^2 - t_b\left(\frac{\partial u_b}{\partial t}\right)\left(\frac{\partial w}{\partial x \partial t}\right) + \frac{t_b^2}{4}\left(\frac{\partial w}{\partial x \partial t}\right)^2 - t_s\left(\frac{\partial u_b}{\partial t}\right)\left(\frac{\partial \psi}{\partial t}\right) + \frac{t_b t_s}{2}\left(\frac{\partial w}{\partial x \partial t}\right)\left(\frac{\partial \psi}{\partial t}\right) + \frac{t_s^2}{4}\left(\frac{\partial \psi}{\partial t}\right)^2 + \left(\frac{\partial w}{\partial t}\right)^2 \right] \left[\mathrm{H}(x - x_1) - \mathrm{H}(x - x_2)\right] dx \tag{2.33}$$

$$\mathrm{T}_p = \frac{\rho_p A_p}{2}\int_0^L \left[\left(\frac{\partial u_b}{\partial t}\right)^2 - \left(t_b + t_p\right)\left(\frac{\partial u_b}{\partial t}\right)\left(\frac{\partial w}{\partial x \partial t}\right) + \frac{\left(t_b + t_p\right)^2}{4}\left(\frac{\partial w}{\partial x \partial t}\right)^2 - 2t_s\left(\frac{\partial u_b}{\partial t}\right)\left(\frac{\partial \psi}{\partial t}\right) + \left(t_b + t_p\right)t_s\left(\frac{\partial w}{\partial x \partial t}\right)\left(\frac{\partial \psi}{\partial t}\right) + t_s^2\left(\frac{\partial \psi}{\partial t}\right)^2 + \left(\frac{\partial w}{\partial t}\right)^2 \right] \left[\mathrm{H}(x - x_1) - \mathrm{H}(x - x_2)\right] dx \tag{2.34}$$

$$\mathrm{U}_s = \frac{1}{2}\int_0^L \left[E_s A_s \left\{ \left(\frac{\partial u_b}{\partial x}\right)^2 - t_b\left(\frac{\partial u_b}{\partial x}\right)\left(\frac{\partial^2 w}{\partial x^2}\right) + \frac{t_b^2}{4}\left(\frac{\partial^2 w}{\partial x^2}\right)^2 - t_s\left(\frac{\partial u_b}{\partial x}\right)\left(\frac{\partial \psi}{\partial x}\right) + \frac{t_s t_b}{2}\left(\frac{\partial^2 w}{\partial x^2}\right)\left(\frac{\partial \psi}{\partial x}\right) + \frac{t_s^2}{4}\left(\frac{\partial \psi}{\partial x}\right)^2 \right\} + E_s I_s\left(\frac{\partial \psi}{\partial x}\right)^2 + GA_s\left\{ \left(\frac{\partial w}{\partial x}\right)^2 - 2\left(\frac{\partial w}{\partial x}\right)\psi + \psi^2 \right\} \right] \left[\mathrm{H}(x - x_1) - \mathrm{H}(x - x_2)\right] dx \tag{2.35}$$

$$\mathrm{U}_p = \frac{1}{2}\int_0^L \left[C_{11}^D A_p \left\{ \left(\frac{\partial u_b}{\partial x}\right)^2 - \left(t_b + t_p\right)\left(\frac{\partial u_b}{\partial x}\right)\left(\frac{\partial^2 w}{\partial x^2}\right) + \frac{\left(t_b + t_p\right)^2}{4}\left(\frac{\partial^2 w}{\partial x^2}\right)^2 - 2t_s\left(\frac{\partial u_b}{\partial x}\right)\left(\frac{\partial \psi}{\partial x}\right) + t_s\left(t_b + t_p\right)\left(\frac{\partial^2 w}{\partial x^2}\right)\left(\frac{\partial \psi}{\partial x}\right) + t_s^2\left(\frac{\partial \psi}{\partial x}\right)^2 \right\} + C_{11}^D I_p\left(\frac{\partial^2 w}{\partial x^2}\right)^2 \right] \left[\mathrm{H}(x - x_1) - \mathrm{H}(x - x_2)\right] dx \tag{2.36}$$

Again, the shear modulus is used to account for the damping behavior of the VEM. Note that equations 2.33 and 2.35 are identical to equations 2.26 and 2.28. Equations 2.34 and

2.36 account for the difference in constraining layer, which is active for equations 2.34 and 2.36, and passive for equations 2.27 and 2.29.

2.6.4 Active Damping and PCLD - Same Side of Beam

In this section, the energy equations for a piezoelectric element which is attached to the beam, but is separate from the PCLD treatment, are derived. Figure 2.5 shows the geometry of this configuration. In this case, the piezoelectric treatment will be applied from x_1 to x_2. The PCLD is not allowed to overlap with the piezoelectric treatment and is therefore applied from x_3 to x_4, where $x_4 > x_3 > x_2 > x_1$ or $x_2 > x_1 > x_4 > x_3$. This means that the PZT can be placed at the root, and the PCLD further away, or visa versa. Heaviside's functions, as described 2.10, are used to account for the different treatments.

$$\mathrm{T}_p = \frac{\rho_p A_p}{2}\int_0^L \left[\left(\frac{\partial u_b}{\partial t}\right)^2 - \left(t_b + t_p\right)\left(\frac{\partial u_b}{\partial t}\right)\left(\frac{\partial^2 w}{\partial t \partial x}\right) + \frac{\left(t_b + t_p\right)^2}{4}\left(\frac{\partial^2 w}{\partial t \partial x}\right)^2 + \left(\frac{\partial w}{\partial t}\right)^2\right]\left[\mathrm{H}\left(x - x_1\right) - \mathrm{H}\left(x - x_2\right)\right]dx \tag{2.37}$$

$$\mathrm{T}_s = \frac{\rho_s A_s}{2}\int_0^L \left[\left(\frac{\partial u_b}{\partial t}\right)^2 - t_b\left(\frac{\partial u_b}{\partial t}\right)\left(\frac{\partial w}{\partial x \partial t}\right) + \frac{t_b^2}{4}\left(\frac{\partial w}{\partial x \partial t}\right)^2 - t_s\left(\frac{\partial u_b}{\partial t}\right)\left(\frac{\partial \psi}{\partial t}\right) + \frac{t_b t_s}{2}\left(\frac{\partial w}{\partial x \partial t}\right)\left(\frac{\partial \psi}{\partial t}\right) + \frac{t_s^2}{4}\left(\frac{\partial \psi}{\partial t}\right)^2 + \left(\frac{\partial w}{\partial t}\right)^2\right]\left[\mathrm{H}\left(x - x_3\right) - \mathrm{H}\left(x - x_4\right)\right]dx \tag{2.38}$$

$$\mathrm{T}_c = \frac{\rho_c A_c}{2}\int_0^L \left[\left(\frac{\partial u_b}{\partial t}\right)^2 - \left(t_b + t_c\right)\left(\frac{\partial u_b}{\partial t}\right)\left(\frac{\partial w}{\partial x \partial t}\right) + \frac{\left(t_b + t_c\right)^2}{4}\left(\frac{\partial w}{\partial x \partial t}\right)^2 - 2t_s\left(\frac{\partial u_b}{\partial t}\right)\left(\frac{\partial \psi}{\partial t}\right) + \left(t_b + t_c\right)t_s\left(\frac{\partial w}{\partial x \partial t}\right)\left(\frac{\partial \psi}{\partial t}\right) + t_s^2\left(\frac{\partial \psi}{\partial t}\right)^2 + \left(\frac{\partial w}{\partial t}\right)^2\right]\left[\mathrm{H}\left(x - x_3\right) - \mathrm{H}\left(x - x_4\right)\right]dx \tag{2.39}$$

$$\mathrm{U}_p = \frac{1}{2}\int_0^L \left[C_{11}^D A_p \left\{ \left(\frac{\partial u_b}{\partial x}\right)^2 - \left(t_b + t_p\right)\left(\frac{\partial u_b}{\partial x}\right)\left(\frac{\partial^2 w}{\partial x^2}\right) + \frac{\left(t_b + t_p\right)^2}{4}\left(\frac{\partial^2 w}{\partial x^2}\right)^2 \right\} + C_{11}^D I_p \left(\frac{\partial^2 w}{\partial x^2}\right)^2 \right] \left[\mathrm{H}\left(x - x_1\right) - \mathrm{H}\left(x - x_2\right)\right] dx \tag{2.40}$$

$$\mathrm{U}_s = \frac{1}{2}\int_0^L \left[E_s A_s \left\{ \left(\frac{\partial u_b}{\partial x}\right)^2 - t_b\left(\frac{\partial u_b}{\partial x}\right)\left(\frac{\partial^2 w}{\partial x^2}\right) + \frac{t_b^2}{4}\left(\frac{\partial^2 w}{\partial x^2}\right)^2 - t_s\left(\frac{\partial u_b}{\partial x}\right)\left(\frac{\partial \psi}{\partial x}\right) + \frac{t_s t_b}{2}\left(\frac{\partial^2 w}{\partial x^2}\right)\left(\frac{\partial \psi}{\partial x}\right) + \frac{t_s^2}{4}\left(\frac{\partial \psi}{\partial x}\right)^2 \right\} + E_s I_s \left(\frac{\partial \psi}{\partial x}\right)^2 + GA_s \left\{ \left(\frac{\partial w}{\partial x}\right)^2 - 2\left(\frac{\partial w}{\partial x}\right)\psi + \psi^2 \right\} \right] \left[\mathrm{H}\left(x - x_3\right) - \mathrm{H}\left(x - x_4\right)\right] dx \tag{2.41}$$

$$\mathrm{U}_c = \frac{1}{2}\int_0^L \left[E_c A_c \left\{ \left(\frac{\partial u_b}{\partial x}\right)^2 - \left(t_b + t_c\right)\left(\frac{\partial u_b}{\partial x}\right)\left(\frac{\partial^2 w}{\partial x^2}\right) + \frac{\left(t_b + t_c\right)^2}{4}\left(\frac{\partial^2 w}{\partial x^2}\right)^2 - 2t_s\left(\frac{\partial u_b}{\partial x}\right)\left(\frac{\partial \psi}{\partial x}\right) + t_s\left(t_b + t_c\right)\left(\frac{\partial^2 w}{\partial x^2}\right)\left(\frac{\partial \psi}{\partial x}\right) + t_s^2\left(\frac{\partial \psi}{\partial x}\right)^2 \right\} + E_c I_c \left(\frac{\partial^2 w}{\partial x^2}\right)^2 \right] \left[\mathrm{H}\left(x - x_3\right) - \mathrm{H}\left(x - x_4\right)\right] dx \tag{2.42}$$

Since the piezoelectric material is bonded directly to the beam, equations 2.37 and 2.40 are identical to equations 2.31 and 2.32. Equations 2.26-2.29 are modified such that the PCLD treatment is from x_3 to x_4, as described in equations 2.38-2.39 and 2.41-2.42. Note that Heaviside's function is modified to place the PZT from x_1 to x_2, and the PCLD from x_3 to x_4.

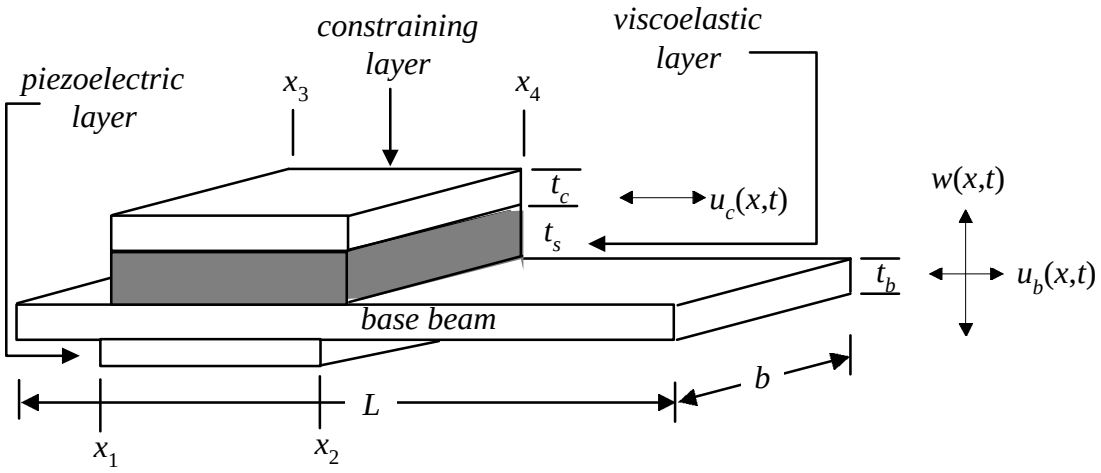

Figure 2. 6 Geometry of a Beam with PCLD and Active Element on Opposite Side

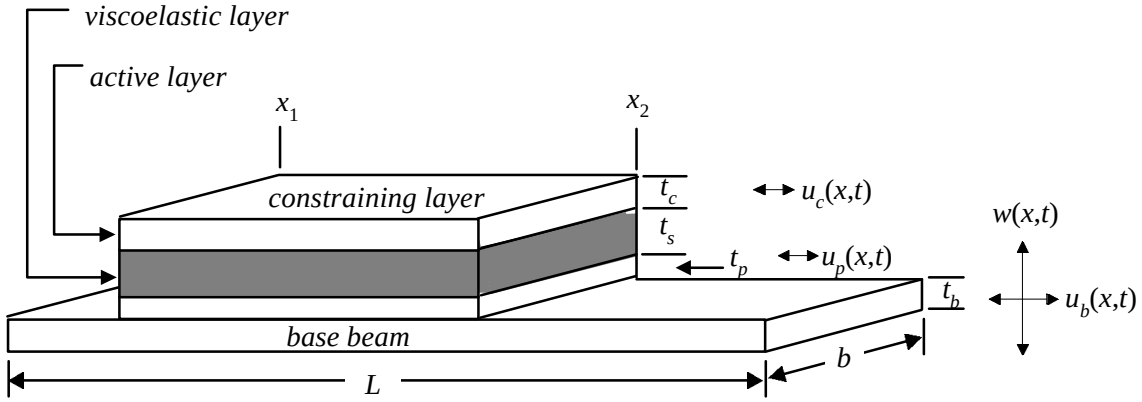

Figure 2. 7 Geometry of a Beam with an Active Element under PCLD

2.6.5 Active Damping and PCLD - Opposite Sides of Beam

Another hybrid configuration places the active element separate from the passive element, but on the other side of the beam (see Fig 2.6). The equations for the last section and this are very similar, except there is a sign change on some of the piezoelectric terms. In this case, the piezoelectric and the PCLD are allowed to be in the same position along the beam, and they are not constrained to be the same length. Therefore the energy for the piezoelectric layer is integrated from x_1 to x_2 while the energy for the PCLD is integrated from x_3 to x_4. The kinematic relationship for a piezoelectric material mounted underneath the beam is

$$u_p = u_b + \frac{t_b + t_p}{2}\frac{\partial w}{\partial x}.$$

The equations for the kinetic and potential energies are given by

$$\mathrm{T}_p = \frac{\rho_p A_p}{2}\int_0^L \left[\left(\frac{\partial u_b}{\partial t}\right)^2 + \left(t_b + t_c\right)\left(\frac{\partial u_b}{\partial t}\right)\left(\frac{\partial^2 w}{\partial t \partial x}\right) + \frac{\left(t_b + t_c\right)^2}{4}\left(\frac{\partial^2 w}{\partial t \partial x}\right)^2 + \left(\frac{\partial w}{\partial t}\right)^2\right] \left[\mathrm{H}\left(x - x_1\right) - \mathrm{H}\left(x - x_2\right)\right] dx \tag{2.43}$$

$$\mathrm{T}_s = \frac{\rho_s A_s}{2}\int_0^L \left[\left(\frac{\partial u_b}{\partial t}\right)^2 - t_b\left(\frac{\partial u_b}{\partial t}\right)\left(\frac{\partial w}{\partial x \partial t}\right) + \frac{t_b^2}{4}\left(\frac{\partial w}{\partial x \partial t}\right)^2 - t_s\left(\frac{\partial u_b}{\partial t}\right)\left(\frac{\partial \psi}{\partial t}\right) + \frac{t_b t_s}{2}\left(\frac{\partial w}{\partial x \partial t}\right)\left(\frac{\partial \psi}{\partial t}\right) + \frac{t_s^2}{4}\left(\frac{\partial \psi}{\partial t}\right)^2 + \left(\frac{\partial w}{\partial t}\right)^2\right] \left[\mathrm{H}\left(x - x_3\right) - \mathrm{H}\left(x - x_4\right)\right] dx \tag{2.44}$$

$$\mathrm{T}_c = \frac{\rho_c A_c}{2}\int_0^L \Bigg[\left(\frac{\partial u_b}{\partial t}\right)^2 - \left(t_b + t_c\right)\left(\frac{\partial u_b}{\partial t}\right)\left(\frac{\partial w}{\partial x \partial t}\right) + \frac{\left(t_b + t_c\right)^2}{4}\left(\frac{\partial w}{\partial x \partial t}\right)^2 - 2t_s\left(\frac{\partial u_b}{\partial t}\right)\left(\frac{\partial \psi}{\partial t}\right) + \left(t_b + t_c\right)t_s\left(\frac{\partial w}{\partial x \partial t}\right)\left(\frac{\partial \psi}{\partial t}\right) + t_s^2\left(\frac{\partial \psi}{\partial t}\right)^2 + \left(\frac{\partial w}{\partial t}\right)^2 \Bigg] \left[\mathrm{H}\left(x - x_3\right) - \mathrm{H}\left(x - x_4\right)\right] dx \tag{2.45}$$

$$\mathrm{U}_p = \frac{1}{2}\int_0^L \Bigg[C_{11}^D A_p \left\{ \left(\frac{\partial u_b}{\partial x}\right)^2 + \left(t_b + t_c\right)\left(\frac{\partial u_b}{\partial x}\right)\left(\frac{\partial^2 w}{\partial x^2}\right) + \frac{\left(t_b + t_c\right)^2}{4}\left(\frac{\partial^2 w}{\partial x^2}\right)^2 \right\} + C_{11}^D I_p \left(\frac{\partial^2 w}{\partial x^2}\right)^2 \Bigg] \left[\mathrm{H}\left(x - x_1\right) - \mathrm{H}\left(x - x_2\right)\right] dx \tag{2.46}$$

$$\mathrm{U}_s = \frac{1}{2}\int_0^L \Bigg[E_s A_s \left\{ \left(\frac{\partial u_b}{\partial x}\right)^2 - t_b\left(\frac{\partial u_b}{\partial x}\right)\left(\frac{\partial^2 w}{\partial x^2}\right) + \frac{t_b^2}{4}\left(\frac{\partial^2 w}{\partial x^2}\right)^2 - t_s\left(\frac{\partial u_b}{\partial x}\right)\left(\frac{\partial \psi}{\partial x}\right) + \frac{t_s t_b}{2}\left(\frac{\partial^2 w}{\partial x^2}\right)\left(\frac{\partial \psi}{\partial x}\right) + \frac{t_s^2}{4}\left(\frac{\partial \psi}{\partial x}\right)^2 \right\} + E_s I_s \left(\frac{\partial \psi}{\partial x}\right)^2 + GA_s \left\{ \left(\frac{\partial w}{\partial x}\right)^2 - 2\left(\frac{\partial w}{\partial x}\right)\psi + \psi^2 \right\} \Bigg] \left[\mathrm{H}\left(x - x_3\right) - \mathrm{H}\left(x - x_4\right)\right] dx \tag{2.47}$$

$$\mathrm{U}_c = \frac{1}{2}\int_0^L \Bigg[E_c A_c \left\{ \left(\frac{\partial u_b}{\partial x}\right)^2 - \left(t_b + t_c\right)\left(\frac{\partial u_b}{\partial x}\right)\left(\frac{\partial^2 w}{\partial x^2}\right) + \frac{\left(t_b + t_c\right)^2}{4}\left(\frac{\partial^2 w}{\partial x^2}\right)^2 - 2t_s\left(\frac{\partial u_b}{\partial x}\right)\left(\frac{\partial \psi}{\partial x}\right) + t_s\left(t_b + t_c\right)\left(\frac{\partial^2 w}{\partial x^2}\right)\left(\frac{\partial \psi}{\partial x}\right) + t_s^2\left(\frac{\partial \psi}{\partial x}\right)^2 \right\} + E_c I_c \left(\frac{\partial^2 w}{\partial x^2}\right)^2 \Bigg] \left[\mathrm{H}\left(x - x_3\right) - \mathrm{H}\left(x - x_4\right)\right] dx \tag{2.48}$$

Note that x_3 is no longer constrained to be greater than x_2. In fact, x_1 and x_3, the location and length of the piezoelectric element and the PCLD element can be equal.

2.6.6 Active Damping Underneath PCLD

This variation is like PCLD, but it has a piezoelectric layer underneath the PCLD (see Fig. 2.7). The lengths of all the treatments are assumed to be the same. The equations for the kinetic and potential energies are

$$\mathrm{T}_p = \frac{\rho_p A_p}{2}\int_0^L \left[\left(\frac{\partial u_b}{\partial t}\right)^2 - \left(t_b + t_c\right)\left(\frac{\partial u_b}{\partial t}\right)\left(\frac{\partial^2 w}{\partial t \partial x}\right) + \frac{\left(t_b + t_p\right)^2}{4}\left(\frac{\partial^2 w}{\partial t \partial x}\right)^2 + \left(\frac{\partial w}{\partial t}\right)^2\right] \left[\mathrm{H}\left(x - x_1\right) - \mathrm{H}\left(x - x_2\right)\right] dx \tag{2.49}$$

$$\mathrm{T}_s = \frac{\rho_s A_s}{2}\int_0^L \left[\left(\frac{\partial u_b}{\partial t}\right)^2 - \left(t_b + 2t_p\right)\left(\frac{\partial u_b}{\partial t}\right)\left(\frac{\partial w}{\partial x \partial t}\right) + \frac{\left(t_b + 2t_p\right)^2}{4}\left(\frac{\partial w}{\partial x \partial t}\right)^2 - t_s\left(\frac{\partial u_b}{\partial t}\right)\left(\frac{\partial \psi}{\partial t}\right) + \frac{\left(t_b + 2t_p\right)t_s}{2}\left(\frac{\partial w}{\partial x \partial t}\right)\left(\frac{\partial \psi}{\partial t}\right) + \frac{t_s^2}{4}\left(\frac{\partial \psi}{\partial t}\right)^2 + \left(\frac{\partial w}{\partial t}\right)^2\right] \left[\mathrm{H}\left(x - x_1\right) - \mathrm{H}\left(x - x_2\right)\right] dx \tag{2.50}$$

$$\mathrm{T}_c = \frac{\rho_c A_c}{2}\int_0^L \left[\left(\frac{\partial u_b}{\partial t}\right)^2 - \left(t_b + 2t_p + t_c\right)\left(\frac{\partial u_b}{\partial t}\right)\left(\frac{\partial w}{\partial x \partial t}\right) + \frac{\left(t_b + 2t_p + t_c\right)^2}{4}\left(\frac{\partial w}{\partial x \partial t}\right)^2 - 2t_s\left(\frac{\partial u_b}{\partial t}\right)\left(\frac{\partial \psi}{\partial t}\right) + \frac{\left(t_b + 2t_p + t_c\right)t}{2}{}_s\left(\frac{\partial w}{\partial x \partial t}\right)\left(\frac{\partial \psi}{\partial t}\right) + t_s^2\left(\frac{\partial \psi}{\partial t}\right)^2 + \left(\frac{\partial w}{\partial t}\right)^2\right] \left[\mathrm{H}\left(x - x_1\right) - \mathrm{H}\left(x - x_2\right)\right] dx \tag{2.51}$$

$$\mathrm{U}_p = \frac{1}{2}\int_0^L \left[C_{11}^D A_p \left\{ \left(\frac{\partial u_b}{\partial x}\right)^2 - \left(t_b + t_p\right)\left(\frac{\partial u_b}{\partial x}\right)\left(\frac{\partial^2 w}{\partial x^2}\right) + \frac{\left(t_b + t_p\right)^2}{4}\left(\frac{\partial^2 w}{\partial x^2}\right)^2 \right\} \right.$$
$$\left. + C_{11}^D I_p \left(\frac{\partial^2 w}{\partial x^2}\right)^2 \right] \left[\mathrm{H}\left(x - x_1\right) - \mathrm{H}\left(x - x_2\right)\right] dx \qquad 2.52$$

$$\mathrm{U}_s = \frac{1}{2}\int_0^L \left[E_s A_s \left\{ \left(\frac{\partial u_b}{\partial x}\right)^2 - \left(t_b + 2t_p\right)\left(\frac{\partial u_b}{\partial x}\right)\left(\frac{\partial^2 w}{\partial x^2}\right) + \frac{\left(t_b + 2t_p\right)^2}{4}\left(\frac{\partial^2 w}{\partial x^2}\right)^2 \right.\right.$$
$$\left. - t_s \left(\frac{\partial u_b}{\partial x}\right)\left(\frac{\partial \psi}{\partial x}\right) + \frac{t_s\left(t_b + 2t_p\right)}{2}\left(\frac{\partial^2 w}{\partial x^2}\right)\left(\frac{\partial \psi}{\partial x}\right) + \frac{t_s^2}{4}\left(\frac{\partial \psi}{\partial x}\right)^2 \right\} \qquad 2.53$$
$$\left. + E_s I_s \left(\frac{\partial \psi}{\partial x}\right)^2 + GA_s \left\{ \left(\frac{\partial w}{\partial x}\right)^2 - 2\left(\frac{\partial w}{\partial x}\right)\psi + \psi^2 \right\} \right]$$
$$\left[\mathrm{H}\left(x - x_1\right) - \mathrm{H}\left(x - x_2\right)\right] dx$$

$$\mathrm{U}_c = \frac{1}{2}\int_0^L \left[E_c A_c \left\{ \left(\frac{\partial u_b}{\partial x}\right)^2 - \left(t_b + 2t_p + t_c\right)\left(\frac{\partial u_b}{\partial x}\right)\left(\frac{\partial^2 w}{\partial x^2}\right) \right.\right.$$
$$+ \frac{\left(t_b + 2t_p + t_c\right)^2}{4}\left(\frac{\partial^2 w}{\partial x^2}\right)^2 - 2t_s \left(\frac{\partial u_b}{\partial x}\right)\left(\frac{\partial \psi}{\partial x}\right) \qquad 2.54$$
$$\left. \left. + t_s\left(t_b + 2t_p + t_c\right)\left(\frac{\partial^2 w}{\partial x^2}\right)\left(\frac{\partial \psi}{\partial x}\right) + t_s^2 \left(\frac{\partial \psi}{\partial x}\right)^2 \right\} + E_c I_c \left(\frac{\partial^2 w}{\partial x^2}\right)^2 \right]$$
$$\left[\mathrm{H}\left(x - x_1\right) - \mathrm{H}\left(x - x_2\right)\right] dx$$

This configuration is not to be confused with the treatment as described by Baz [31]. Baz places a piezoelectric film under the ACLD treatment to use as a sensor. Here the piezoelectric element is used as an actuator.

2.7 Discretization and Lagrange Equations

The assumed modes method is used to discretize the energy equations [61]. Assumed modes, which are in terms of generalized coordinates, are used to expand the transverse and longitudinal displacements, w and u_b respectively, and shear angle, ψ, functions.

$$\begin{aligned} w(x,t) &= \sum_{i=1}^{n} W_i(x)\theta_i(t) = \left[W(x)\right]^T\left[\theta(t)\right] \\ u_b(x,t) &= \sum_{i=1}^{n} U_i(x)\phi_i(t) = \left[U(x)\right]^T\left[\phi(t)\right] \\ \psi(x,t) &= \sum_{i=1}^{n} \Psi_i(x)\xi_i(t) = \left[\Psi(x)\right]^T\left[\xi(t)\right] \end{aligned} \qquad 2.55$$

The displacement functions, $W(x)$, $U(x)$ and $\Psi(x)$, are sets of admissible functions which are chosen for each generalized coordinate, $\theta(t)$, $\phi(t)$, and $\xi(t)$, respectively.

Lagrange's equation will be used to obtain equations of motion for the different treatments. The basic form of Lagrange's equation is

$$\frac{d}{dt}\left(\frac{\partial \mathcal{L}}{\partial \dot{q}_i}\right) - \frac{\partial \mathcal{L}}{\partial q_i} = \mathrm{Q}_i \qquad (i = 1,2,\ldots,n) \qquad 2.56$$

where $\mathcal{L} = \mathrm{T} - \mathrm{U}$, q_i is the generalized displacement, and Q_i the generalized force. The kinetic, T, and potential energy, U, terms will consist of summations of the energies due to the different layers. For example, for a beam with PCLD, the total kinetic energy is given as $\mathrm{T} = \mathrm{T}_b + \mathrm{T}_s + \mathrm{T}_c$, and the total potential energy is given as $\mathrm{U} = \mathrm{U}_b + \mathrm{U}_s + \mathrm{U}_c$. Recall the subscript b denotes the beam, s the VEM and c the constraining layer. The

Table 2. 1 Notation Used to Write Discretized Energy Equations

$\langle \alpha,\beta \rangle_{mb} \equiv \rho_b A_b \int_0^L \alpha\beta^T dx$	$\langle \alpha,\beta \rangle_{kb} \equiv E_b I_b \int_0^L \alpha\beta^T dx$
$\langle \alpha,\beta \rangle_{mp} \equiv \rho_p A_p \int_0^L \alpha\beta^T \left[\mathrm{H}(x-x_1) - \mathrm{H}(x-x_2) \right] dx$	$\langle \alpha,\beta \rangle_{kp} \equiv C_{11}^D A_p \int_0^L \alpha\beta^T \left[\mathrm{H}(x-x_1) - \mathrm{H}(x-x_2) \right] dx$
$\langle \alpha,\beta \rangle_{ms} \equiv \rho_s A_s \int_0^L \alpha\beta^T \left[\mathrm{H}(x-x_1) - \mathrm{H}(x-x_2) \right] dx$	$\langle \alpha,\beta \rangle_{ks} \equiv E_s A_s \int_0^L \alpha\beta^T \left[\mathrm{H}(x-x_1) - \mathrm{H}(x-x_2) \right] dx$
$\langle \alpha,\beta \rangle_{mc} \equiv \rho_c A_c \int_0^L \alpha\beta^T \left[\mathrm{H}(x-x_1) - \mathrm{H}(x-x_2) \right] dx$	$\langle \alpha,\beta \rangle_{kc} \equiv E_c A_c \int_0^L \alpha\beta^T \left[\mathrm{H}(x-x_1) - \mathrm{H}(x-x_2) \right] dx$
	$\langle \alpha,\beta \rangle_{kg} \equiv G A_c \int_0^L \alpha\beta^T \left[\mathrm{H}(x-x_1) - \mathrm{H}(x-x_2) \right] dx$

Table 2. 2 Notation for PCLD if Separate from Active Element

$\langle \alpha,\beta \rangle_{ms} \equiv \rho_s A_s \int_0^L \alpha\beta^T \left[\mathrm{H}(x-x_3) - \mathrm{H}(x-x_4) \right] dx$	$\langle \alpha,\beta \rangle_{ks} \equiv E_s A_s \int_0^L \alpha\beta^T \left[\mathrm{H}(x-x_3) - \mathrm{H}(x-x_4) \right] dx$
$\langle \alpha,\beta \rangle_{mc} \equiv \rho_c A_c \int_0^L \alpha\beta^T \left[\mathrm{H}(x-x_3) - \mathrm{H}(x-x_4) \right] dx$	$\langle \alpha,\beta \rangle_{kc} \equiv E_c A_c \int_0^L \alpha\beta^T \left[\mathrm{H}(x-x_3) - \mathrm{H}(x-x_4) \right] dx$
	$\langle \alpha,\beta \rangle_{kg} \equiv G A_c \int_0^L \alpha\beta^T \left[\mathrm{H}(x-x_3) - \mathrm{H}(x-x_4) \right] dx$

complete derivation to obtain a matrix equation of motion is included in section 2.7.1. For subsequent sections, the same methods are applied, but only the final results are reported.

2.7.1 Passive Constrained Layer Damping

Equations 2.7, 2.8 and 2.26-2.29 describe the energy for a beam with passive constrained layer damping. Discretizing the system using equation 2.55 and the notation outlined inTable 2.1, the kinetic and potential energy equations for the beam, VEM and constraining layer can be written in matrix form such that

$$\mathrm{T}_b = \frac{1}{2}\left[\dot{\phi}^T \mathbf{M}_1^b \dot{\phi} + \dot{\theta}^T \mathbf{M}_2^b \dot{\theta}\right] \tag{2.57}$$

$$\mathrm{T}_s = \frac{1}{2}\left[\dot{\phi}^T \mathbf{M}_1^s \dot{\phi} + \dot{\phi}^T \mathbf{M}_2^s \dot{\theta} + \dot{\theta}^T \mathbf{M}_3^s \dot{\theta} + \dot{\phi}^T \mathbf{M}_4^s \dot{\xi} + \dot{\theta}^T \mathbf{M}_5^s \dot{\xi} + \dot{\xi}^T \mathbf{M}_6^s \dot{\xi}\right] \tag{2.58}$$

$$\mathrm{T}_c = \frac{1}{2}\left[\dot{\phi}^T \mathbf{M}_1^c \dot{\phi} + \dot{\phi}^T \mathbf{M}_2^c \dot{\theta} + \dot{\theta}^T \mathbf{M}_3^c \dot{\theta} + \dot{\phi}^T \mathbf{M}_4^c \dot{\xi} + \dot{\theta}^T \mathbf{M}_5^c \dot{\xi} + \dot{\xi}^T \mathbf{M}_6^c \dot{\xi}\right] \tag{2.59}$$

$$\mathrm{U}_b = \frac{1}{2}\left[\phi^T \mathbf{K}_1^b \phi + \theta^T \mathbf{K}_2^b \theta\right] \tag{2.60}$$

$$\begin{aligned}\mathrm{U}_s = \frac{1}{2}\Big[&\phi^T \mathbf{K}_1^s \phi + \phi^T \mathbf{K}_2^s \theta + \theta^T \mathbf{K}_3^s \theta + \phi^T \mathbf{K}_4^s \xi + \theta^T \mathbf{K}_5^s \xi + \xi^T \mathbf{K}_6^s \xi \\ &+ \theta^T \mathbf{K}_1^g \theta + \theta^T \mathbf{K}_2^g \xi + \xi^T \mathbf{K}_3^g \xi\Big]\end{aligned} \tag{2.61}$$

$$\mathrm{U}_c = \frac{1}{2}\left[\phi^T \mathbf{K}_1^c \phi + \phi^T \mathbf{K}_2^c \theta + \theta^T \mathbf{K}_3^c \theta + \phi^T \mathbf{K}_4^c \xi + \theta^T \mathbf{K}_5^c \xi + \xi^T \mathbf{K}_6^c \xi\right] \tag{2.62}$$

Note that the subscripts on the terms in Table 2.1 describe whether the term is associated with mass or stiffness, as well as layer of treatment. Also note that the superscript on the

mass and stiffness terms in equations 2.57-2.62 denote the layer. Recall subscript or superscript *b* describes the base beam, *s* the VEM, and *c* the constraining layer. The mass, **M**, and stiffness, **K**, matrices are of equations 2.57-2.62 are defined as

$$\mathbf{M}_1^b = \langle U, U \rangle_{mb} \qquad \mathbf{M}_4^c = -2t_s \langle U, \Psi \rangle_{mc} \qquad \mathbf{K}_6^s = \left(\frac{t_s^2}{4} + \frac{I_s}{A_s} \right) \langle \Psi', \Psi' \rangle_{ks}$$

$$\mathbf{M}_2^b = \langle W, W \rangle_{mb} \qquad \mathbf{M}_5^c = t_s (t_b + t_c) \langle W', \Psi \rangle_{mc} \qquad \mathbf{K}_1^c = \langle U', U' \rangle_{kc}$$

$$\mathbf{M}_1^s = \langle U, U \rangle_{ms} \qquad \mathbf{M}_6^c = t_s^2 \langle \Psi, \Psi \rangle_{mc} \qquad \mathbf{K}_2^c = -(t_b + t_c) \langle U', W'' \rangle_{kc}$$

$$\mathbf{M}_2^s = -t_b \langle U, W' \rangle_{ms} \qquad \mathbf{K}_1^b = \langle U', U' \rangle_{kb} \qquad \mathbf{K}_3^c = \left(\frac{(t_b + t_c)^2}{4} + \frac{I_c}{A_c} \right) \langle W'', W'' \rangle_{kc}$$

$$\mathbf{M}_3^s = \frac{t_b^2}{4} \langle W', W' \rangle_{ms} + \langle W, W \rangle_{ms} \qquad \mathbf{K}_2^b = \frac{I_b}{A_b} \langle W'', W'' \rangle_{kb} \qquad \mathbf{K}_4^c = -2t_s \langle U', \Psi' \rangle_{kc}$$

$$\mathbf{M}_4^s = -t_s \langle U, \Psi \rangle_{ms} \qquad \mathbf{K}_1^s = \langle U', U' \rangle_{ks} \qquad \mathbf{K}_5^c = t_s (t_b + t_c) \langle W'', \Psi' \rangle_{kc}$$

$$\mathbf{M}_5^s = \frac{t_b t_s}{2} \langle W', \Psi \rangle_{ms} \qquad \mathbf{K}_2^s = -t_b \langle U', W'' \rangle_{ks} \qquad \mathbf{K}_6^c = t_s^2 \langle \Psi', \Psi' \rangle_{kc}$$

$$\mathbf{M}_6^s = \frac{t_s^2}{4} \langle \Psi, \Psi \rangle_{ms} \qquad \mathbf{K}_3^s = \frac{t_b^2}{4} \langle W'', W'' \rangle_{ks} \qquad \mathbf{K}_1^g = \langle W', W' \rangle_{kg}$$

$$\mathbf{M}_1^c = \langle U, U \rangle_{mc} \qquad \mathbf{K}_4^s = -t_s \langle U', \Psi' \rangle_{ks} \qquad \mathbf{K}_2^g = -\langle W', \Psi \rangle_{kg}$$

$$\mathbf{M}_2^c = -(t_b + t_c) \langle U, W' \rangle_{mc} \qquad \mathbf{K}_5^s = \frac{t_b t_s}{2} \langle W'', \Psi' \rangle_{ks} \qquad \mathbf{K}_3^g = \langle \Psi, \Psi \rangle_{kg}$$

$$\mathbf{M}_3^c = \frac{(t_b + t_c)^2}{4} \langle W', W' \rangle_{mc} + \langle W, W \rangle_{mc}$$

Here the single apostrophe denotes one derivative with respect to *x*. A double apostrophe denotes two derivatives with respect to *x*.

The Lagrangian is given as $\mathcal{L} = \mathrm{T} - \mathrm{U} = \mathrm{T}_b + \mathrm{T}_s + \mathrm{T}_c - \mathrm{U}_b - \mathrm{U}_s - \mathrm{U}_c$. Next, Lagrange's equation, equation 2.56, is applied to equations 2.57-2.62. Taking the partial derivatives of the kinetic and potential energy of equations 2.57-2.62 with respect to the

displacements and velocities of the generalized coordinates, the following set of equations is obtained.

$$\frac{d}{dt}\left(\frac{\partial \mathscr{L}}{\partial \dot{\theta}}\right) = \left(\mathbf{M}_2^b + \mathbf{M}_3^s + \mathbf{M}_3^c\right)\ddot{\theta} + \frac{1}{2}\left(\mathbf{M}_2^s + \mathbf{M}_2^c\right)^T \ddot{\phi} + \frac{1}{2}\left(\mathbf{M}_5^s + \mathbf{M}_5^c\right)\ddot{\xi} \tag{2.63}$$

$$\frac{d}{dt}\left(\frac{\partial \mathscr{L}}{\partial \dot{\phi}}\right) = \frac{1}{2}\left(\mathbf{M}_2^s + \mathbf{M}_2^c\right)\ddot{\theta} + \left(\mathbf{M}_1^b + \mathbf{M}_1^s + \mathbf{M}_1^c\right)\ddot{\phi} + \frac{1}{2}\left(\mathbf{M}_4^s + \mathbf{M}_4^c\right)\ddot{\xi} \tag{2.64}$$

$$\frac{d}{dt}\left(\frac{\partial \mathscr{L}}{\partial \dot{\xi}}\right) = \frac{1}{2}\left(\mathbf{M}_5^s + \mathbf{M}_5^c\right)^T \ddot{\theta} + \frac{1}{2}\left(\mathbf{M}_4^s + \mathbf{M}_4^c\right)^T \ddot{\phi} + \left(\mathbf{M}_6^s + \mathbf{M}_6^c\right)\ddot{\xi} \tag{2.65}$$

$$\frac{\partial \mathscr{L}}{\partial \theta} = \left(\mathbf{K}_2^b + \mathbf{K}_3^s + \mathbf{K}_3^c + \mathbf{K}_1^g\right)\theta + \frac{1}{2}\left(\mathbf{K}_2^s + \mathbf{K}_2^c\right)^T \phi + \frac{1}{2}\left(\mathbf{K}_5^s + \mathbf{K}_5^c + \mathbf{K}_2^g\right)\xi \tag{2.66}$$

$$\frac{\partial \mathscr{L}}{\partial \phi} = \frac{1}{2}\left(\mathbf{K}_2^s + \mathbf{K}_2^c\right)\theta + \left(\mathbf{K}_1^b + \mathbf{K}_1^s + \mathbf{K}_1^c\right)\phi + \frac{1}{2}\left(\mathbf{K}_4^s + \mathbf{K}_4^c\right)\xi \tag{2.67}$$

$$\frac{\partial \mathscr{L}}{\partial \xi} = \frac{1}{2}\left(\mathbf{K}_5^s + \mathbf{K}_5^c + \mathbf{K}_2^g\right)^T \theta + \frac{1}{2}\left(\mathbf{K}_4^s + \mathbf{K}_4^c\right)^T \phi + \left(\mathbf{K}_6^s + \mathbf{K}_6^c + \mathbf{K}_3^g\right)\xi \tag{2.68}$$

These equations can be written in matrix form such that

$$\begin{bmatrix} \mathbf{M}_{\theta\theta} & \mathbf{M}_{\theta\phi} & \mathbf{M}_{\theta\xi} \\ \mathbf{M}_{\theta\phi}^T & \mathbf{M}_{\phi\phi} & \mathbf{M}_{\phi\xi} \\ \mathbf{M}_{\theta\xi}^T & \mathbf{M}_{\phi\xi}^T & \mathbf{M}_{\xi\xi} \end{bmatrix} \begin{bmatrix} \ddot{\theta} \\ \ddot{\phi} \\ \ddot{\xi} \end{bmatrix} + \begin{bmatrix} \mathbf{K}_{\theta\theta} & \mathbf{K}_{\theta\phi} & \mathbf{K}_{\theta\xi} \\ \mathbf{K}_{\theta\phi}^T & \mathbf{K}_{\phi\phi} & \mathbf{K}_{\phi\xi} \\ \mathbf{K}_{\theta\xi}^T & \mathbf{K}_{\phi\xi}^T & \mathbf{K}_{\xi\xi} \end{bmatrix} \begin{bmatrix} \theta \\ \phi \\ \xi \end{bmatrix} = \begin{bmatrix} \mathrm{Q}_\theta \\ \mathrm{Q}_\phi \\ \mathrm{Q}_\xi \end{bmatrix} \tag{2.69}$$

where

$$\mathbf{M}_{\theta\theta} = \mathbf{M}_2^b + \mathbf{M}_3^s + \mathbf{M}_3^c \qquad \mathbf{M}_{\phi\xi} = \frac{1}{2}\left(\mathbf{M}_4^s + \mathbf{M}_4^c\right) \qquad \mathbf{K}_{\theta\xi} = \frac{1}{2}\left(\mathbf{K}_5^s + \mathbf{K}_5^c + \mathbf{K}_2^g\right)$$

$$\mathbf{M}_{\theta\phi} = \frac{1}{2}\left(\mathbf{M}_2^s + \mathbf{M}_2^c\right)^T \qquad \mathbf{M}_{\xi\xi} = \mathbf{M}_6^s + \mathbf{M}_6^c \qquad \mathbf{K}_{\phi\phi} = \mathbf{K}_1^b + \mathbf{K}_1^s + \mathbf{K}_1^c$$

$$\mathbf{M}_{\theta\xi} = \frac{1}{2}\left(\mathbf{M}_5^s + \mathbf{M}_5^c\right) \qquad \mathbf{K}_{\theta\theta} = \mathbf{K}_2^b + \mathbf{K}_3^s + \mathbf{K}_3^c + \mathbf{K}_1^g \qquad \mathbf{K}_{\phi\xi} = \frac{1}{2}\left(\mathbf{K}_4^s + \mathbf{K}_4^c\right)$$

$$\mathbf{M}_{\phi\phi} = \mathbf{M}_1^b + \mathbf{M}_1^s + \mathbf{M}_1^c \qquad \mathbf{K}_{\theta\phi} = \frac{1}{2}\left(\mathbf{K}_2^s + \mathbf{K}_2^c\right)^T \qquad \mathbf{K}_{\xi\xi} = \mathbf{K}_6^s + \mathbf{K}_6^c + \mathbf{K}_3^g$$

Note the subscripts of equation 2.69 denote which generalized coordinates the mass matrix, stiffness matrix and forcing function are associated with. While each submatrix of equation 2.69 is not necessarily symmetric, symmetry of the complete mass and stiffness matrices is maintained. The forcing terms are determined from the virtual work equations. In this case, there is only an externally applied load, as described in equation 2.25. Taking the variation of equation 2.25 yields

$$\begin{bmatrix} Q_\theta \\ Q_\phi \\ Q_\xi \end{bmatrix} = \begin{bmatrix} \int_0^L W^T f(x,t)dx \\ 0 \\ 0 \end{bmatrix} \qquad 2.70$$

Equations 2.69 and 2.70 fully describe the motion of a beam with PCLD treatment. The boundary conditions will dictate the displacement functions to be used.

2.7.2 Active Damping

The kinetic and potential energy equations for a piezoelectric patch are given in equations 2.21 and 2.23. Along with the energy equations for the base beam, equations 2.7 and 2.9, the energy equations for a beam with active damping can be rewritten as

$$\mathrm{T}_b = \frac{1}{2}\left[\dot{\phi}^T \mathbf{M}_1^b \dot{\phi} + \dot{\theta}^T \mathbf{M}_2^b \dot{\theta}\right] \tag{2.71}$$

$$\mathrm{T}_p = \frac{1}{2}\left[\dot{\phi}^T \mathbf{M}_1^p \dot{\phi} + \dot{\phi}^T \mathbf{M}_2^p \dot{\theta} + \dot{\theta}^T \mathbf{M}_3^p \dot{\theta}\right] \tag{2.72}$$

$$\mathrm{U}_b = \frac{1}{2}\left[\dot{\phi}^T \mathbf{K}_1^b \dot{\phi} + \dot{\theta}^T \mathbf{K}_2^b \dot{\theta}\right] \tag{2.73}$$

$$\mathrm{U}_p = \frac{1}{2}\left[\dot{\phi}^T \mathbf{K}_1^p \dot{\phi} + \dot{\phi}^T \mathbf{K}_2^p \dot{\theta} + \dot{\theta}^T \mathbf{K}_3^p \dot{\theta}\right] \tag{2.74}$$

where the mass and stiffness matrices are defined as

$$\mathbf{M}_1^b = \langle U, U \rangle_{mb} \qquad \mathbf{M}_3^p = \frac{\left(t_p + t_b\right)^2}{4}\langle W', W' \rangle_{mp} + \langle W, W \rangle_{mp} \qquad \mathbf{K}_1^p = \langle U', U' \rangle_{kp}$$

$$\mathbf{M}_2^b = \langle W, W \rangle_{mb} \qquad \mathbf{K}_1^b = \langle U', U' \rangle_{kb} \qquad \mathbf{K}_2^p = -\left(t_b + t_p\right)\langle U', W'' \rangle_{kp}$$

$$\mathbf{M}_1^p = \langle U, U \rangle_{mp} \qquad \mathbf{K}_2^b = \frac{I_b}{A_b}\langle W'', W'' \rangle_{kb} \qquad \mathbf{K}_3^p = \left(\frac{\left(t_b + t_p\right)^2}{4} + \frac{I_b}{A_b}\right)\langle W'', W'' \rangle_{kp}$$

$$\mathbf{M}_2^p = -\left(t_b + t_p\right)\langle U, W' \rangle_{mp}$$

Again, the superscipt on the mass and stiffness terms denote the layer. Recall that the subscript or superscript *p* denotes the piezoelectric layer. Applying Lagrange's equation to equations 2.71-2.74 and taking the partial derivatives yields the following matrix equation

$$\begin{bmatrix} \mathbf{M}_{\theta\theta} & \mathbf{M}_{\theta\phi} \\ \mathbf{M}_{\theta\phi}^T & \mathbf{M}_{\phi\phi} \end{bmatrix} \begin{bmatrix} \ddot{\theta} \\ \ddot{\phi} \end{bmatrix} + \begin{bmatrix} \mathbf{K}_{\theta\theta} & \mathbf{K}_{\theta\phi} \\ \mathbf{K}_{\theta\phi}^T & \mathbf{K}_{\phi\phi} \end{bmatrix} \begin{bmatrix} \theta \\ \phi \end{bmatrix} = \begin{bmatrix} Q_\theta \\ Q_\phi \end{bmatrix} \tag{2.75}$$

where

$$\mathbf{M}_{\theta\theta} = \mathbf{M}_2^b + \mathbf{M}_3^p \qquad \mathbf{M}_{\phi\phi} = \mathbf{M}_1^b + \mathbf{M}_1^p \qquad \mathbf{K}_{\theta\phi} = \frac{1}{2}\left(\mathbf{K}_2^p\right)^T$$

$$\mathbf{M}_{\theta\phi} = \frac{1}{2}\left(\mathbf{M}_2^p\right)^T \qquad \mathbf{K}_{\theta\theta} = \mathbf{K}_2^b + \mathbf{K}_3^p \qquad \mathbf{K}_{\phi\phi} = \mathbf{K}_1^b + \mathbf{K}_1^p$$

The virtual work done by an outside force and the piezoelectric treatment is described in equations 2.24 and 2.25 Taking the variation yields

$$\begin{bmatrix} Q_\theta \\ Q_\phi \end{bmatrix} = \begin{bmatrix} \int_0^L W^T f(x,t)dx \\ 0 \end{bmatrix} + bd_{31}C_{11}^D V(t) \begin{bmatrix} -\int_0^L W^T\left(\delta'\left(x-x_2\right) - \delta'\left(x-x_1\right)\right)dx \\ -\int_0^L U^T\left(\delta\left(x-x_2\right) - \delta\left(x-x_1\right)\right)dx \end{bmatrix} \qquad 2.76$$

where $\delta(x - x_1)$ denotes the Dirac delta function such that

$$\int_0^\infty f(x)\delta\left(x-x_1\right)dx = f\left(x_1\right)$$

and $\delta'(x - x_1)$ denotes the Doublet function such that

$$\int_0^\infty f(x)\delta'\left(x-x_1\right)dx = -f'\left(x_1\right).$$

Note to be careful not to confuse δ, used to describe the variation, with $\delta(x-x_0)$, which describes the Dirac delta function. Since the variational derivations are completed, the symbol δ will be used to describe the Dirac delta function in the future.

2.7.3 Active Constrained Layer Damping

The kinetic and potential energy equations for a beam with active constrained layer damping is described by equations 2.33-2.36. Applying the Lagrange equation, and using the same notation as described in Table 2.1, the following equation of motions is obtained.

$$\begin{bmatrix} \mathbf{M}_{\theta\theta} & \mathbf{M}_{\theta\phi} & \mathbf{M}_{\theta\xi} \\ \mathbf{M}_{\theta\phi}^T & \mathbf{M}_{\phi\phi} & \mathbf{M}_{\phi\xi} \\ \mathbf{M}_{\theta\xi}^T & \mathbf{M}_{\phi\xi}^T & \mathbf{M}_{\xi\xi} \end{bmatrix} \begin{bmatrix} \ddot{\theta} \\ \ddot{\phi} \\ \ddot{\xi} \end{bmatrix} + \begin{bmatrix} \mathbf{K}_{\theta\theta} & \mathbf{K}_{\theta\phi} & \mathbf{K}_{\theta\xi} \\ \mathbf{K}_{\theta\phi}^T & \mathbf{K}_{\phi\phi} & \mathbf{K}_{\phi\xi} \\ \mathbf{K}_{\theta\xi}^T & \mathbf{K}_{\phi\xi}^T & \mathbf{K}_{\xi\xi} \end{bmatrix} \begin{bmatrix} \theta \\ \phi \\ \xi \end{bmatrix} = \begin{bmatrix} Q_\theta \\ Q_\phi \\ Q_\xi \end{bmatrix} \qquad 2.77$$

where

$$\mathbf{M}_{\theta\theta} = \mathbf{M}_2^b + \mathbf{M}_3^s + \mathbf{M}_3^p \qquad \mathbf{M}_{\phi\xi} = \frac{1}{2}\left(\mathbf{M}_4^s + \mathbf{M}_4^p\right) \qquad \mathbf{K}_{\theta\xi} = \frac{1}{2}\left(\mathbf{K}_5^s + \mathbf{K}_5^p + \mathbf{K}_2^g\right)$$

$$\mathbf{M}_{\theta\phi} = \frac{1}{2}\left(\mathbf{M}_2^s + \mathbf{M}_2^p\right)^T \qquad \mathbf{M}_{\xi\xi} = \mathbf{M}_6^s + \mathbf{M}_6^p \qquad \mathbf{K}_{\phi\phi} = \mathbf{K}_1^b + \mathbf{K}_1^s + \mathbf{K}_1^p$$

$$\mathbf{M}_{\theta\xi} = \frac{1}{2}\left(\mathbf{M}_5^s + \mathbf{M}_5^p\right) \qquad \mathbf{K}_{\theta\theta} = \mathbf{K}_2^b + \mathbf{K}_3^s + \mathbf{K}_3^p + \mathbf{K}_1^g \qquad \mathbf{K}_{\phi\xi} = \frac{1}{2}\left(\mathbf{K}_4^s + \mathbf{K}_4^p\right)$$

$$\mathbf{M}_{\phi\phi} = \mathbf{M}_1^b + \mathbf{M}_1^s + \mathbf{M}_1^p \qquad \mathbf{K}_{\theta\phi} = \frac{1}{2}\left(\mathbf{K}_2^s + \mathbf{K}_2^p\right)^T \qquad \mathbf{K}_{\xi\xi} = \mathbf{K}_6^s + \mathbf{K}_6^p + \mathbf{K}_3^g$$

and the mass and stiffness matrices are defined as

$$\mathbf{M}_1^b = \langle U, U\rangle_{mb} \qquad \mathbf{M}_4^p = -2t_s\langle U, \Psi\rangle_{mp} \qquad \mathbf{K}_6^s = \left(\frac{t_s^2}{4} + \frac{I_s}{A_s}\right)\langle \Psi', \Psi'\rangle_{ks}$$

$$\mathbf{M}_2^b = \langle W, W\rangle_{mb} \qquad \mathbf{M}_5^p = t_s\left(t_b + t_p\right)\langle W', \Psi\rangle_{mp} \qquad \mathbf{K}_1^p = \langle U', U'\rangle_{kp}$$

$$\mathbf{M}_1^s = \langle U, U\rangle_{ms} \qquad \mathbf{M}_6^p = t_s^2\langle \Psi, \Psi\rangle_{mp} \qquad \mathbf{K}_2^p = \left(t_b + t_p\right)\langle U', W''\rangle_{kp}$$

$$\mathbf{M}_2^s = -t_b\langle U, W'\rangle_{ms} \qquad \mathbf{K}_1^b = \langle U', U'\rangle_{kb} \qquad \mathbf{K}_3^p = \left(\frac{\left(t_b + t_p\right)^2}{4} + \frac{C_{11}^D}{A_p}\right)\langle W'', W''\rangle_{kp}$$

$$\mathbf{M}_3^s = \frac{t_b^2}{4}\langle W', W'\rangle_{ms} + \langle W, W\rangle_{ms} \qquad \mathbf{K}_2^b = \frac{I_b}{A_b}\langle W'', W''\rangle_{kb} \qquad \mathbf{K}_4^p = -2t_s\langle U', \Psi'\rangle_{kp}$$

$$\mathbf{M}_4^s = -t_s\langle U,\Psi\rangle_{ms} \qquad \mathbf{K}_1^s = \langle U',U'\rangle_{ks} \qquad \mathbf{K}_5^p = t_s\left(t_b + t_p\right)\langle W'',\Psi'\rangle_{kp}$$

$$\mathbf{M}_5^s = \frac{t_b t_s}{2}\langle W',\Psi\rangle_{ms} \qquad \mathbf{K}_2^s = -t_b\langle U',W''\rangle_{ks} \qquad \mathbf{K}_6^p = t_s^2\langle \Psi',\Psi'\rangle_{kp}$$

$$\mathbf{M}_6^s = \frac{t_s^2}{4}\langle \Psi,\Psi\rangle_{ms} \qquad \mathbf{K}_3^s = \frac{t_b^2}{4}\langle W'',W''\rangle_{ks} \qquad \mathbf{K}_1^g = \langle W',W'\rangle_{kg}$$

$$\mathbf{M}_1^p = \langle U,U\rangle_{mp} \qquad \mathbf{K}_4^s = -t_s\langle U',\Psi'\rangle_{ks} \qquad \mathbf{K}_2^g = -\langle W',\Psi\rangle_{kg}$$

$$\mathbf{M}_2^p = -\left(t_b + t_p\right)\langle U,W'\rangle_{mp} \qquad \mathbf{K}_5^s = \frac{t_b t_s}{2}\langle W'',\Psi'\rangle_{ks} \qquad \mathbf{K}_3^g = \langle \Psi,\Psi\rangle_{kg}$$

$$\mathbf{M}_3^p = \frac{\left(t_b + t_p\right)^2}{4}\langle W',W'\rangle_{mp} + \langle W,W\rangle_{mp}$$

Again, the generalized force is obtained from taking the variation of equations 2.24 and 2.25

$$\begin{bmatrix} Q_\theta \\ Q_\phi \\ Q_\xi \end{bmatrix} = \begin{bmatrix} \int_0^L W^T f(x,t)dx \\ 0 \\ 0 \end{bmatrix} + bd_{31}C_{11}^D V(t)\begin{bmatrix} -\int_0^L W^T\left(\delta'\left(x-x_2\right)-\delta'\left(x-x_1\right)\right)dx \\ -\int_0^L U^T\left(\delta\left(x-x_2\right)-\delta\left(x-x_1\right)\right)dx \\ \int_0^L \Psi^T\left(\delta\left(x-x_2\right)-\delta\left(x-x_1\right)\right)dx \end{bmatrix} \qquad 2.78$$

Note the piezoelectric material has to apply force through the VEM, thereby creating the Q_ξ. The delta functions are the Dirac delta function and the doublet function as described in the previous section.

2.7.4 Active Damping and PCLD Treatment - Same Side of Beam

Since the active and passive elements are not in the same location, the notation from Table 2.1 is supplemented with the notation from Table 2.2. Using equations 2.37-2.42, the equation of motion for this system becomes

$$\begin{bmatrix} \mathbf{M}_{\theta\theta} & \mathbf{M}_{\theta\phi} & \mathbf{M}_{\theta\xi} \\ \mathbf{M}_{\theta\phi}^T & \mathbf{M}_{\phi\phi} & \mathbf{M}_{\phi\xi} \\ \mathbf{M}_{\theta\xi}^T & \mathbf{M}_{\phi\xi}^T & \mathbf{M}_{\xi\xi} \end{bmatrix} \begin{bmatrix} \ddot{\theta} \\ \ddot{\phi} \\ \ddot{\xi} \end{bmatrix} + \begin{bmatrix} \mathbf{K}_{\theta\theta} & \mathbf{K}_{\theta\phi} & \mathbf{K}_{\theta\xi} \\ \mathbf{K}_{\theta\phi}^T & \mathbf{K}_{\phi\phi} & \mathbf{K}_{\phi\xi} \\ \mathbf{K}_{\theta\xi}^T & \mathbf{K}_{\phi\xi}^T & \mathbf{K}_{\xi\xi} \end{bmatrix} \begin{bmatrix} \theta \\ \phi \\ \xi \end{bmatrix} = \begin{bmatrix} Q_\theta \\ Q_\phi \\ Q_\xi \end{bmatrix} \qquad 2.79$$

where

$$\mathbf{M}_{\theta\theta} = \mathbf{M}_2^b + \mathbf{M}_3^p + \mathbf{M}_3^s + \mathbf{M}_3^c \qquad \mathbf{K}_{\theta\theta} = \mathbf{K}_2^b + \mathbf{K}_3^p + \mathbf{K}_3^s + \mathbf{K}_3^c + \mathbf{K}_1^g$$

$$\mathbf{M}_{\theta\phi} = \frac{1}{2}\left(\mathbf{M}_2^p + \mathbf{M}_2^s + \mathbf{M}_2^c\right)^T \qquad \mathbf{K}_{\theta\phi} = \frac{1}{2}\left(\mathbf{K}_2^p + \mathbf{K}_2^s + \mathbf{K}_2^c\right)^T$$

$$\mathbf{M}_{\theta\xi} = \frac{1}{2}\left(\mathbf{M}_5^s + \mathbf{M}_5^c\right) \qquad \mathbf{K}_{\theta\xi} = \frac{1}{2}\left(\mathbf{K}_5^s + \mathbf{K}_5^c + \mathbf{K}_2^g\right)$$

$$\mathbf{M}_{\phi\phi} = \mathbf{M}_1^b + \mathbf{M}_1^p + \mathbf{M}_1^s + \mathbf{M}_1^c \qquad \mathbf{K}_{\phi\phi} = \mathbf{K}_1^b + \mathbf{K}_1^p + \mathbf{K}_1^s + \mathbf{K}_1^c$$

$$\mathbf{M}_{\phi\xi} = \frac{1}{2}\left(\mathbf{M}_4^s + \mathbf{M}_4^c\right) \qquad \mathbf{K}_{\phi\xi} = \frac{1}{2}\left(\mathbf{K}_4^s + \mathbf{K}_4^c\right)$$

$$\mathbf{M}_{\xi\xi} = \mathbf{M}_6^s + \mathbf{M}_6^c \qquad \mathbf{K}_{\xi\xi} = \mathbf{K}_6^s + \mathbf{K}_6^c + \mathbf{K}_3^g$$

where the mass and stiffness matrices are defined as

$$\mathbf{M}_1^b = \langle U, U \rangle_{mb}$$

$$\mathbf{M}_2^b = \langle W, W \rangle_{mb}$$

$$\mathbf{M}_1^p = \langle U, U \rangle_{mp}$$

$$\mathbf{M}_2^p = -\left(t_b + t_p\right)\langle U, W' \rangle_{mp}$$

$$\mathbf{M}_3^p = \frac{\left(t_p + t_b\right)^2}{4}\langle W', W' \rangle_{mp} + \langle W, W \rangle_{mp}$$

$$\mathbf{M}_1^s = \langle U, U \rangle_{ms}$$

$$\mathbf{M}_2^s = -t_b \langle U, W' \rangle_{ms}$$

$$\mathbf{M}_3^s = \frac{t_b^2}{4}\langle W', W' \rangle_{ms} + \langle W, W \rangle_{ms}$$

$$\mathbf{M}_3^c = \frac{\left(t_b + t_c\right)^2}{4}\langle W', W' \rangle_{mc} + \langle W, W \rangle_{mc}$$

$$\mathbf{M}_4^c = -2t_s \langle U, \Psi \rangle_{mc}$$

$$\mathbf{M}_5^c = t_s\left(t_b + t_c\right)\langle W', \Psi \rangle_{mc}$$

$$\mathbf{M}_6^c = t_s^2 \langle \Psi, \Psi \rangle_{mc}$$

$$\mathbf{K}_1^b = \langle U', U' \rangle_{kb}$$

$$\mathbf{K}_2^b = \frac{I_b}{A_b}\langle W'', W'' \rangle_{kb}$$

$$\mathbf{K}_1^p = \langle U', U' \rangle_{kp}$$

$$\mathbf{K}_2^p = -\left(t_b + t_p\right)\langle U', W'' \rangle_{kp}$$

$$\mathbf{K}_4^s = -t_s \langle U', \Psi' \rangle_{ks}$$

$$\mathbf{K}_5^s = \frac{t_b t_s}{2}\langle W'', \Psi' \rangle_{ks}$$

$$\mathbf{K}_6^s = \left(\frac{t_s^2}{4} + \frac{I_s}{A_s}\right)\langle \Psi', \Psi' \rangle_{ks}$$

$$\mathbf{K}_1^c = \langle U', U' \rangle_{kc}$$

$$\mathbf{K}_2^c = -\left(t_b + t_c\right)\langle U', W'' \rangle_{kc}$$

$$\mathbf{K}_3^c = \left(\frac{\left(t_b + t_c\right)^2}{4} + \frac{I_c}{A_c}\right)\langle W'', W'' \rangle_{kc}$$

$$\mathbf{K}_4^c = -2t_s \langle U', \Psi' \rangle_{kc}$$

$$\mathbf{K}_5^c = t_s\left(t_b + t_c\right)\langle W'', \Psi' \rangle_{kc}$$

$$\mathbf{M}_4^s = -t_s\langle U,\Psi\rangle_{ms} \qquad \mathbf{K}_3^p = \left(\frac{\left(t_b+t_p\right)^2}{4}+\frac{I_b}{A_b}\right)\langle W'',W''\rangle_{kp} \qquad \mathbf{K}_6^c = t_s^2\langle \Psi',\Psi'\rangle_{kc}$$

$$\mathbf{M}_5^s = \frac{t_b t_s}{2}\langle W',\Psi\rangle_{ms} \qquad \mathbf{K}_1^s = \langle U',U'\rangle_{ks} \qquad \mathbf{K}_1^g = \langle W',W'\rangle_{kg}$$

$$\mathbf{M}_6^s = \frac{t_s^2}{4}\langle \Psi,\Psi\rangle_{ms} \qquad \mathbf{K}_2^s = -t_b\langle U',W''\rangle_{ks} \qquad \mathbf{K}_2^g = -\langle W',\Psi\rangle_{kg}$$

$$\mathbf{M}_1^c = \langle U,U\rangle_{mc} \qquad \mathbf{K}_3^s = \frac{t_b^2}{4}\langle W'',W''\rangle_{ks} \qquad \mathbf{K}_3^g = \langle \Psi,\Psi\rangle_{kg}$$

$$\mathbf{M}_2^c = -\left(t_b+t_c\right)\langle U,W'\rangle_{mc}$$

and the generalized force is defined as

$$\begin{bmatrix} Q_\theta \\ Q_\phi \\ Q_\xi \end{bmatrix} = \begin{bmatrix} \int_0^L W^T f(x,t)dx \\ 0 \\ 0 \end{bmatrix} + bd_{31}C_{11}^D V(t)\begin{bmatrix} -\int_0^L W^T\left(\delta'\left(x-x_2\right)-\delta'\left(x-x_1\right)\right)dx \\ -\int_0^L U^T\left(\delta\left(x-x_2\right)-\delta\left(x-x_1\right)\right)dx \\ 0 \end{bmatrix} \qquad 2.80$$

Since the piezoelectric material is attached directly to the beam, its forcing function is not dependent on the shear angle as was the case for ACLD. Since the piezoelectric force is not applied through the VEM, and there is no Q_ξ.

2.7.5 Active Damping and PCLD Treatment - Opposite Side of Beam

The energy equations for a beam with an active treatment on the opposite side of the beam from the PCLD treatment use the same basic notation as the application of an active patch on the same side of the beam as the PCLD. The equations for this system are identical to section 2.7.4, except for a mass and stiffness term associated with the piezoelectric material which are given as

$$\mathbf{M}_2^p = \left(t_b + t_p\right)\langle U, W'\rangle_{mp} \qquad \mathbf{K}_2^p = \left(t_b + t_p\right)\langle U', W''\rangle_{kp}$$

Therefore, equation 2.79 with all definitions, except for the two terms given here, describe the motion of the beam. Note the sign change on the mass and stiffness terms associated with the piezoelectric element. The generalized force also has a sign change associated with it such that

$$\begin{bmatrix} Q_\theta \\ Q_\phi \\ Q_\xi \end{bmatrix} = \begin{bmatrix} \int_0^L W^T f(x,t)dx \\ 0 \\ 0 \end{bmatrix} + bd_{31}C_{11}^D V(t) \begin{bmatrix} \int_0^L W^T \left(\delta'\left(x - x_2\right) - \delta'\left(x - x_1\right)\right)dx \\ -\int_0^L U^T \left(\delta\left(x - x_2\right) - \delta\left(x - x_1\right)\right)dx \\ 0 \end{bmatrix} \qquad 2.81$$

The piezoelectric layer and the PCLD are not constrained to the same length or location. Therefore, x_2-x_1 denotes the length of the piezoelectric, and x_4-x_3 denotes the length of the PCLD.

2.7.6 Active Damping Underneath PCLD

In this case, the derivation is very similar to the PCLD treatment, except there is an additional active layer underneath the PCLD. The notation as explained in Table 2.1 is used to describe the mass and stiffness terms. Again, the equations of motion are written as

$$\begin{bmatrix} \mathbf{M}_{\theta\theta} & \mathbf{M}_{\theta\phi} & \mathbf{M}_{\theta\xi} \\ \mathbf{M}_{\theta\phi}^T & \mathbf{M}_{\phi\phi} & \mathbf{M}_{\phi\xi} \\ \mathbf{M}_{\theta\xi}^T & \mathbf{M}_{\phi\xi}^T & \mathbf{M}_{\xi\xi} \end{bmatrix} \begin{bmatrix} \ddot{\theta} \\ \ddot{\phi} \\ \ddot{\xi} \end{bmatrix} + \begin{bmatrix} \mathbf{K}_{\theta\theta} & \mathbf{K}_{\theta\phi} & \mathbf{K}_{\theta\xi} \\ \mathbf{K}_{\theta\phi}^T & \mathbf{K}_{\phi\phi} & \mathbf{K}_{\phi\xi} \\ \mathbf{K}_{\theta\xi}^T & \mathbf{K}_{\phi\xi}^T & \mathbf{K}_{\xi\xi} \end{bmatrix} \begin{bmatrix} \theta \\ \phi \\ \xi \end{bmatrix} = \begin{bmatrix} Q_\theta \\ Q_\phi \\ Q_\xi \end{bmatrix} \qquad 2.82$$

where

$$\mathbf{M}_{\theta\theta} = \mathbf{M}_2^b + \mathbf{M}_3^p + \mathbf{M}_3^s + \mathbf{M}_3^c \qquad \mathbf{M}_{\phi\xi} = \frac{1}{2}\left(\mathbf{M}_4^s + \mathbf{M}_4^c\right) \qquad \mathbf{K}_{\theta\xi} = \frac{1}{2}\left(\mathbf{K}_5^s + \mathbf{K}_5^c + \mathbf{K}_2^g\right)$$

$$\mathbf{M}_{\theta\phi} = \frac{1}{2}\left(\mathbf{M}_2^p + \mathbf{M}_2^s + \mathbf{M}_2^c\right)^T \qquad \mathbf{M}_{\xi\xi} = \mathbf{M}_6^s + \mathbf{M}_6^c \qquad \mathbf{K}_{\phi\phi} = \mathbf{K}_1^b + \mathbf{K}_1^p + \mathbf{K}_1^s + \mathbf{K}_1^c$$

$$\mathbf{M}_{\theta\xi} = \frac{1}{2}\left(\mathbf{M}_5^s + \mathbf{M}_5^c\right) \qquad \mathbf{K}_{\theta\theta} = \mathbf{K}_2^b + \mathbf{K}_3^p + \mathbf{K}_3^s + \mathbf{K}_3^c + \mathbf{K}_1^g \qquad \mathbf{K}_{\phi\xi} = \frac{1}{2}\left(\mathbf{K}_4^s + \mathbf{K}_4^c\right)$$

$$\mathbf{M}_{\phi\phi} = \mathbf{M}_1^b + \mathbf{M}_1^p + \mathbf{M}_1^s + \mathbf{M}_1^c \qquad \mathbf{K}_{\theta\phi} = \frac{1}{2}\left(\mathbf{K}_2^p + \mathbf{K}_2^s + \mathbf{K}_2^c\right)^T \qquad \mathbf{K}_{\xi\xi} = \mathbf{K}_6^s + \mathbf{K}_6^c + \mathbf{K}_3^g$$

and

$$\mathbf{M}_1^b = \langle U, U\rangle_{mb} \qquad \mathbf{M}_3^c = \frac{\left(t_n + t_c\right)^2}{4}\langle W', W'\rangle_{mc} + \langle W, W\rangle_{mc} \qquad \mathbf{K}_4^s = -t_s\langle U', \Psi'\rangle_{ks}$$

$$\mathbf{M}_2^b = \langle W, W\rangle_{mb} \qquad \mathbf{M}_4^c = -2t_s\langle U, \Psi\rangle_{mc} \qquad \mathbf{K}_5^s = \frac{t_n t_s}{2}\langle W'', \Psi'\rangle_{ks}$$

$$\mathbf{M}_1^p = \langle U, U\rangle_{mp} \qquad \mathbf{M}_5^c = t_s\left(t_n + t_c\right)\langle W', \Psi\rangle_{mc} \qquad \mathbf{K}_6^s = \left(\frac{t_s^2}{4} + \frac{I_s}{A_s}\right)\langle \Psi', \Psi'\rangle_{ks}$$

$$\mathbf{M}_2^p = -\left(t_b + t_p\right)\langle U, W'\rangle_{mp} \qquad \mathbf{M}_6^c = t_s^2\langle \Psi, \Psi\rangle_{mc} \qquad \mathbf{K}_1^c = \langle U', U'\rangle_{kc}$$

$$\mathbf{M}_3^p = \frac{\left(t_p + t_b\right)^2}{4}\langle W', W'\rangle_{mp} + \langle W, W\rangle_{mp} \qquad \mathbf{K}_1^b = \langle U', U'\rangle_{kb} \qquad \mathbf{K}_2^c = -\left(t_n + t_c\right)\langle U', W''\rangle_{kc}$$

$$\mathbf{M}_1^s = \langle U, U\rangle_{ms} \qquad \mathbf{K}_2^b = \frac{I_b}{A_b}\langle W'', W''\rangle_{kb} \qquad \mathbf{K}_3^c = \left(\frac{\left(t_n + t_c\right)^2}{4} + \frac{I_c}{A_c}\right)\langle W'', W''\rangle_{kc}$$

$$\mathbf{M}_2^s = -t_n\langle U, W'\rangle_{ms} \qquad \mathbf{K}_1^p = \langle U', U'\rangle_{kp} \qquad \mathbf{K}_4^c = -2t_s\langle U', \Psi'\rangle_{kc}$$

$$\mathbf{M}_3^s = \frac{t_n^2}{4}\langle W', W'\rangle_{ms} + \langle W, W\rangle_{ms} \qquad \mathbf{K}_2^p = -\left(t_b + t_p\right)\langle U', W''\rangle_{kp} \qquad \mathbf{K}_5^c = t_s\left(t_n + t_c\right)\langle W'', \Psi'\rangle_{kc}$$

$$\mathbf{M}_4^s = -t_s\langle U, \Psi\rangle_{ms} \qquad \mathbf{K}_3^p = \left(\frac{\left(t_b + t_p\right)^2}{4} + \frac{I_b}{A_b}\right)\langle W'', W''\rangle_{kp} \qquad \mathbf{K}_6^c = t_s^2\langle \Psi', \Psi'\rangle_{kc}$$

$$\mathbf{M}_5^s = \frac{t_n t_s}{2}\langle W', \Psi\rangle_{ms} \qquad \mathbf{K}_1^s = \langle U', U'\rangle_{ks} \qquad \mathbf{K}_1^g = \langle W', W'\rangle_{kg}$$

$$\mathbf{M}_6^s = \frac{t_s^2}{4}\langle \Psi, \Psi\rangle_{ms} \qquad \mathbf{K}_2^s = -t_n\langle U', W''\rangle_{ks} \qquad \mathbf{K}_2^g = -\langle W', \Psi\rangle_{kg}$$

$$\mathbf{M}_1^c = \langle U, U\rangle_{mc} \qquad \mathbf{K}_3^s = \frac{t_n^2}{4}\langle W'', W''\rangle_{ks} \qquad \mathbf{K}_3^g = \langle \Psi, \Psi\rangle_{kg}$$

$$\mathbf{M}_2^c = -\left(t_n + t_c\right)\langle U, W'\rangle_{mc}$$

where $t_n = t_b + 2t_p$. The forcing function is

$$\begin{bmatrix} Q_\theta \\ Q_\phi \\ Q_\xi \end{bmatrix} = \begin{bmatrix} \int_0^L W^T f(x,t)dx \\ 0 \\ 0 \end{bmatrix} + bd_{31}C_{11}^D V(t) \begin{bmatrix} -\int_0^L W^T \left(\delta'\left(x-x_2\right) - \delta'\left(x-x_1\right)\right)dx \\ -\int_0^L U^T \left(\delta\left(x-x_2\right) - \delta\left(x-x_1\right)\right)dx \\ 0 \end{bmatrix} \qquad 2.83$$

At this point general equations of motion for the different treatments are available. No mention has been made about the boundary conditions. The set of admissible displacement functions used in all equations will depend upon the boundary conditions chosen.

DAMPING MODELING METHOD

3.1 Introduction

A system which has viscoelastic damping is often modeled as having a complex modulus. However, use of the complex modulus directly in the equation of motion leads to a dynamic model useful only at single-frequency steady-state excitations. The Golla-Hughes-McTavish (GHM) modeling approach [20] provides an alternative method which includes viscoelastic damping effects without the restriction of steady-state motion by providing extra coordinates. GHM models hysteretic damping by adding additional "dissipation coordinates" to the system to achieve a linear non hysteretic model providing the same damping properties. The dissipation coordinates are used with a standard finite element approach or, as in this work, with assumed modes method. Linear second-order matrix form is maintained as well as symmetry and definiteness of the augmented system matrices. The time domain stress relaxation is modeled by a modulus function in the Laplace domain.

3.2 Golla-Hughes-McTavish Damping Model

The derivation of the GHM equations starts with the constitutive relation for a one-dimensional stress-strain system using the theory of linear viscoelasticity [62].

$$\sigma(t) = G(t)\varepsilon(0) + \int_0^t G(t-\tau)\frac{d}{d\tau}\varepsilon(\tau)d\tau \qquad 3.1$$

where σ is the stress. It is assumed that the strain, ε, is zero for all time less than zero, and $G(t)$ is defined as a material relaxation function. The stress relaxation function represents the energy loss of the material, which is damping. The strain, ε, is restricted to

be zero for all time less than or equal to zero. In other words, the system is at static equilibrium at time $t = 0$. Taking the Laplace transform of equation 3.1 yields

$$\sigma(s) = sG(s)\varepsilon(s). \tag{3.2}$$

where s is the Laplace domain operator. If the material modulus function, $sG(s)$, is evaluated along the imaginary axis of the s-plane, in other words in the frequency domain, the result is the complex modulus, $G^*(\omega)$,

$$G^*(\omega) \equiv j\omega G(j\omega) = G'(\omega) + jG''(\omega). \tag{3.3}$$

The real part of the complex modulus is known as the storage modulus, and the imaginary part as the loss modulus. This complex modulus is the standard representation of viscoelastic damping and models the viscoelastic effect in steady state at a single frequency, ω. In this approach, the loss factor, η, is defined as

$$\eta(\omega) = \frac{G''(\omega)}{G'(\omega)} \tag{3.4}$$

which is the ratio of energy dissipated to the energy stored. In steady state, the loss factor η can be related to the standard damping ration ζ by $\eta = 2\zeta$. However, this equivalence of models is only valid at a single frequency, giving rise to the phrase "frequency dependent damping" often associated with VEM. The usefulness of this concept is that steady state experiments can be performed on material components to generate $\eta(\omega)$. Unfortunately $\eta(\omega)$ is not useful by itself in predicting transient or broad band responses of viscoelastic systems.

The GHM method used here provides a convenient connection between the steady state characteristics of VEM's through $\eta(\omega)$ measurements. A dynamic model is obtained which useful in calculating the transient response.

The GHM method approximates the viscoelastic properties as a series of mini-oscillators (see Fig. 3.1). Therefore, the complex modulus can be written in Laplace domain as

$$G^*(s) = G_0(1+h(s)) = G_0\left(1+\sum_{n=1}^{k}\hat{\alpha}_n \frac{s^2+2\hat{\zeta}_n\hat{\omega}_n s}{s^2+2\hat{\zeta}_n\hat{\omega}_n s+\hat{\omega}_n^2}\right) \qquad 3.5$$

where G_0 is the modulus of elasticity, and the hatted terms are obtained from the curve fit to the complex modulus data for a particular viscoelastic material. The expansion of $h(s)$ represents the material modulus as a series of mini-oscillators (second order) terms [20]. The number of terms kept in the expansion will be determined by the high or low frequency dependence of the complex modulus. In many cases only two to four terms are necessary.

The equation of motion, for a system which uses a complex shear modulus to describe damping, in the Laplace domain is

$$\mathbf{M}\left(s^2\mathbf{x}(s) - s\mathbf{x}_0 - \dot{\mathbf{x}}_0\right) + \mathbf{K}(s)\mathbf{x}(s) = \mathbf{F}(s) \qquad 3.6$$

where **M** is the mass matrix, **K** the complex stiffness matrix, **F** the forcing function, and $\mathbf{x}_0$ and $\dot{\mathbf{x}}_0$ the initial conditions. The mass and stiffness matrices and the forcing vector are obtained from equations of motion as derived in chapter 2. The complex stiffness matrix can be written as the summation of the contributions of the *n* complex moduli to the stiffness matrix such that

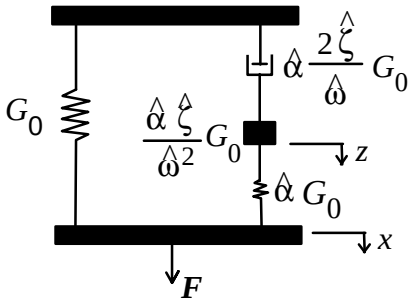

Figure 3. 1 Mini-oscillator used in GHM method

$$\mathbf{K}(s) = \left(G_1^*(s)\overline{\mathbf{K}}_1 + G_2^*(s)\overline{\mathbf{K}}_2 + \cdots + G_n^*(s)\overline{\mathbf{K}}_n\right) \tag{3.7}$$

where G_n^* refers to the n^{th} complex modulus and $\overline{\mathbf{K}}_n$ to the contribution of the n^{th} modulus to the stiffness matrix. For simplicity, assume a complex modulus model with a single expansion term and zero initial conditions, so equation 3.6 can be written as

$$\mathbf{M}s^2\mathbf{x}(s) + G_0\left(1 + \hat{\alpha}\frac{s^2 + 2\hat{\zeta}\hat{\omega}s}{s^2 + 2\hat{\zeta}\hat{\omega}s + \hat{\omega}^2}\right)\overline{\mathbf{K}}(s)\mathbf{x}(s) = \mathbf{F}(s) \tag{3.8}$$

Comparing equations 3.5 and 3.8 we find that

$$h(s) = \hat{\alpha}\frac{s^2 + 2\hat{\zeta}\hat{\omega}s}{s^2 + 2\hat{\zeta}\hat{\omega}s + \hat{\omega}^2} \tag{3.9}$$

In other words, the GHM method adds two zeros, at $s = 0$ and $s = -2\hat{\zeta}\hat{\omega}$, and two poles at $s = \dfrac{-2\hat{\zeta}\hat{\omega} \pm j2\hat{\omega}\sqrt{\hat{\zeta}^2 - 1}}{2}$. Figure 3.2 is a root locus diagram of $1 + \hat{\alpha}h(s)$ for arbitrary values of $\hat{\alpha}$, $\hat{\zeta}$, and $\hat{\omega}$.

By introducing a vector of dissipation coordinates, **z**, defined as

$$\mathbf{z}(s) = \frac{\hat{\omega}^2}{s^2 + 2\varsigma\hat{\omega}s + \hat{\omega}^2}\mathbf{x}(s),$$

equation 3.8 can be separated into two equations such that

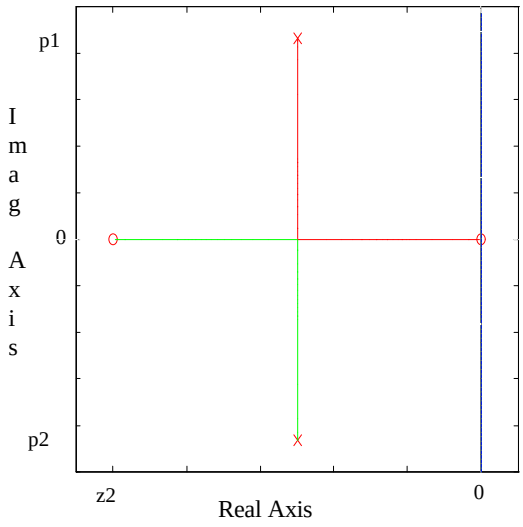

Figure 3. 2 Root locus diagram of $1+\hat{\alpha}h(s)$

$$\mathbf{M}s^2\mathbf{x}(s) + G_0(1+\hat{\alpha})\overline{\mathbf{K}}(s)\mathbf{x}(s) - G_0\hat{\alpha}\mathbf{z}(s) = \mathbf{F}(s) \tag{3.10}$$

and

$$\mathbf{0} = \frac{\hat{\alpha}}{\hat{\omega}^2}s^2\mathbf{z}(s) + \frac{2\hat{\zeta}\hat{\omega}}{\hat{\omega}}s\mathbf{z}(s) + \hat{\alpha}\mathbf{z}(s) - \hat{\alpha}\mathbf{x}(s) \tag{3.11}$$

Such added degrees of freedom are also called internal variables. Equation 3.11 can be multiplied by G_0, and the following equation of motion can be assembled

$$\begin{bmatrix} \mathbf{M} & \mathbf{0} \\ \mathbf{0} & \frac{\hat{\alpha}}{\hat{\omega}^2}G_0\overline{\mathbf{K}} \end{bmatrix}\begin{bmatrix} \mathbf{x}(s) \\ \mathbf{z}(s) \end{bmatrix}s^2 + \begin{bmatrix} \mathbf{0} & \mathbf{0} \\ \mathbf{0} & \frac{2\hat{\alpha}\hat{\zeta}}{\hat{\omega}}G_0\overline{\mathbf{K}} \end{bmatrix}\begin{bmatrix} \mathbf{x}(s) \\ \mathbf{z}(s) \end{bmatrix}s + \tag{3.12}$$

$$\begin{bmatrix} (1+\hat{\alpha})G_0\overline{\mathbf{K}} & -\hat{\alpha}G_0\overline{\mathbf{K}} \\ -\hat{\alpha}G_0\overline{\mathbf{K}} & \hat{\alpha}G_0\overline{\mathbf{K}} \end{bmatrix}\begin{bmatrix} \mathbf{x}(s) \\ \mathbf{z}(s) \end{bmatrix} = \begin{bmatrix} \mathbf{F}(s) \\ \mathbf{0} \end{bmatrix}$$

This is the final form of the Golla-Hughes-McTavish model as described by McTavish and Hughes [20]. Note that the mass, damping and stiffness matrices remain symmetric.

One problem with this form of the GHM equations is the possible creation of an ill-conditioned mass matrix. The magnitude of the dissipation coordinates can be many orders different from the state coordinates. In these cases, it may be advantageous to write equation 3.12 as

$$\begin{bmatrix} \mathbf{M} & \mathbf{0} \\ \mathbf{0} & \dfrac{\hat{\alpha}}{\hat{\omega}^2} G_0 \mathbf{I} \end{bmatrix} \begin{bmatrix} \mathbf{x}(s) \\ \mathbf{z}(s) \end{bmatrix} s^2 + \begin{bmatrix} \mathbf{0} & \mathbf{0} \\ \mathbf{0} & \dfrac{2\hat{\alpha}\hat{\zeta}}{\hat{\omega}} G_0 \mathbf{I} \end{bmatrix} \begin{bmatrix} \mathbf{x}(s) \\ \mathbf{z}(s) \end{bmatrix} s +$$
$$\begin{bmatrix} (1+\hat{\alpha}) G_0 \overline{\mathbf{K}} & -\hat{\alpha} G_0 \overline{\mathbf{K}} \\ -\hat{\alpha} G_0 \mathbf{I} & \hat{\alpha} G_0 \mathbf{I} \end{bmatrix} \begin{bmatrix} \mathbf{x}(s) \\ \mathbf{z}(s) \end{bmatrix} = \begin{bmatrix} \mathbf{F}(s) \\ \mathbf{0} \end{bmatrix} \qquad 3.13$$

In this case, the system looses symmetry of the stiffness matrix. However, if state space methods are used to analyze the model, this loss of symmetry is not as important as the reduced risk of an ill-conditioned mass matrix.

The GHM terms, $\hat{\alpha}$, $\hat{\zeta}$, and $\hat{\omega}$, are obtained by curve-fitting the parameters to actual data of the shear modulus. Data curves of the storage modulus and loss factor versus temperature and displacement are available from manufacturers such as 3M [68].

In order to model the behavior of the viscoelastic material which partially covers a beam, the stiffness and mass matrices for the covered area are first assembled. The effects of the dissipation modes on the system are calculated as described above. The full mass and stiffness matrices for the whole beam are assembled, using the mass, damping and stiffness matrices obtained from equation 3.12 or 3.13, to model the effects of the viscoelastic material on the whole structure. The order of the system increases as the number of terms in the expansion are kept, which increases the accuracy for modeling the damping effects. The number of elastic modes of the stiffness matrix also increases the order of the system, i.e. for every elastic mode there is a dissipation mode. It is also possible to use the GHM method to model different materials for each VEM element, i.e. different stiffness properties over each segment of beam.

3.3 Internally Balanced Model Reduction

One major disadvantage in using GHM to model the damping of the VEM is the creation of additional dissipation coordinates. The order of the system quickly increases as the number of oscillators used in the summation is increased. This size is determined by the nature of the loss factor versus frequency curve. It is therefore advantageous to look at model reduction to reduce the system to its original size.

The standard reduction method used in finite element codes is Guyan's reduction which removes some "insignificant" physical coordinates. Specific coordinates can be removed and new symmetric mass and stiffness matrices are obtained. Guyan's reduction does not allow damping and therefore can not be used on a model which includes GHM damping. In balanced reduction, the states to be removed are dynamically chosen. This method does not allow a choice of states to be reduced, but chooses them by examining the dynamics. There is also a loss of symmetry. Yae and Inman [64] combine a balancing method with a Guyan type reduction. Balancing is used to compute the states to be removed, and then a transformation is developed so that the desired states can be removed. By using the internal balancing method, the reduced system can be expressed in terms of the original states. In other words, when GHM is used to model damping, the internal balancing method removes the dissipation states but retain the damping so that the original states now fully model the damping effects.

In order to employ the internally balanced model reduction, the damping matrix must be proportional. When using GHM, the damping matrix is not proportional, and it is therefore necessary to add some structural damping. Next, the system needs to be converted into the state space form, such that

$$\dot{\mathbf{x}} = \mathbf{A}\mathbf{x} + \mathbf{B}\mathbf{u} \tag{3.14}$$

where $\mathbf{A} = \begin{bmatrix} \mathbf{0} & \mathbf{I} \\ -\mathbf{M}^{-1}\mathbf{K} & -\mathbf{M}^{-1}\mathbf{D} \end{bmatrix}$ is defined as the state matrix, $\mathbf{B} = \begin{bmatrix} \mathbf{0} \\ \mathbf{M}^{-1} \end{bmatrix}$ the input matrix, **x** the state vector, and **u** the input vector. The mass, **M**, damping, **D**, and stiffness, **K**, matrices include the effects of damping via the GHM modeling approach. The measured states are defined in output equation

$$\mathbf{y} = \mathbf{C}\mathbf{x} \tag{3.15}$$

where **C** defines the choice of outputs.

In order to use the model reduction method, the system must be controllable and observable. In other words, the controllability test matrix and the observability test matrix must be full rank, where the controllability and observability test matrices are defined as

$$\mathbf{U}_c = \begin{bmatrix} \mathbf{B} & \mathbf{AB} & \cdots & \mathbf{A}^{2n-1}\mathbf{B} \end{bmatrix} \quad \text{and} \quad \mathbf{U}_o = \begin{bmatrix} \mathbf{C} \\ \mathbf{CA} \\ \vdots \\ \mathbf{CA}^{2n-1} \end{bmatrix} \tag{3.16}$$

respectively. If *n* is the size of the second-order matrix equation, defined in equation 3.12 or 3.13, and the controllability and observability test matrices are full rank if the rank is 2*n*.

The issue of controllability and observability is crucial for the internal balanced model reduction. The observability and controllability of each state is examined. The internal balanced model reduction method then removes those states which least affect the response.

If the system is controllable and observable and the state matrix is asymptotically stable, the controllability grammian, $\mathbf{W}_c$, and observability grammian, $\mathbf{W}_o$, are defined as

$$\mathbf{W}_c = \int_0^\infty e^{\mathbf{A}t}\mathbf{B}\mathbf{B}^T e^{\mathbf{A}^T t}dt \tag{3.17}$$

and

$$\mathbf{W}_o = \int_0^\infty e^{\mathbf{A}^T t}\mathbf{C}^T\mathbf{C}e^{\mathbf{A}t}dt \tag{3.18}$$

where $e^{\mathbf{A}t}$ is the matrix exponential function. These grammians provide a measure of the controllability and observability of the structure, given its inputs and outputs. $\mathbf{W}_c$ and $\mathbf{W}_o$ are unique semi-positive definite matrices which satisfy the Lyapunov matrix equations given by

$$\mathbf{A}\mathbf{W}_c + \mathbf{W}_c\mathbf{A}^T = -\mathbf{B}\mathbf{B}^T \tag{3.19}$$

$$\mathbf{A}^T\mathbf{W}_o + \mathbf{W}_o\mathbf{A} = -\mathbf{C}^T\mathbf{C} \tag{3.20}$$

The objective of the balanced model reduction method is to find a system where the controllability and observability grammians are equal and diagonal. This is achieved through transformation matrix, **P**, such that equations 3.14 and 3.15 can be written as

$$\begin{aligned}\dot{\hat{\mathbf{x}}} &= \hat{\mathbf{A}}\hat{\mathbf{x}} + \hat{\mathbf{B}}\mathbf{u}\\ \mathbf{y} &= \hat{\mathbf{C}}\hat{\mathbf{x}}\end{aligned} \tag{3.21}$$

where $\hat{\mathbf{A}} = \mathbf{P}^{-1}\mathbf{A}\mathbf{P}$, $\hat{\mathbf{B}} = \mathbf{P}^{-1}\mathbf{B}$, $\hat{\mathbf{C}} = \mathbf{C}\mathbf{P}$, and $\hat{\mathbf{x}} = \mathbf{P}^{-1}\mathbf{x}$. Equation 3.21 is the balanced model. The transformation matrix is obtained through a method developed by Laub [65].

Given the controllability and observability grammians calculated using equations 3.19 and 3.20, the lower triangular form of controllability grammian, using Cholesky decomposition for example, is found such that

$$\mathbf{W}_c = \mathbf{L}_c\mathbf{L}_c^T. \tag{3.22}$$

Next, **H** is defined as

$$\mathbf{H} = \mathbf{L}_c^T\mathbf{W}_o\mathbf{L}_c \tag{3.23}$$

The eigenvalues, Λ, and eigenvectors, **U**, of **H** are found such that

$$\mathbf{U}^T\mathbf{H}\mathbf{U} = \Lambda^2 \tag{3.24}$$

The transformation matrix, **P**, which transforms the system into the balanced coordinate system, is

$$\mathbf{P} = \mathbf{L}_c\mathbf{U}\left((\Lambda)^{1/2}\right)^{-1/2} \tag{3.25}$$

The balanced system, described in equation 3.21, can now be partitioned such that

$$\begin{bmatrix} \dot{\hat{\mathbf{x}}}_r \\ \dot{\hat{\mathbf{x}}}_d \end{bmatrix} = \begin{bmatrix} \hat{\mathbf{A}}_{11} & \hat{\mathbf{A}}_{12} \\ \hat{\mathbf{A}}_{21} & \hat{\mathbf{A}}_{22} \end{bmatrix} \begin{bmatrix} \hat{\mathbf{x}}_r \\ \hat{\mathbf{x}}_d \end{bmatrix} + \begin{bmatrix} \hat{\mathbf{B}}_r \\ \hat{\mathbf{B}}_d \end{bmatrix} \mathbf{u} \qquad 3.26$$

$$\mathbf{y} = \begin{bmatrix} \hat{\mathbf{C}}_r & \hat{\mathbf{C}}_d \end{bmatrix} \begin{bmatrix} \hat{\mathbf{x}}_r \\ \hat{\mathbf{x}}_d \end{bmatrix}$$

where the subscript *r* denotes those states which are retained, and *d* those states which are deleted. The system is reduced to the original size by deleting the appropriate columns and rows from the transformation and state matrices. Assume there are *k* states which are to be eliminated. First, the rows consisting of *k* coordinates to be eliminated are deleted, in this case the dissipation states. Next, the last *k* columns of **P** are removed, to form a reduced transformation matrix, $\mathbf{P}_r$. These *k* columns represent the least controllable states. In other words, the internal balancing method allows the elimination of the dissipation states, keeping only the physical states. Reduced balanced state matrices are obtained from the balanced state matrices by eliminating the last *k* columns and/or rows, creating $\hat{\mathbf{A}}_r$, $\hat{\mathbf{B}}_r$, and $\hat{\mathbf{C}}_r$. The order of these matrices is 2*n* - *k*. The reduced balanced system can now be transformed back to the reduced state space form such that

$$\begin{aligned} \dot{\mathbf{x}}_r &= \mathbf{A}_r \mathbf{x}_r + \mathbf{B}_r \mathbf{u} \\ \mathbf{y} &= \mathbf{C}_r \mathbf{x}_r \end{aligned} \qquad 3.27$$

where $\mathbf{A}_r = \mathbf{P}_r \hat{\mathbf{A}}_r \mathbf{P}_r^{-1}$, $\mathbf{B}_r = \mathbf{P}_r \hat{\mathbf{B}}_r$, $\mathbf{C} = \hat{\mathbf{C}}_r \mathbf{P}_r^{-1}$, and $\mathbf{x} = \mathbf{P}\hat{\mathbf{x}}_r$. This is the reduced model as described by Yae and Inman [64].

3.4 Experimental Verification of the GHM Damping Model

In order to verify the accuracy of the GHM model, an experiment is performed on a fully covered, free-free aluminum beam. The dimensions of the beam are 0.381 m long, 0.0381 m wide and 0.0032 m thick (15 × 1.5 × 0.125 in.). It is suspended from the ceiling with

fish wire which is attached 0.0254 m from either end. The beam is excited using an impact hammer, applied at the center of the beam. The accelerometer is placed on the other side of the beam also in the center. A Tektronix 2630 Fourier Analyzer is used which does all the data acquisition as well as the computations of the FFT, transfer functions and coherence functions. Figure 3.3 is a diagram of the experimental setup. The placement of the impact and sensor is chosen to minimize excitation of the torsional modes and to excite only one rigid body mode, swinging back and forth. The constraining layer is a beam the same dimensions as the base beam, thus creating a sandwich beam. The beam is tested with 0.127 mm (5 mil) and 0.254 mm (10 mil) thick 3M ISD 112 VEM [66]. This is done to insure that the GHM model accounted for the increase in damping with the increase in thickness of the VEM. Due to the placement of the sensor, only the odd modes are observable.

A calibration test is performed on the hammer and accelerometer in order to account for the calibration constant. The accelerometer is attached to a large mass, in this case an aluminum block about the size of a brick, weighting 6.34 kg (13.94 lb). The large mass minimizes excitation of modes other than the rigid body mode. The hammer is used to input an impulse into the system, and acceleration data is collected by the accelerometer. In theory, the transfer function is a straight line and the calibration constant, H_{calib}, is

$$H_{calib} = \frac{1}{M_c} \tag{3.28}$$

where M_c is the mass of the block. This is rarely the case, and an error constant, H_{error}, is introduced, such that

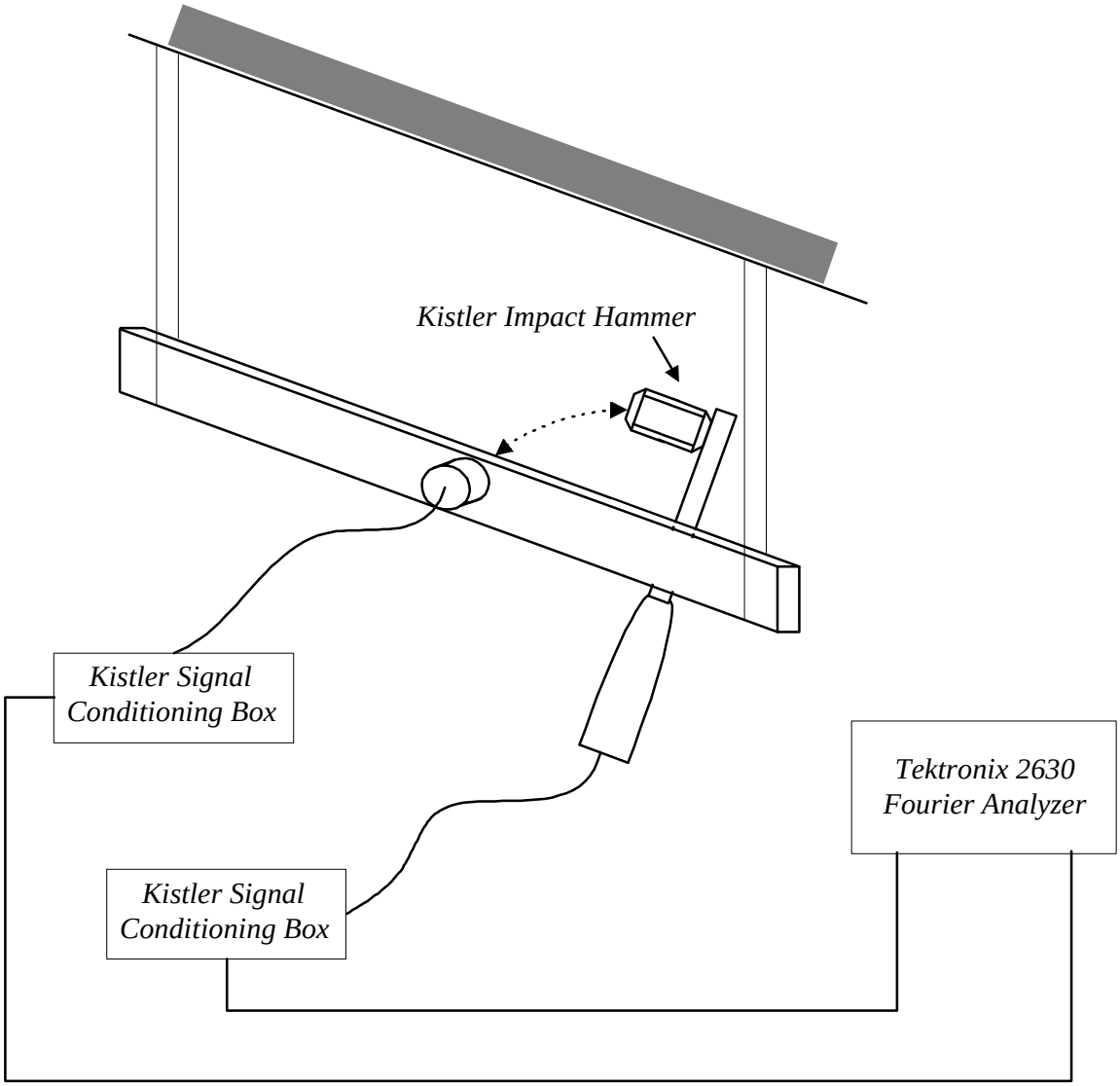

Figure 3. 3 Test Equipment and Beam

$$H_{calib} = H_{error} \frac{1}{M_c} \tag{3.29}$$

Figure 3.4 is the plot of the transfer function between accelerometer and the impulse hammer. Note the spike at 60 Hz, which is due to electrical noise. The calibration constant is 0.15, and the error constant is calculated using equation 3.29 and found to be 0.95.

Figures 3.5 and 3.6 show the acceleration bode plots for the experimental (dash-dot) and the analytical (solid) transfer functions. In Fig. 3.5 the thickness of the VEM is 0.127 mm (5 mil), while in Fig. 3.6 the thickness is increased to 0.254 mm (10 mil). The units of the magnitude curves are g/N. As can be seen on both figures, there is good correlation in both the magnitude and phase for the first and third mode. There is 10% difference between the experimental and analytical peak magnitude for the first mode and only a 3 % difference in magnitude for the second mode. The correlation starts to break down for the fifth mode. This is due to the fact that the accelerometer was attached to the beam using wax. The accurate data range for wax is about 0 - 2000 Hz [67].

The GHM model includes three summations in the expansion of the material properties. Using the data provided by 3M [68], the constants were found to be $G_0 = 5 \times 10^4$, $\hat{\alpha} = [9.6 \quad 99.1 \quad 26.2]$, $\hat{\zeta} = [73.4 \quad 1.1 \quad 3.28]$, and $\hat{\omega} = [1 \quad 2 \quad 0.5] \times 10^4$. The curve fit for the storage and loss modulus is shown in Fig. 3.7. It was necessary to include three terms to assure that the damping was modeled accurately over the full frequency range of interest.

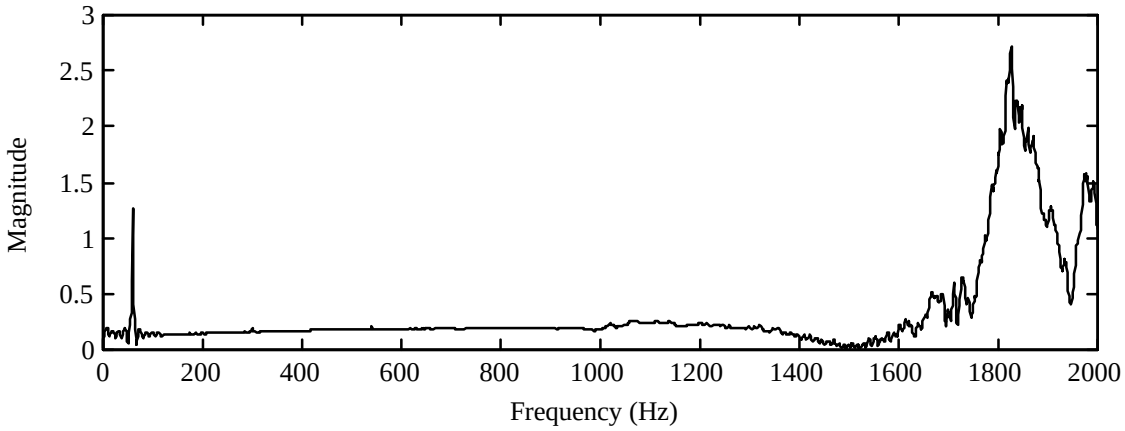

Figure 3. 4 Calibration Transfer Function

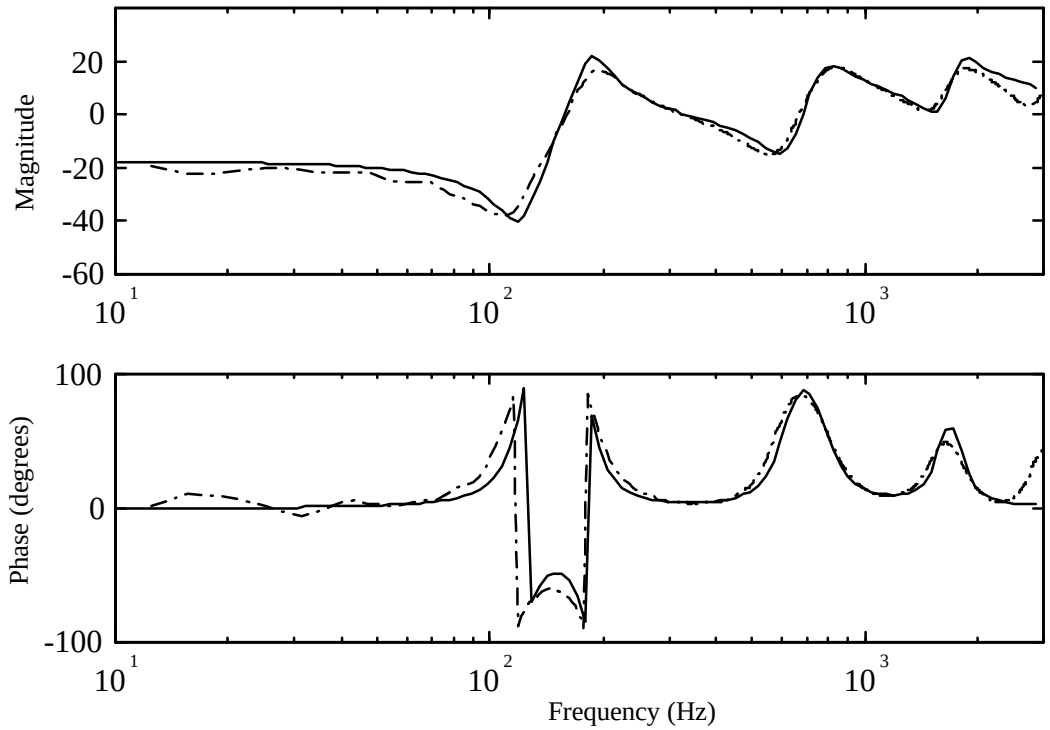

Figure 3. 5 Transfer Functions for 5 mil ISD 112 with 3 mini-oscillators
(solid = theoretical, dash-dot = experimental)

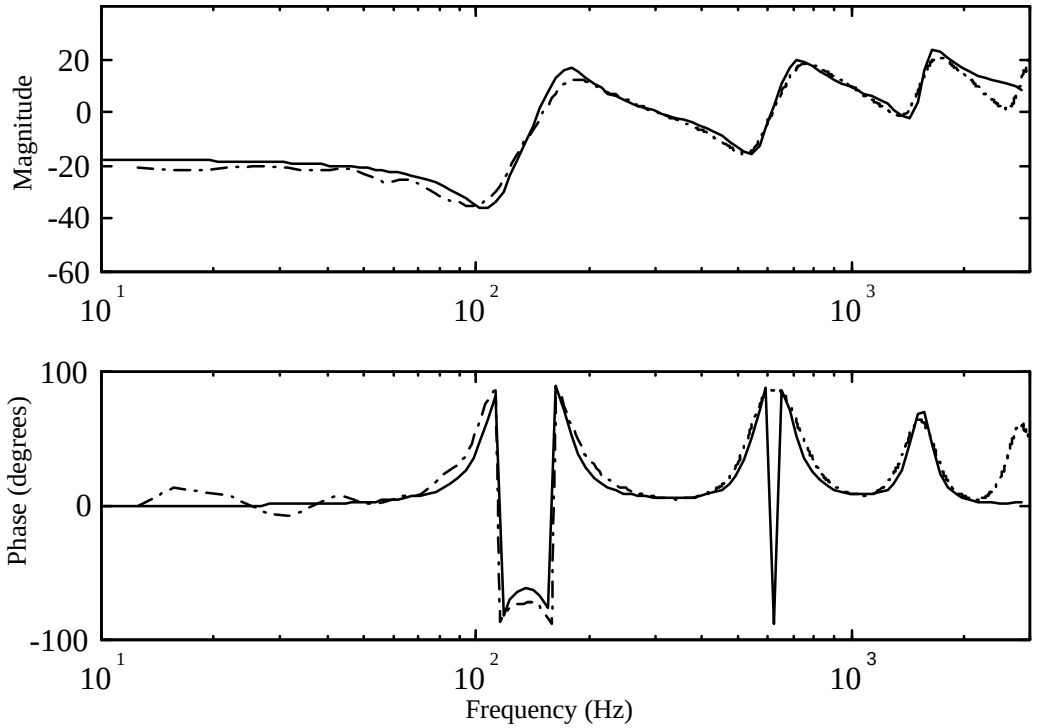

Figure 3. 6 Transfer Functions for 10 mil ISD 112 with 3 mini-oscillators
(solid = theoretical, dash-dot = experimental)

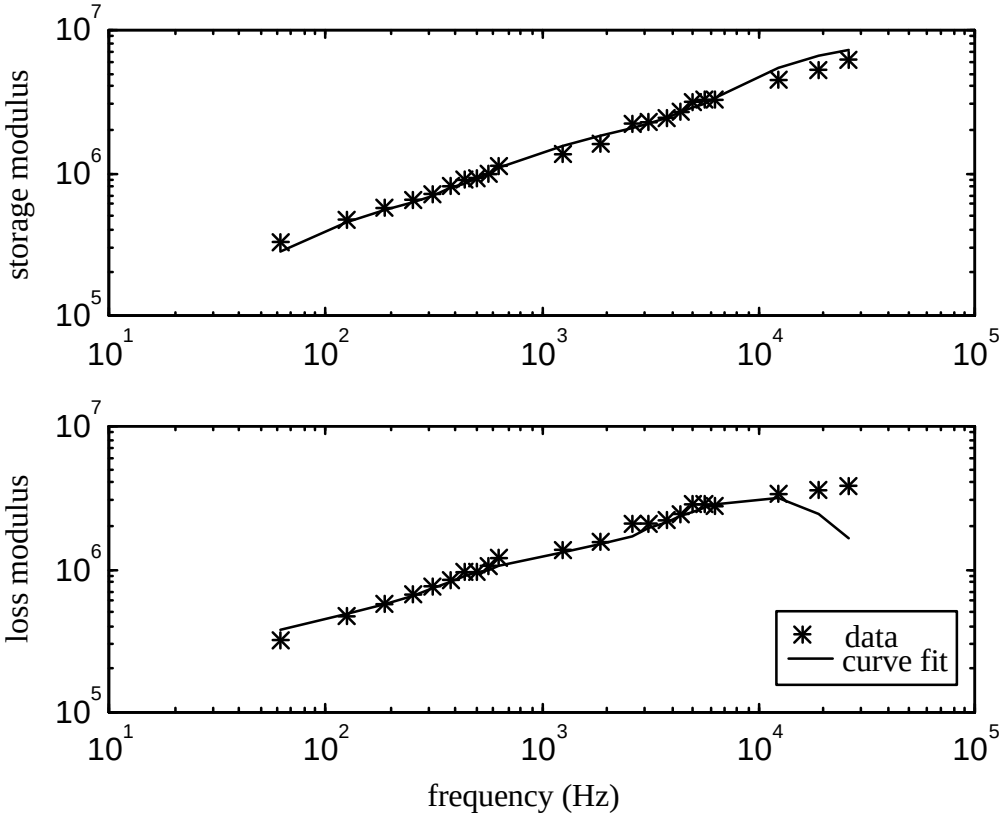

Figure 3. 7 Curve fit for GHM parameters

CONTROL LAW DEVELOPMENT & OPTIMIZATION

4.1 Introduction

Previous work in controlling the piezoelectric material has involved proportional (P) and proportional plus derivative (PD) controllers, as well as linear quadratic regulators (LQR). For beams with ACLD, Baz ([30], [36]), Azvine et al. [34], Lesieutre et al. [52], and Shen [31] used P and PD controllers while Liao and Wang [33] used LQR. Veley and Rao [46] addresses both PD and LQR control, but only shows results for PD. LQR control is used in this work to suppress vibration.

One drawback of LQR is that all states must be known in order to control the vibration of the structure. Since it is not always possible to obtain all states, output feedback will also be used to control the vibration.

The issue of optimal placement of the active, passive and hybrid damping treatment is addressed. Most of the work in passive and active control has optimized the thickness of the treatment ([11], [12], [27]). Here, the optimal thickness for constraining layer is assumed, while the PZT thickness is arbitrarily chosen from known thicknesses. Equal thickness of base layer and constraining layer should be used to maximize passive damping. It is usually desirable to have a constraining layer that is as stiff as possible without exceeding the stiffness of the base structure [68]. One way to achieve this is to use a constraining layer that is the same thickness and material as the base beam. The length of treatment is optimized using several different criteria: vibration suppression performance and required control effort, as well as settling time and overshoot of the output and control force.

4.2 Linear Quadratic Regulator

The control will be implemented using a linear quadratic regulator [69]. The control output is a linear combination of the states, such that

$$\mathbf{u} = -\mathbf{K}_c\mathbf{x} \tag{4.1}$$

Here **u** is the input vector, **x** is the state vector and $\mathbf{K}_c$ is the gain matrix. Equation 4.1 assumes full state feedback. The cost function used to determine the gain matrix is given as

$$J_{LQR} = \int_0^\infty \left(\mathbf{y}^T\mathbf{Q}\mathbf{y} + \mathbf{u}^T\mathbf{R}\mathbf{u}\right)dt \tag{4.2}$$

where **y** is the output vector, and **Q** and **R** are semi-positive definite and positive definite weighting functions, respectively. Increasing gain **Q** will give more vibration suppression on the output, while increasing gain **R** signifies greater limit on the control effort. The gain matrix is defined as

$$\mathbf{K}_c = \mathbf{R}^{-1}\mathbf{B}^T\mathbf{P} \tag{4.3}$$

where **P** satisfies the Ricatti equation

$$\mathbf{P}\mathbf{A} + \mathbf{A}^T\mathbf{P} - \mathbf{P}\mathbf{B}\mathbf{R}^{-1}\mathbf{B}^T\mathbf{P} = -\mathbf{Q}\,. \tag{4.4}$$

Recall that **A** is the state matrix and **B** the input matrix.

4.3 Output Feedback

Linear quadratic regulators assume that all states of the system are known. Since this is unlikely, a control scheme is developed which uses only the output as feedback [70]. First, the system is written in state space, such that

$$\dot{\mathbf{x}} = \mathbf{A}\mathbf{x} + \mathbf{B}\mathbf{u} \tag{4.5}$$

where **A** is the state matrix, **B** the input matrix, **x** the state vector and **u** the input vector. The output is measured as

$$\mathbf{y} = \mathbf{C}\mathbf{x} \tag{4.6}$$

where **C** is the output matrix which identifies the states to be measured, and **y** is the output vector. Linear quadratic regulators assume the all states are known and fed back (equation 4.1). However, if only the output is known, then equation 4.1 becomes

$$\mathbf{u}_o = \mathbf{K}_o\mathbf{y} = \mathbf{K}_o\mathbf{C}\mathbf{x} \tag{4.7}$$

where $\mathbf{K}_o$ is the gain matrix for output feedback. The state equation, equation 4.5 becomes

$$\begin{aligned} \dot{\mathbf{x}} &= \mathbf{A}\mathbf{x} + \mathbf{B}\mathbf{K}_o\mathbf{C}\mathbf{x} \\ &= \left(\mathbf{A} + \mathbf{B}\mathbf{K}_o\mathbf{C}\right)\mathbf{x} = \mathbf{A}_c\mathbf{x} \end{aligned} \tag{4.8}$$

where $\mathbf{A}_c$ is the new state matrix which incorporates output feedback. Now define the function

$$\phi = \left[\mathbf{u}_o - \mathbf{u}\right]^T \left[\mathbf{u}_o - \mathbf{u}\right] \tag{4.9}$$

where **u** is the input obtained by using full state feedback and defined in equation 4.1. The minimum ϕ with respect to the gain matrix, $\mathbf{K}_o$, is determined by setting $\frac{\partial \phi}{\partial \mathbf{K}_o} = 0$ and solving for $\mathbf{K}_o$, such that

$$\mathbf{K}_o = \left[\mathbf{y}^T \mathbf{y}\right]^{-1} \mathbf{y}^T \mathbf{u} \tag{4.10}$$

The least squares approximation for the solution of the output feedback gain matrix is obtained [76].

4.4 Optimization Criteria

There are many different schemes to optimize the treatment for active, passive and hybrid damping. Section 4.2 derives the optimal cost function for an active system, using LQR control. To obtain further insight, the following functions are defined.

$$J_{VS} = \int_0^\infty \mathbf{y}_a^T \mathbf{y}_a dt \tag{4.11}$$

and

$$J_{CE} = \int_0^\infty \mathbf{u}^T \mathbf{u} dt \tag{4.12}$$

Here J_{VS} represents the vibration suppression and J_{CE} represents the control effort. The active output is denoted by $\mathbf{y}_a$. Lower values of J_{VS} and J_{CE} indicate better performance. In order to maximize the passive vibration suppression, $J_{passive}$ is defined as

$$J_{passive} = \int_0^\infty \mathbf{y}_p^T \mathbf{y}_p dt \tag{4.13}$$

where $\mathbf{y}_p$ is the passive response. Again, lower values of the cost function, $J_{passive}$, indicates more vibration suppression.

If the system has a limited range of motion, it is important to look at the overshoot of the output. One example of a system with limited movement is the payload inside the cargo bay on the shuttle. On the other hand, if the system has solar panels, for example the Hubble space telescope or any satellite, it is important to limit the settling time of the output. The overshoot is defined as the maximum displacement of the output or

$$OS_{output} = \max\left(\mathbf{y}(t)\right). \tag{4.14}$$

Traditionally, the settling time uses two percent criteria, or

$$t_{s_y} = \frac{3}{\varsigma_y \omega_y} \tag{4.15}$$

where ζ_y is the damping ratio and ω_y the natural frequency of the output. This definition of the settling time depends on the overshoot of the output. Recall that the damping ratio of the overshoot can be found directly from the output through $OS_{output} = e^{\zeta\pi/\sqrt{1-\varsigma^2}}$. A lower settling time can therefore be achieved by increasing the overshoot. In this work, the settling time is defined as the time in which the system reaches some ε, where ε is a small value. This means that the individual settling times are not directly dependent on the overshoot and can be compared directly to each other. An example is described to clarify

this principle. Imagine a beam which has an overshoot of 10 and a 2% settling time of 2 sec. According to 2% settling time criteria, the vibration is within 2% if it is less than 0.2 for all time greater than the settling time. If a comparison is made with a system whose overshoot is 0.15 with a 2% settling time of 4 sec, it is assumed that the first configuration settles more quickly. However, the second system never reaches the value of 0.2, and is therefore more desirable.

For some systems, it is important to look more closely at the required voltage. When using power supplies, peak magnitude of the voltage may have to be limited. It is also desirable to limit the duration of the voltage applied. The equation for the overshoot of the voltage, assuming LQR control, is given as

$$OS_{voltage} = \max\left(-K_c \mathbf{x}(t)\right) \tag{4.16}$$

and again, traditionally the settling time is

$$t_{s_v} = \frac{3}{\varsigma_v \omega_v}. \tag{4.17}$$

However, the same concerns are valid here as with the output. Therefore a small value, ε, will be chosen to find the minimum settling time for each configuration.

NUMERIC SIMULATIONS OF HYBRID DAMPING TREATMENTS

5.1 Introduction

The equations of motion for beams with different damping treatments are derived in Chapter 2. They include a beam with a piezoelectric element (PZT), passive constrained layer damping (PCLD), active constrained layer damping (ACLD), placing the PZT under the PCLD and two new hybrid treatments. The hybrid treatments separate the active and passive elements. In one variation, the piezoelectric element is on the same side as the passive treatment, while the other variation allows the piezoelectric element to be on the opposite side of the beam. The damping effect of the viscoelastic material (VEM) is modeled using Golla-Hughes-McTavish (GHM) by adding dissipation coordinates as outlined in Chapter 3. Model reduction will be used to reduce the equations of motion to the original size. In this chapter, the equations of motion as derived in Chapter 2 are used to numerically simulate the response of a cantilevered beam. The effects of the different treatments is reported given different optimization criteria. A linear quadratic regulator and output feedback are used to control vibration. The optimization criteria and control schemes are derived in chapter 4.

First, the settling time of the response is investigated. It can be important to minimize the settling time of structures, as exemplified by the Hubble Space Telescope. Unwanted vibration induced by a thermal snap caused vibration which lasted most of the thermal cycle before the next temperature change induced new vibrations. In order to obtain data from the telescope, it was important to reduce the settling time of the vibrations to a minimum value. Section 5.3.1 explores the settling time of the passive response, while section 5.3.2 discusses the settling time of the active response. The settling time of the passive response is defined as the time when the response remains within 0.01 mm. When

the active response remains within 0.0001 mm, the active settling time has been reached. The settling time of the control force indicates the duration of the control and is discussed in section 5.3.3. This value indicates the length the power source is active, and the settling time is reached when the response remains within 0.01 V.

In some cases, such as confined spaces like the payload in a cargo bay, it may be important to minimize the maximum overshoot of the response. Equations 4.14 and 4.16 define the maximum overshoot of the output and control force, respectively. In section 5.3.4, the overshoot of the passive response is studied. Section 5.3.5 addresses the overshoot of active response, while section 5.3.6 addresses the overshoot of the control force. Depending on the power source, the magnitude of the control force may be an important factor in the control of vibration.

In order to obtain further insight into vibration suppression, equations 4.11 and 4.13 define an active and passive vibration suppression index, respectively. Section 5.3.7 investigates vibration suppression of the passive response, and section 5.3.8 addresses vibration suppression of the active response. The control effort index is defined in equation 4.12, and the minimum values are addressed in section 5.3.9. Finally, the minimum values of the LQR cost function are addressed in section 5.3.10. Technically, the integration is performed from zero to infinity. However, since there is no response after a certain time, the integration is only performed over a limited range.

5.2 Dimensions and Properties of Materials

An aluminum cantilevered beam is considered and the VEM is assumed to be ISD 112 [68]. The dimensions for the piezoelectric material (PZT), VEM, cover plate and beam are chosen based on easily available materials. The material properties and dimensions of the beam, PZT, VEM and constraining layer are given in Table 5.1. The

Table 5. 1 System Parameters

L	0.381 m (15 in.)	d_{31}	-109×10^{-12}
b	0.038 m (1.5 in.)	t_s	0.13 mm (5 mil)
t_b	0.0032 m (0.125 in.)	ρ_s	1000 kg/m^3
ρ_b	2710 kg/m^3	E_s	14×10^6 Pa
E_b	70×10^9 Pa	G_0	5×10^4
t_p	0.5 mm (0.02 in.)	$\hat{\alpha}$	[9.6 99.1 26.2]
ρ_p	7600 kg/m^3	$\hat{\zeta}$	[73.4 1.1 3.28]
E_p	6.3×10^{10} Pa	$\hat{\omega}$	$[1\ 5\ 0.5] \times 10^4$

electromechanical properties of the piezoelectric material are given in [73]. The properties of the VEM include the GHM damping terms, which were determined in section 3.4. Three GHM mini-oscillators are included. The constraining layer is assumed to be aluminum with the same thickness as the beam. Equal thickness of base layer and constraining layer should be used to maximize passive damping. It is usually desirable to have a constraining layer that is as stiff as possible without exceeding the stiffness of the base structure [70]. The minimal length for any treatment is set at 1 cm. Since neither the PCLD nor the PZT can be clamped, the constraint on its placement is 1 mm from the base. In the case where the active and passive treatments are separated but placed on the same side of the beam, a 1 mm space is assumed between treatments. The respective equations of motion for the different treatments are discretized using a five term expansion [74]. The excitation force is an impulse applied at $0.9L$, where L is the length of the base beam. The transverse displacement is measured at the tip.

A linear quadratic regulator (LQR) approach (equations 4.1-4.4) is used to model the effects of the PZT. The weighting matrix, $\mathbf{Q}$, is $10^{10}\mathbf{I}$ for the transverse modes, and zeros for all others. The weighting function, $\mathbf{R}$, is assumed to be 1. Since there is no VEM damping associated with a beam with PZT, only optimization results for the active response or control force will be reported.

The geometry of the different treatments are given in chapter 2. Figure 2.1 depicts the geometry of a beam with PCLD treatment. The geometry of a beam with PZT and ACLD are shown in Fig. 2.3 and Fig. 2.4, respectively. Figure 2.5 shows the geometry of a beam with PZT and PCLD on the same side of the beam, while Fig. 2.6 allows the PCLD and PZT to be placed on opposite sides of the beam. Figure 2.7 shows the geometry of a beam with the PZT mounted on the beam and the PCLD mounted on top of the PZT.

5.3 Optimization Results

5.3.1 Minimum Settling Time of Passive Response

The time responses for tip displacements for optimal treatment lengths, in the transverse direction of a clamped aluminum beam with the different treatments is shown in Fig. 5.1. The optimal lengths and placements of the different treatments, as well as the minimum settling times can be found in Table 5.2. The optimal length for PCLD is 24.5 cm with treatment starting 1 mm from the base of the beam. The settling time is 0.23 sec and the tip displacement is shown in Fig. 5.1(a). The optimal length of ACLD is 23.8 cm, with a settling time of 1.19 sec. The tip displacement is shown in Fig. 5.1(b). When the PZT is placed on the same side as the PCLD, the optimal length of the PZT and PCLD are 1 cm and 24.5 cm, respectively. The PCLD is placed 1 mm from the root and the PZT is placed directly after, or 24.7 cm from the base of the beam. The optimal settling time is 0.23 sec, and the time response is shown in Fig. 5.1(c). When the PZT is placed on the opposite side of the beam, the optimal length of the PZT and PCLD are 9 cm and 26 cm, respectively. Both treatments are placed 1 mm from the root, and the optimal settling time is 0.20 sec. Figure 5.1(d) shows the time response for this configuration. When placing the PZT underneath the PCLD, the optimal length of treatment is 23.6 cm, placed 1 mm from the base of the beam. The optimal settling time is 0.21 sec and Fig. 5.1(e) shows the time response for this configuration.

PCLD is an effective method to settle the system. Note that ACLD treatment is the least effective. It has both the longest settling time and the highest overshoot. The use of PZT as a constraining layer does not add enough stiffness to the system [70]. Placing the PZT and PCLD on the same side of the beam is not as effective as pure PCLD. In fact, the treatment tries to be PCLD by placing a long PCLD at the root, and making the active element as short as possible. The most effective treatment is to place the PZT on the

Table 5. 2 Minimum Values for Passive Response Settling Time for Different Treatments

	L_{pzt} (m)	Loc_{pzt} (m)	L_{pcld} (m)	Loc_{pcld} (m)	ts_y (sec)
PCLD			0.245	0.001	0.2314
ACLD	0.238	0.001	0.238	0.001	1.1890
PZT/PCLD same side	0.010	0.247	0.245	0.001	0.2330
PZT/PCLD opposite	0.090	0.001	0.260	0.001	0.2020
PZT under PCLD	0.236	0.001	0.236	0.001	0.2132

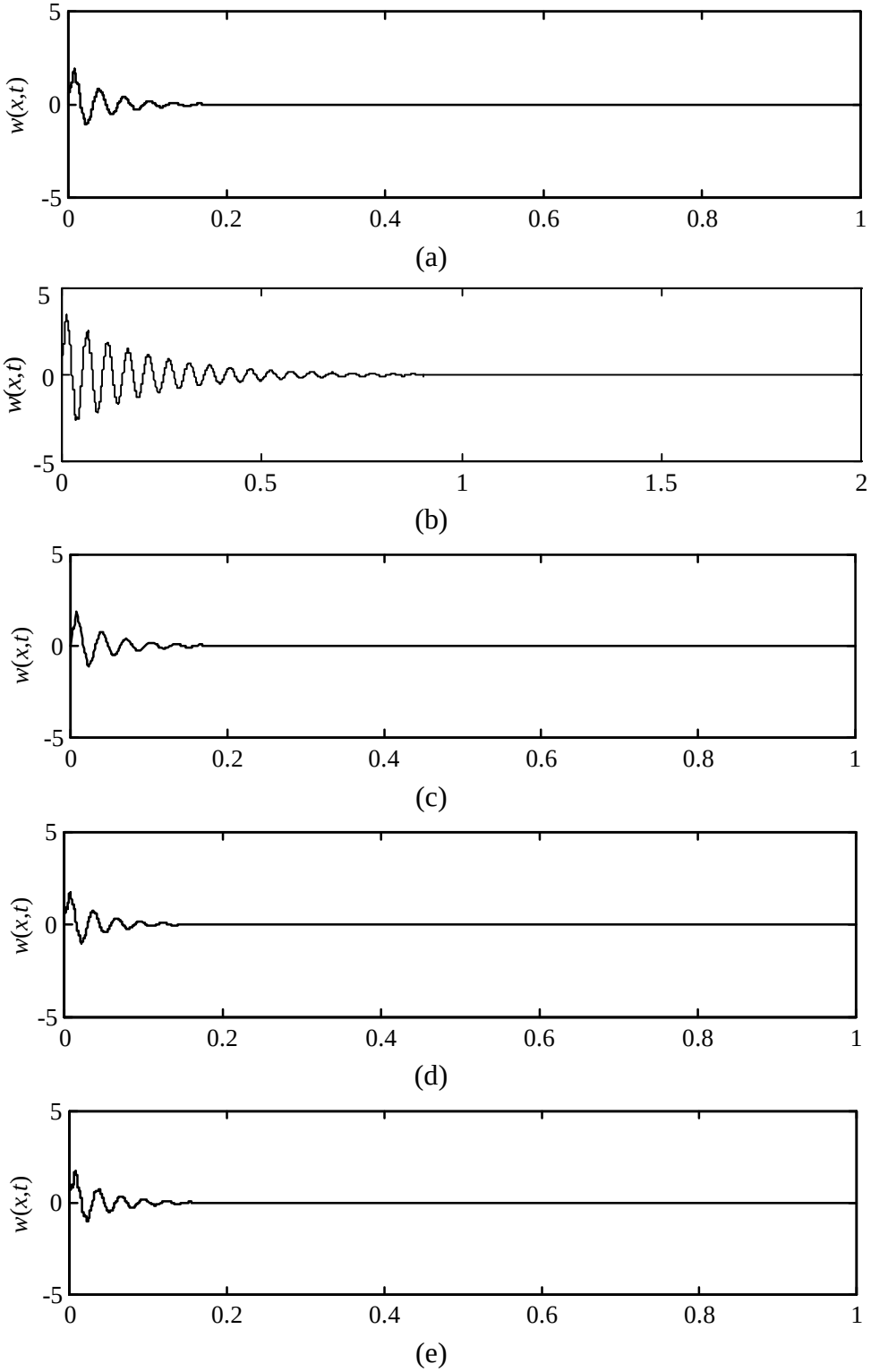

Figure 5. 1 Tip Displacement (mm) vs Time (sec) for Optimal Passive Settling Time: a) PCLD, b) ACLD, c) PZT Same Side, d) PZT Opposite Side, e) PZT Under

opposite side of the beam, as seen in Fig. 5.1(d). However, since the opposite surface is not always available for treatment, a suitable alternative places the PZT underneath the PCLD.

5.3.2 Minimum Settling Time of Active Response

In this section, the optimal configurations to minimize the settling time of the active response are investigated. Figure 5.2 shows the passive time responses for tip displacement in the transverse direction of a clamped aluminum beam with the different treatments. Figure 5.3 shows the active time responses, and Fig. 5.4 the control force needed to achieve these active time responses. The optimal lengths and placements of the different treatments, as well as the minimum active response settling times can be found in Table 5.3. The optimal length for a PZT is 12.7 cm, placed 9.2 cm from the root of the beam. This gives an active response settling time of 0.60 sec. The optimal length of ACLD is 25.1 cm, placed 3.6 cm from the root, giving an active response settling time of 0.18 sec. Placing the PZT and PCLD on the same side, a settling time of 0.20 sec can be achieved by placing a 13.6 cm long PZT at the root, and a 13.9 cm long PCLD 13.8 cm from the root. By allowing the PZT and PCLD to be placed on opposite sides of the beam, an active response settling time of 0.16 sec can be achieved. The PZT must be 28 cm long, placed at the root, and the PCLD must be 23.4 cm long, also placed at the root. When placing the PZT underneath the PCLD, the optimal treatment length is 24 cm, where the active response settling time is 0.23 sec.

The passive and active tip displacements are shown in Fig. 5.2 and Fig. 5.3, respectively. The control force response is shown in Fig. 5.4. Since the PZT does not have any inherent passive damping, only the active tip displacement and control force are shown in Fig. 5.3(a) and 5.4(a), respectively. As can be seen both in the Fig. 5.3(a), Fig. 5.4(a), and Table 5.3, the active response settling time and the control force settling time take the longest to settle. The active response overshoot is also the largest in magnitude. The

Table 5. 3 Minimum Values of Active Response Settling Time for Different Treatments

	L_{pzt} (m)	Loc_{pzt} (m)	L_{pcld} (m)	Loc_{pcld} (m)	ts_{yn} (sec)
PZT	0.127	0.092			0.600
ACLD	0.251	0.036	0.251	0.036	0.184
PZT/PCLD same side	0.136	0.001	0.139	0.138	0.198
PZT/PCLD opposite	0.280	0.001	0.234	0.001	0.158
PZT under PCLD	0.240	0.001	0.240	0.001	0.230

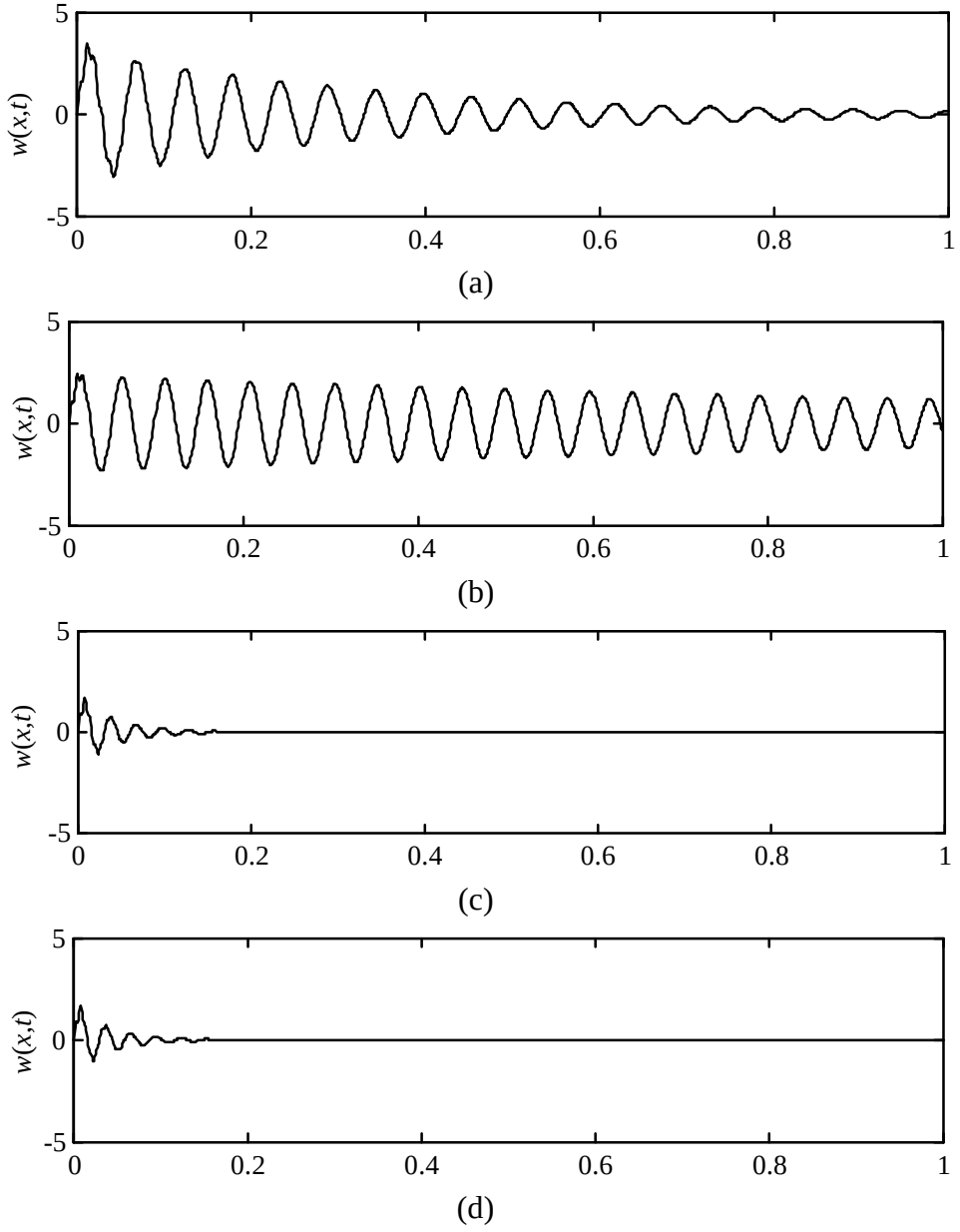

Figure 5. 2 Passive Tip Displacement (mm) vs Time (sec) for Optimal Active Settling Time: a) ACLD, b) PZT Same Side, c) PZT Opposite, d) PZT Under

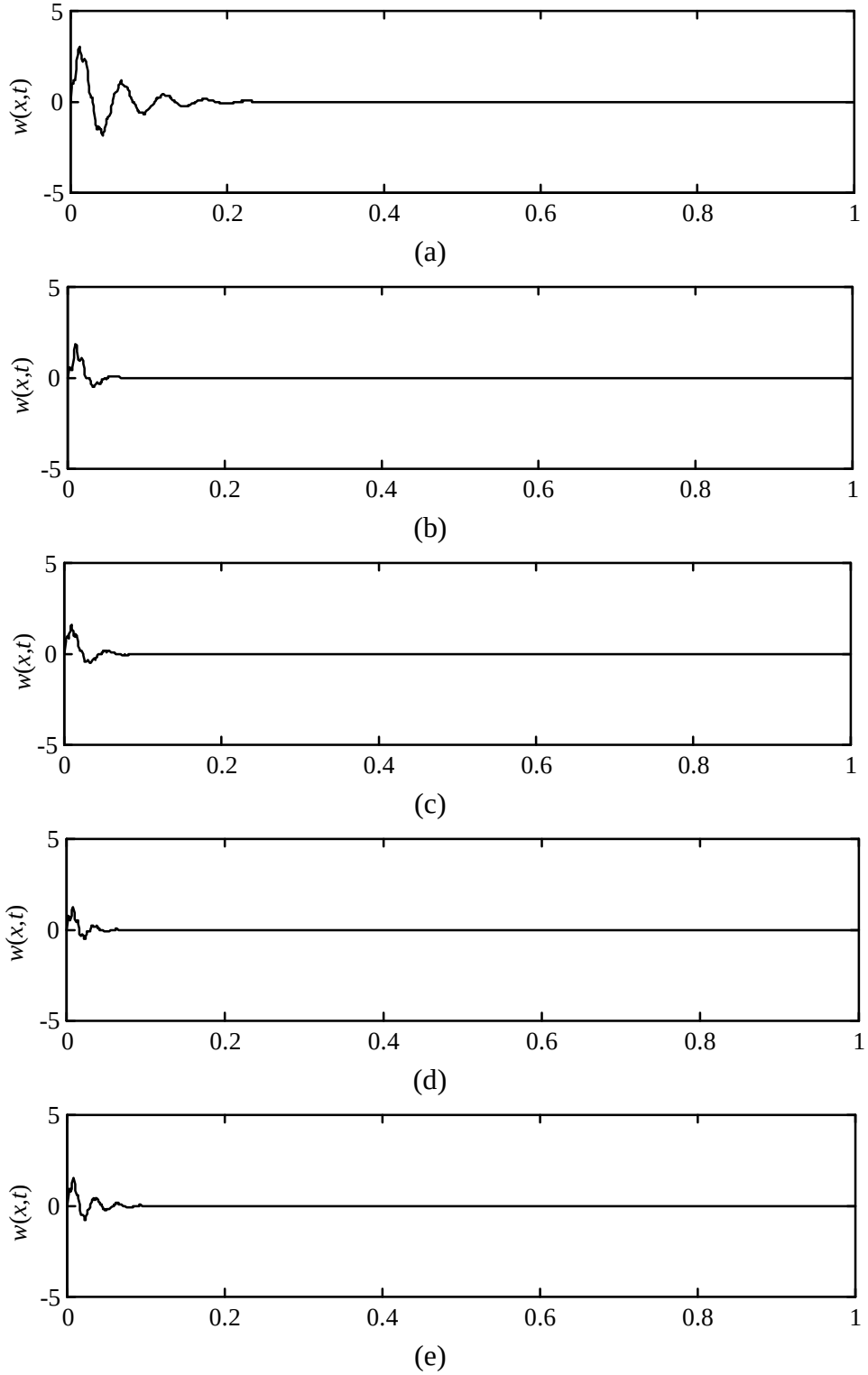

Figure 5. 3 Active Tip Displacement (mm) vs Time (sec) for Optimal Active Settling Time: a) PZT, b) ACLD, c) PZT Same Side, d) PZT Opposite Side, e) PZT Under

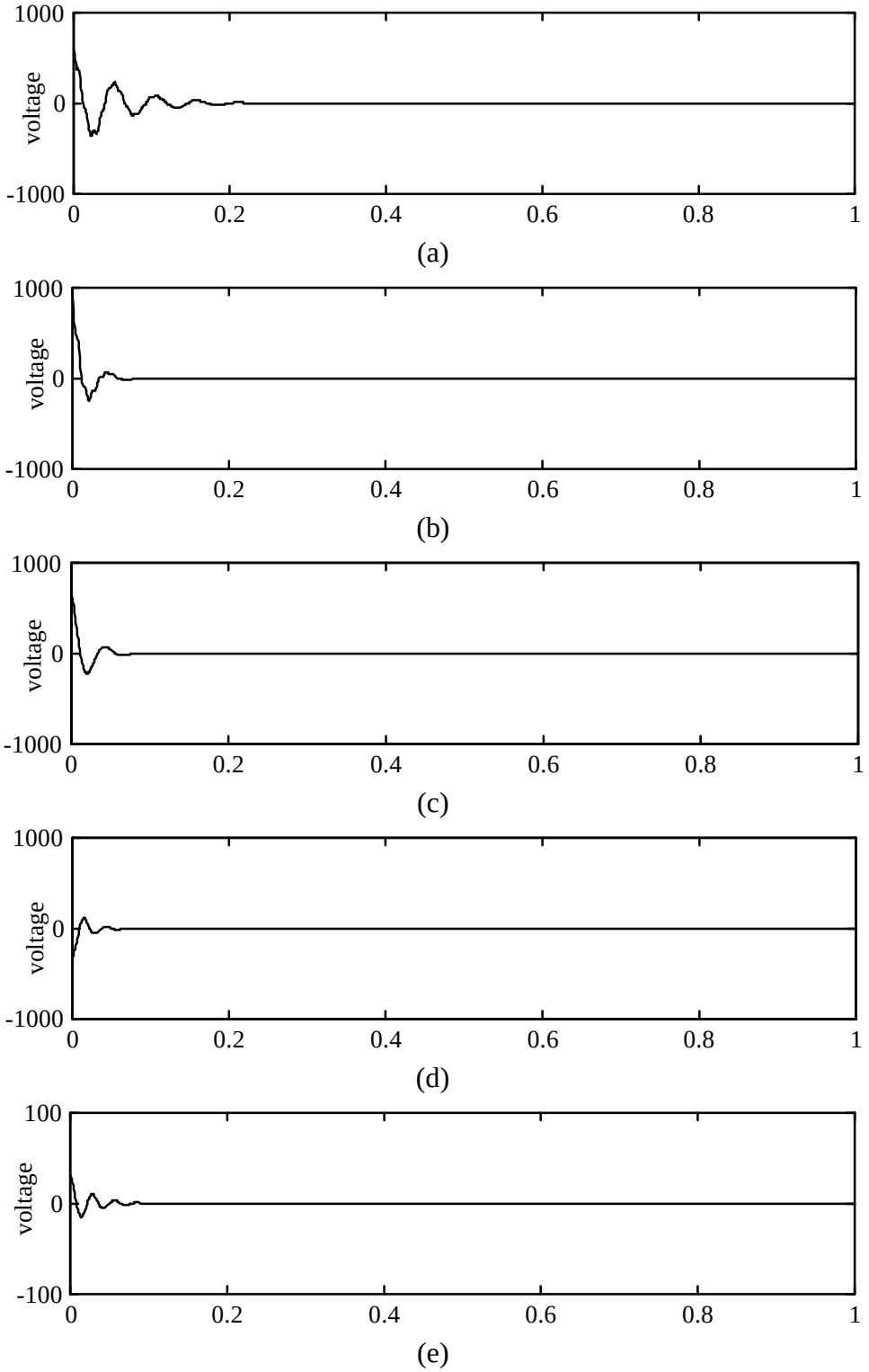

Figure 5. 4 Control Force (V) vs Time (sec) for Optimal Active Settling Time: a) PZT, b) ACLD, c) PZT Same Side, d) PZT Opposite Side, e) PZT Under

passive response of ACLD is shown in Fig. 5.2(a). While the PZT is does not add enough stiffness to the structure when used as a constraining layer, the response is better than placing the PZT and PCLD on the same side of the beam. Since the PCLD is placed 13.8 cm from the root, it does not add enough vibration suppression to the structure. This can be seen in Fig. 5.2(b). The active tip displacement for ACLD is shown in Fig. 5.3(b), with the control force response needed to achieve the active tip response reported in Fig. 5.4(b). Note that the ACLD needs the largest control force in order to achieve an active settling time of 0.18 sec, since the PZT is actuating through the VEM. The active tip displacement and control force response of placing the PZT and PCLD on the same side of the beam is reported in Fig. 5.3(c) and 5.4(c), respectively. The settling time is slightly larger than ACLD, but it takes less control force. ACLD is still preferable, due to the active damping capabilities. Placing the PZT on the opposite side gives the optimal active response settling time. The passive and active tip displacements for this configuration are shown in Fig. 5.2(c) and 5.3(d), respectively. The control force response required is shown in Fig. 5.4(d). Note that this case gives the minimum active and passive overshoot as well as the smallest active response settling time. If the opposite surface is not available for treatment, a good alternative is to place the PZT underneath the PCLD. Here a slight increase in the active response settling time is reported, as can be seen in Fig. 5.3(e). However, it takes much less control effort as seen in Fig. 5.4(e) (note the scale on the axis).

5.3.3 Minimum Settling Time of Control Force

The minimum settling time of the control force response is investigated in this section. The optimal lengths of treatment are reported in Table 5.4. The passive and active tip displacements are shown in Fig. 5.5 and 5.6, respectively. Figure 5.7 shows the control force response. Again, since the PZT does not have inherent passive damping, only the active response and control force are reported. The optimal length for a PZT is 12.7 cm, placed 9.4 cm from the root of the beam. The settling time of the control force is 0.64 sec. An optimal ACLD is 24 cm long and is placed 3.6 cm from the root. The

corresponding settling time is 0.20 cm. Placing the PCLD and PZT on the same side gives an optimal control force settling time of 0.16 sec. This corresponds to a 29.9 cm long PCLD placed at the root, and a 1 cm long PZT placed directly after. By allowing the PZT and PCLD to be placed on opposite sides, the optimal settling time is 0.18 sec. This is achieved by using a 22.5 cm long PZT and 23 cm long PCLD. Both are placed at the root. Placing the PZT underneath the PCLD gives a control force settling time of 25.8 sec where the treatment length is 22.5 cm.

The active tip displacement and control force response for an optimal PZT are shown in Fig. 5.6(a) and Fig. 5.7(a). Note that this configuration gives the highest overshoot of the active response and takes the longest to settle. The passive response for optimal ACLD is shown in Fig. 5.5(a). Again, the passive response is has significant overshoot and takes the longest time to settle, since the PZT is not stiff enough to be an effective constraining layer. The active tip displacement and the control force are shown in Fig. 5.6(b) and 5.6(c). Since the PZT is actuating through a VEM, the control force needed has the largest overshoot. The optimal case is achieved by placing the PZT and PCLD on the same side of the beam. The passive tip displacement is shown in Fig. 5.5(b). Figures 5.6(c) and 5.7(c) show the active tip displacement and the control force, respectively. In other words, the treatment is trying to simulate PCLD. The PZT is only 1 cm long and can not effect the vibration since it is 30.1 cm from the base of the beam. The hybrid treatment is trying to emulate pure passive damping. This is shown by the fact that the PZT is only 1 cm long and is placed 30.1 cm from the root. When comparing Fig. 5.5(b) and 5.6(c), it can be seen that there is no improvement in the active tip displacement when compared to the passive tip displacement. Although this configuration does not have any active control, it is preferable to using PZT only. When comparing Fig. 5.6(a) and 5.6(c), it is seen that the overshoot and settling time of the response of the hybrid treatment is less. However, since the control has not effect, it is not considered a valid configuration. Therefore, allowing the PZT and PCLD to be placed on opposite sides of

Table 5. 4 Minimum Values of Control Force Settling Time for Different Treatments

	L_{pzt} (m)	Loc_{pzt} (m)	L_{pcld} (m)	Loc_{pcld} (m)	ts_{un} (sec)
PZT	0.127	0.094			0.640
ACLD	0.240	0.036	0.240	0.036	0.198
PZT/PCLD same side	0.010	0.301	0.299	0.001	0.163
PZT/PCLD opposite	0.225	0.001	0.230	0.001	0.176
PZT under PCLD	0.225	0.001	0.225	0.001	0.258

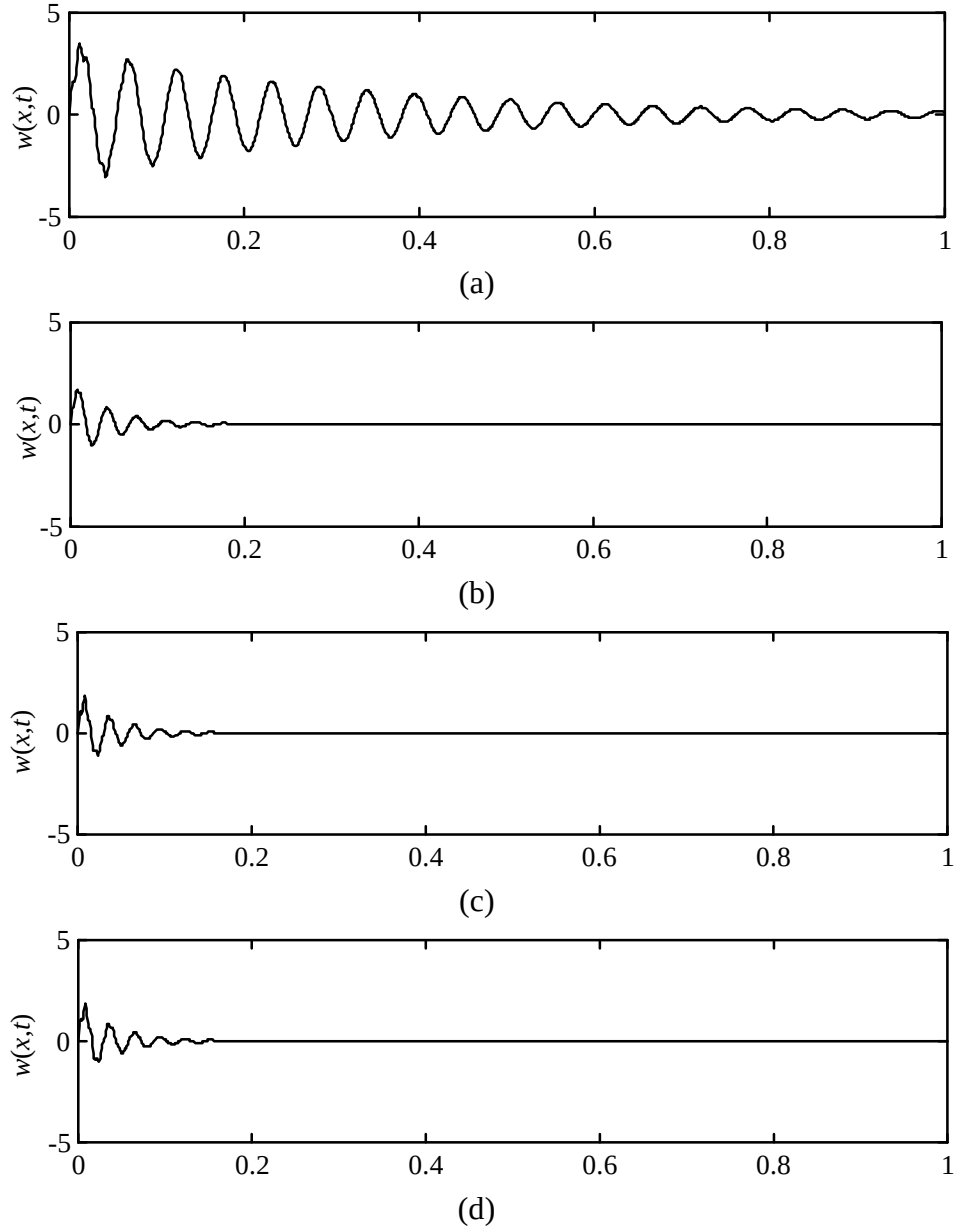

Figure 5. 5 Passive Tip Displacement (mm) vs Time (sec) for Optimal Control Force Settling Time: a) ACLD, b) PZT Same Side, c) PZT Opposite, d) PZT Under

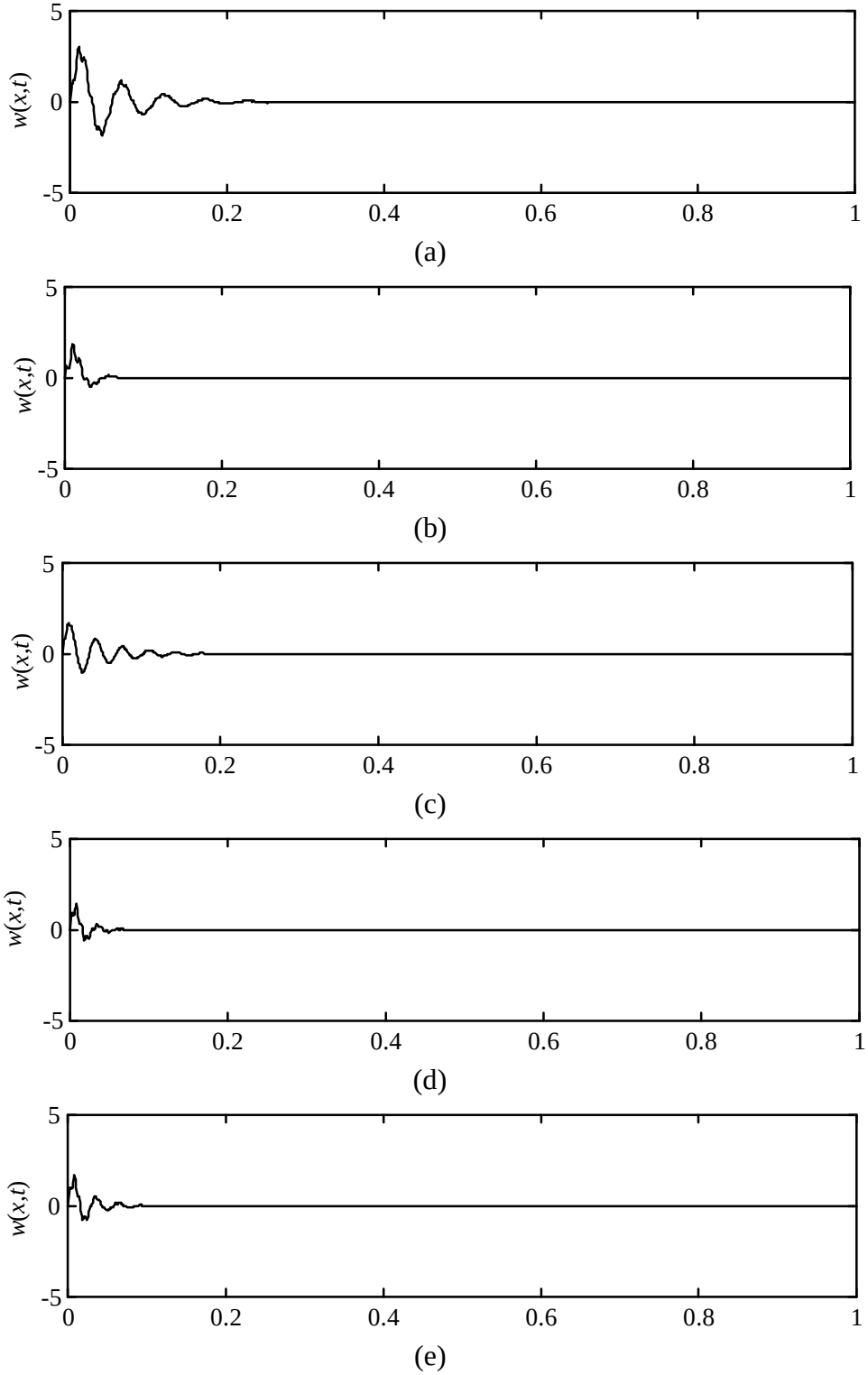

Figure 5. 6 Active Tip Displacement (mm) vs Time (sec) for Optimal Control Force Settling Time: a) PZT, b) ACLD, c) PZT Same Side, d) PZT Opposite, e) PZT Under

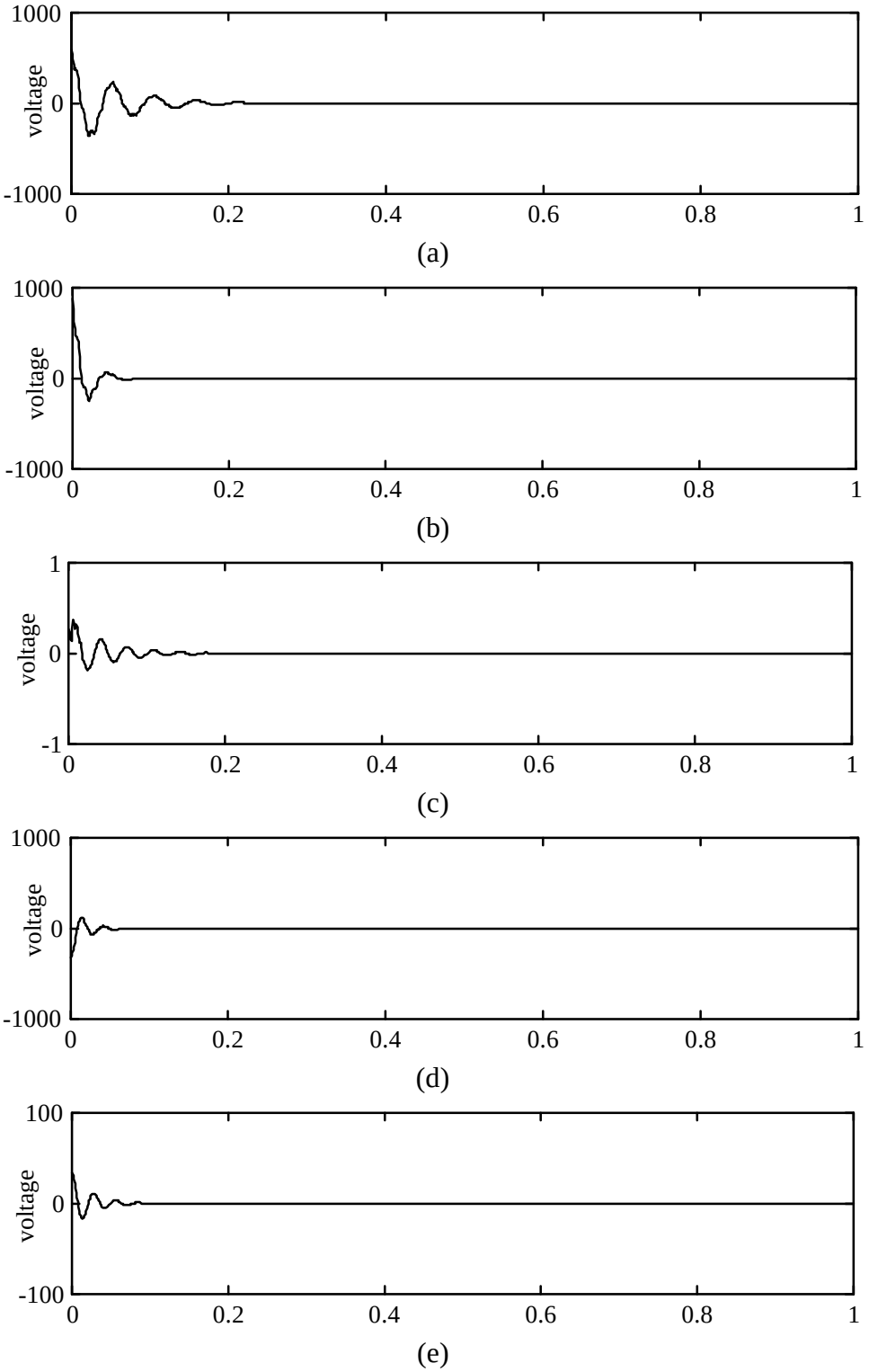

Figure 5. 7 Control Force (V) vs Time (sec) for Optimal Control Force Settling Time: a) PZT, b) ACLD, c) PZT Same Side, d) PZT Opposite Side, e) PZT Under

the beam, the control force settling time is at an optimum value. Note the improvement of the active tip displacement (Fig. 5.6(d)) when compared with the passive tip displacement (Fig. 5.5(c)). The control force is shown in Fig. 5.7(d). The passive tip displacement, active tip displacement and control force for a beam with the PZT underneath the PCLD are shown in Fig. 5.5(d), 5.6(e) and 5.7(e), respectively. Note that although the control force settling time in increased, the maximum magnitude is less than placing the PZT and PCLD on opposite sides of the beam. Unlike placing the PZT and PCLD on the same side of the beam, there is an improvement in the tip displacement for the active case.

5.3.4 Minimizing the Maximum Overshoot of Passive Response

In this section, the overshoot of the passive response will be studied. The passive time responses for tip displacements for a clamped aluminum beam with optimal passive overshoot are shown in Figure 5.8. Only the passive tip displacements are shown. Table 5.5 lists the optimal lengths and placements of the different treatments, as well as the minimum passive overshoot magnitudes. In order to obtain the optimal passive overshoot of 1.67 cm for a beam with PCLD, the treatment must be 28.7 cm long and placed at the root. The optimal length for ACLD is 28.5 cm applied at the root, with an overshoot of 3.33 cm. When the PZT is placed on the same side as the PCLD, the optimal length of the PZT and PCLD is 1 cm and 28.3 cm respectively. The PCLD is placed at the root, and the PZT immediately after, which achieves an optimal passive overshoot of 1.69 cm. The length for the hybrid variation where the PZT is placed on the opposite side of the beam, is 27.5 cm for the PZT and 28.9 cm for the PCLD. Both are placed at the root and the corresponding passive overshoot is 1.44 cm. When mounting the PZT underneath the PCLD, the optimal length of treatment is 28.3 cm, placed at the base of the beam, and the optimal passive overshoot is 1.45 cm.

Figure 5.8 shows the passive time response for the optimal configurations of the different

Table 5. 5 Minimum Values for Maximum Passive Response Overshoot for Different Treatments

	L_{pzt} (m)	Loc_{pzt} (m)	L_{pcld} (m)	Loc_{pcld} (m)	OS_y (mm)
PCLD			0.287	0.001	1.6746
ACLD	0.285	0.001	0.285	0.001	3.3296
PZT/PCLD same side	0.010	0.285	0.283	0.001	1.6893
PZT/PCLD opposite	0.275	0.001	0.289	0.001	1.4405
PZT under PCLD	0.283	0.001	0.283	0.001	1.4483

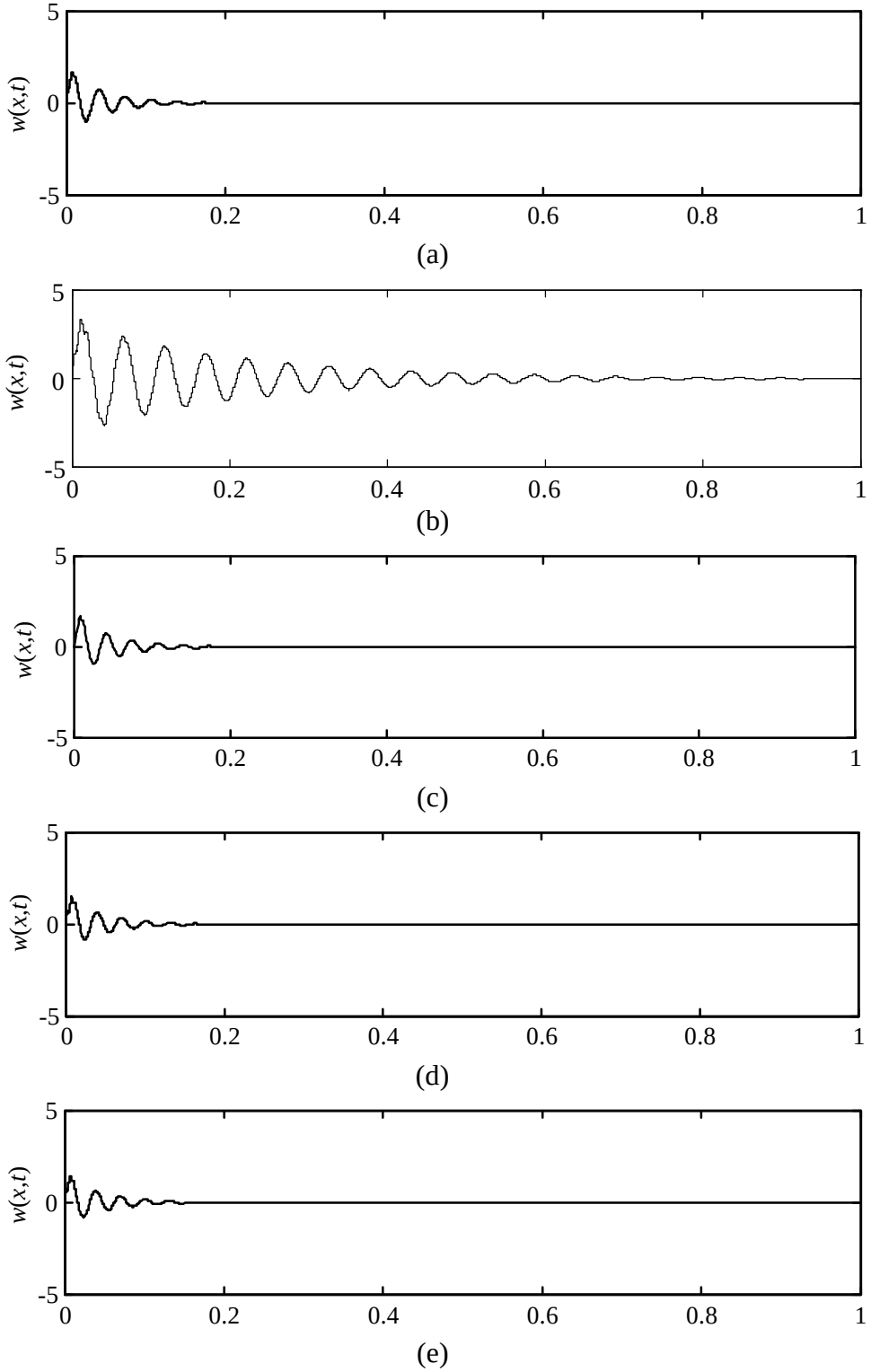

Figure 5. 8 Tip Displacement (mm) vs Time (sec) for Optimal Passive Overshoot: a) PCLD, b) ACLD, c) PZT Same Side, d) PZT Opposite Side, e) PZT Under

treatments. As was seen with all previous optimizations, ACLD (Fig. 5.8b) is least effective due to the lack of stiffness of the PZT constraining layer. Using a PCLD (Fig. 5.8a) is slightly more advantageous than adding a PZT to the same side (Fig. 5.8c). In fact, the treatment where the PZT is added on the same side is trying to become PCLD. This is shown by the fact that the PZT is the minimum value, 1 cm, and placed after the PCLD. As was seen in the previous section, adding a PZT of length 1 cm that far removed from the root does not add the benefit of active control. Therefore, a beam with PCLD is more effective. Adding the PZT on the opposite side of the beam gives the optimal configuration, as seen in Fig. 5.8(d). The overshoot of the passive tip displacement is only increased slightly if the PZT is placed underneath the PCLD. Therefore, if placing the PZT underneath the beam is not an option, placing it underneath the PCLD effectively minimizes the overshoot of the passive response. The added advantage of both treatments is the ability of the PZT to enhance control of vibration.

5.3.5 Minimizing the Maximum Overshoot of Active Response

In this section, the maximum overshoot of the active tip displacement is minimized. The optimal treatment lengths and minimum values of the overshoot are reported in Table 5.6. Figure 5.9-5.11 show the passive and active tip displacement and control force, respectively. Again, due to the lack of frequency dependent damping, only the active response and control force for a PZT are shown. The optimal length of a PZT is 29.2 cm, placed at the base of the beam. This length gives an active response overshoot of 2.06 cm. ACLD can reduce the overshoot to 1.59 cm by setting the treatment length to 26.1 and placing it at the root. Placing the PZT and PCLD on the same side of the beam effectively gives the same overshoot of 1.59 cm. The PZT is 14.5 cm long, placed at the root, and the PCLD is 14.4 cm long, placed directly after the PZT. The minimum value for active response overshoot is achieved by placing the PZT on the opposite side of the PCLD. In this case, the overshoot is 1.10 cm. The PZT is 28.1 cm and the PCLD is 28 cm. Both are placed at the base of the beam. Placing the PZT underneath the PCLD gives an overshoot of 1.30 cm if the treatment length is 28.6 cm.

Table 5. 6 Minimum Values for Maximum Active Response Overshoot for Different Treatments

	L_{pzt} (m)	Loc_{pzt} (m)	L_{pcld} (m)	Loc_{pcld} (m)	OS_{yn} (m)
PZT	0.292	0.001			2.0623
ACLD	0.261	0.001	0.261	0.001	1.5891
PZT/PCLD same side	0.145	0.001	0.144	0.147	1.5887
PZT/PCLD opposite	0.281	0.001	0.280	0.001	1.1014
PZT under PCLD	0.286	0.001	0.286	0.001	1.2954

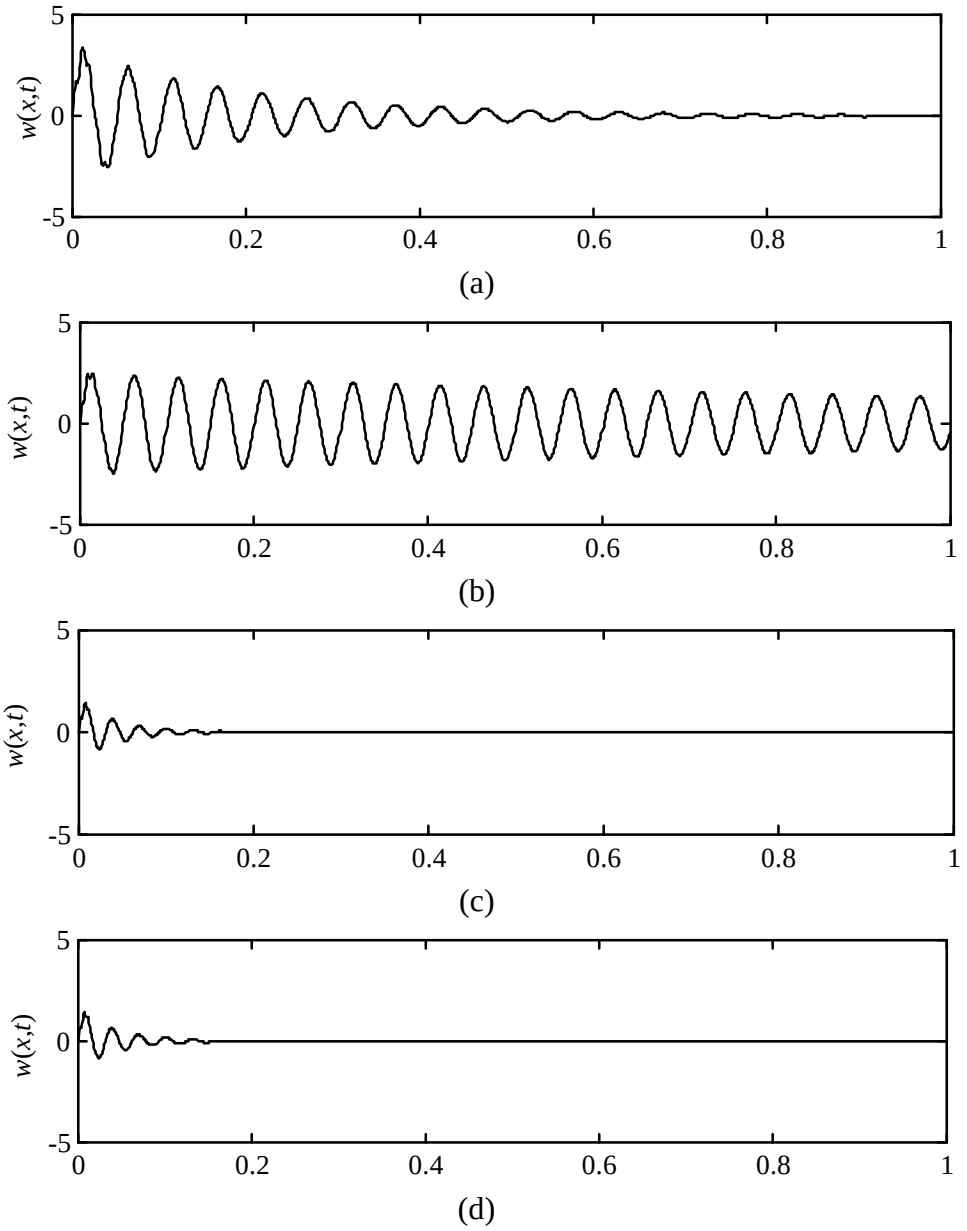

Figure 5. 9 Passive Tip Displacement (mm) vs Time (sec) for Optimal Active Overshoot: a) ACLD, b) PZT Same Side, c) PZT Opposite Side, d) PZT Under

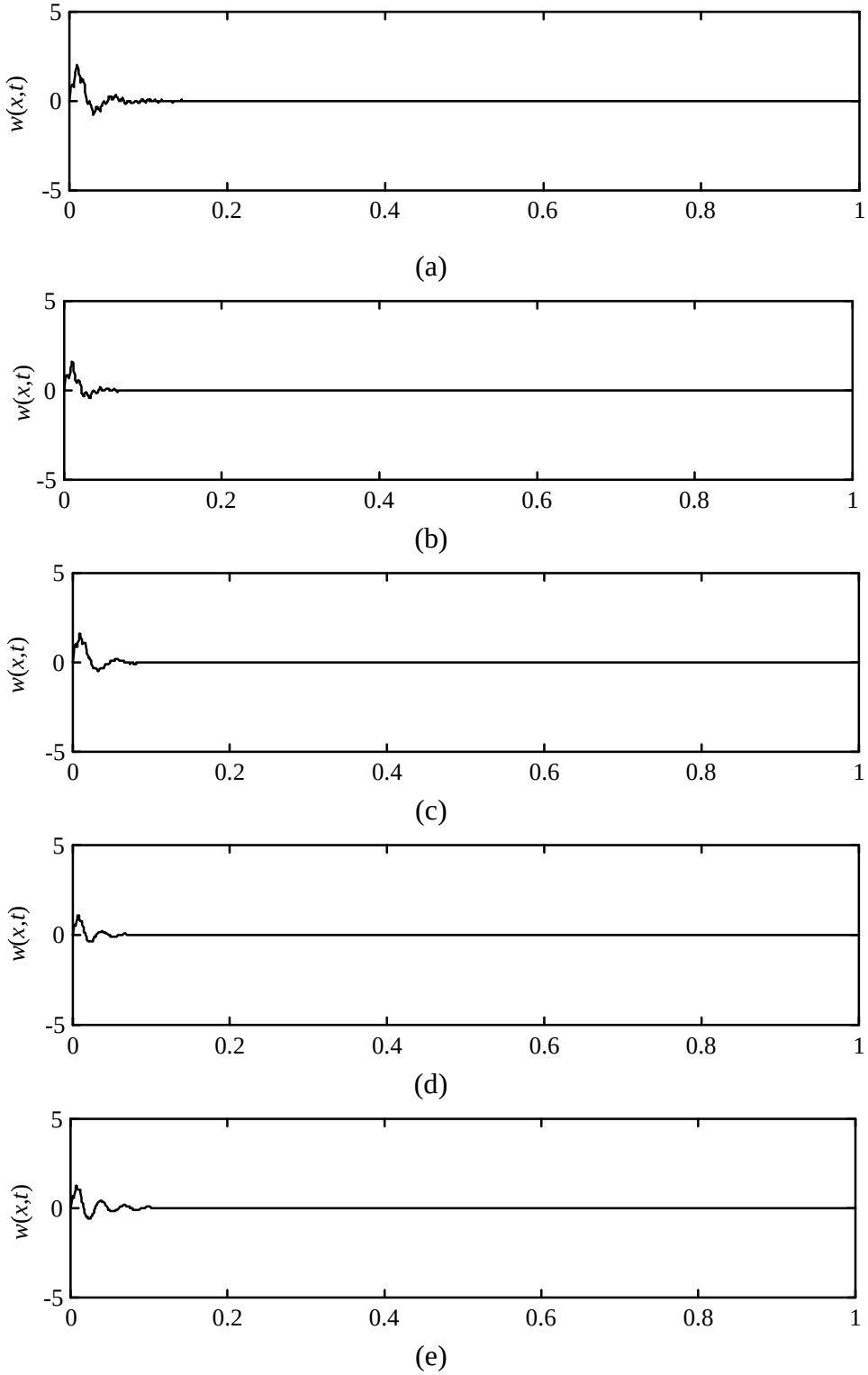

Figure 5. 10 Active Tip Displacement (mm) vs Time (sec) for Optimal Active Overshoot: a) PZT, b) ACLD, c) PZT Same Side, d) PZT Opposite, e) PZT Under

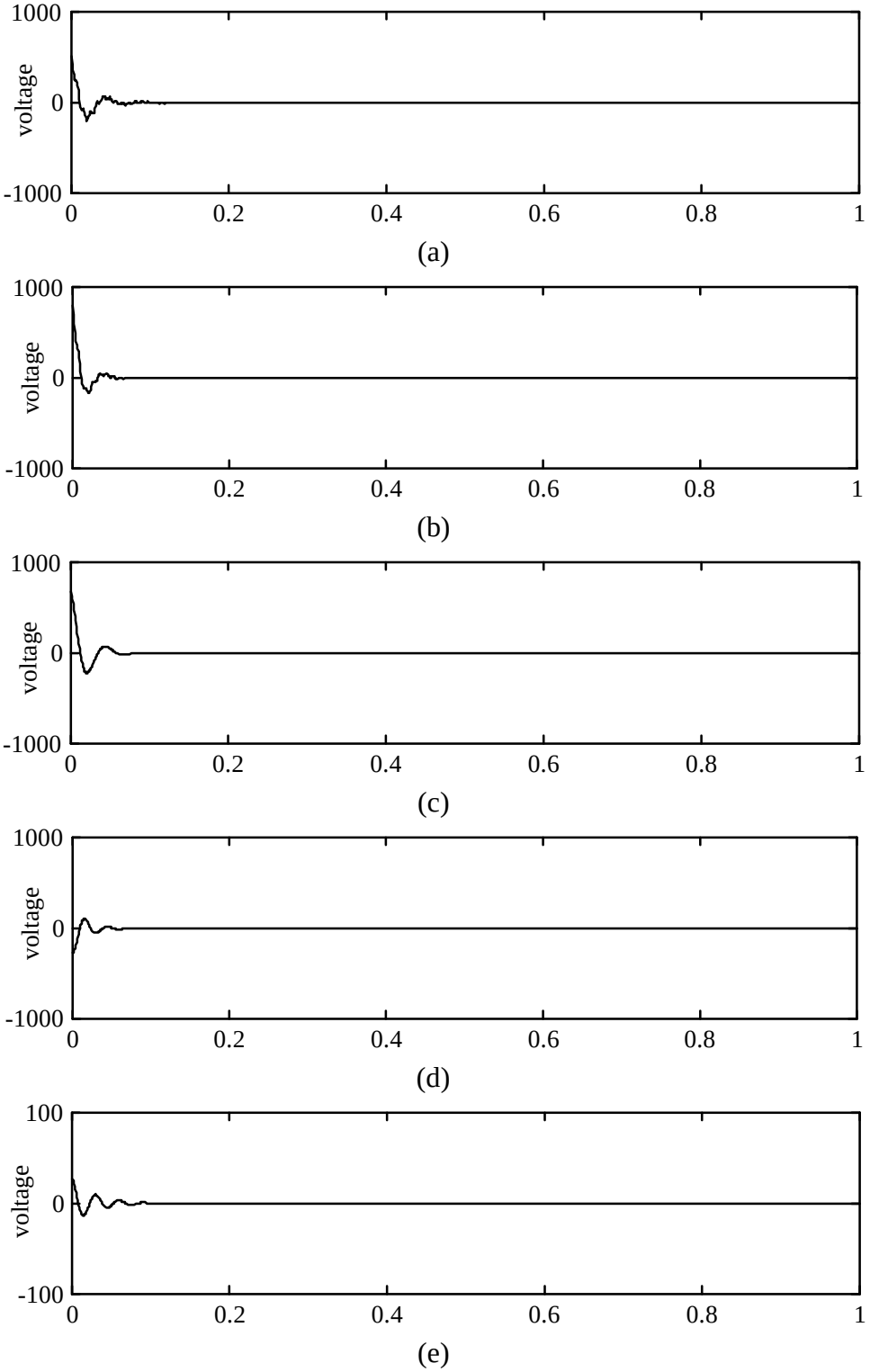

Figure 5. 11 Control Force (V) vs Time (sec) for Optimal Active Overshoot:
a) PZT only, b) ACLD, c) PZT Same Side, d) PZT Opposite Side, e) PZT Under

The active tip displacement for a optimal PZT is shown in Fig. 5.10(a), while the control force is shown in Fig. 5.11(a). When comparing this to ACLD, it is seen that ACLD has less active displacement overshoot, but it takes more control force, as illustrated in Fig. 5.10(b) and 5.11(b). The passive tip displacement is shown in Fig. 5.9(a). As before, the PZT as constraining layer does not have enough stiffness, and the passive response takes a significant amount of time to settle. It is however better than the passive tip displacement for the case where PCLD and PZT are placed on the same side of the beam. Since the PCLD is placed 14.7 cm from the root, not enough passive damping is added to the structure. The active response, as shown in Fig. 5.10(c) is not as good as ACLD and slightly better than PZT. However, the control force, seen in Fig. 5.11(c), is more than either PZT or ACLD. In other words, it would be more advantageous to use ACLD than PZT and PCLD on the same side. The optimal case for minimizing the active response overshoot is obtained by placing the PZT and PCLD on opposite sides of the beam. The passive tip displacement is shown in Fig. 5.9(c). Figure 5.10(d) shows the active tip displacement while Fig. 5.11(e) shows the control force. Note the passive and active displacements also settle quickly. While placing the PZT on the opposite side gives the optimal scenario, it is not always possible to apply a treatment on both surfaces. Byp lacing the PZT underneath the PCLD, the overshoot of the active response is increased, as seen in Fig. 5.10(e). However, Fig. 5.11(e) shows the control force is at a minimum. The passive response is also still adequate, as seen in Fig. 5.9(d).

5.3.6 Minimizing the Maximum Overshoot of Control Force

The minimum values of the control force overshoot for different treatments are reported in Table 5.7. The passive tip displacement, active tip displacement and control force response are shown in Fig. 5.12-14, respectively. A minimum overshoot of 420 V is obtained when a PZT, 18.3 cm long, is applied at the base of the beam. Using an ACLD that is 27.3 cm long increases the minimum overshoot to 794 V. The increase in voltage is due to the fact that the PZT has to actuate through the VEM. The ACLD is applied at the

root. When placing a PZT on the opposite side of the PCLD, the PCLD is placed at the root with the PZT placed directly after it. The optimal length of the PCLD is 30.3 cm, and the PZT is 1 cm. The maximum overshoot of the control force is then 0.3 V. Applying the PZT to the opposite side of the beam increases the maximum overshoot to 36 V, where the PZT is 1 cm and the PCLD is 27.7 cm long and both are applied at the root. The optimal value of the control force overshoot is 215.8 when the PZT is placed underneath the PCLD. The treatment length is 27.5 cm, applied at the root.

The active tip displacement for a PZT is shown in Fig. 5.13(a), and the control forces is shown in Fig. 5.14(a). Even though the control force overshoot is minimized, this is done at the cost of settling time. As can be seen in both the active response and control force, the signal does not settle by 1 sec. This response can be improved by increasing the LQR constant, **Q**, thereby increasing the vibration suppression. However, since a comparison is made between treatments using the same **Q**, this is not shown. As with the previous sections, the passive tip displacement when ACLD is applied does not settle quickly, as seen in Fig. 5.12(a). While the active response settles quickly, it takes significant control force, as seen in Fig. 5.13(b) and 5.14(b). The passive response of a beam with PZT and PCLD on the same side is seen in Fig. 5.12(b). The active response is shown in Fig. 5.13(c), while the control force is shown in Fig. 5.14(c). When placing a PZT on the opposite side of the beam, the passive tip displacement, active tip displacement and control force are shown in Fig. 5.12(c), 5.13(d) and 5.14(d), respectively. For the last two variations, the systems try to emulate PCLD in order to minimize the control force overshoot. This can be seen by the lack of improvement of the active response versus the passive response, and the fact that the lengths of the PZT is set to 1 cm, which is the minimum value. These two configurations are therefore not valid active configurations. Therefore, the optimal treatment is to place the PZT underneath the PCLD. As seen in Fig. 5.12(d), there is good vibration reduction for passive control. When active control is applied, the response, Fig. 5.13(e), and control force, Fig. 5.14(e), are good.

Table 5. 7 Minimum Values for Maximum Control Force Overshoot for Different Treatments

	L_{pzt} (m)	Loc_{pzt} (m)	L_{pcld} (m)	Loc_{pcld} (m)	OS_{un} (V)
PZT	0.183	0.001			420.09
ACLD	0.273	0.001	0.273	0.001	793.75
PZT/PCLD same side	0.010	0.305	0.303	0.001	0.30
PZT/PCLD opposite	0.010	0.001	0.277	0.001	35.97
PZT under PCLD	0.275	0.001	0.275	0.001	215.77

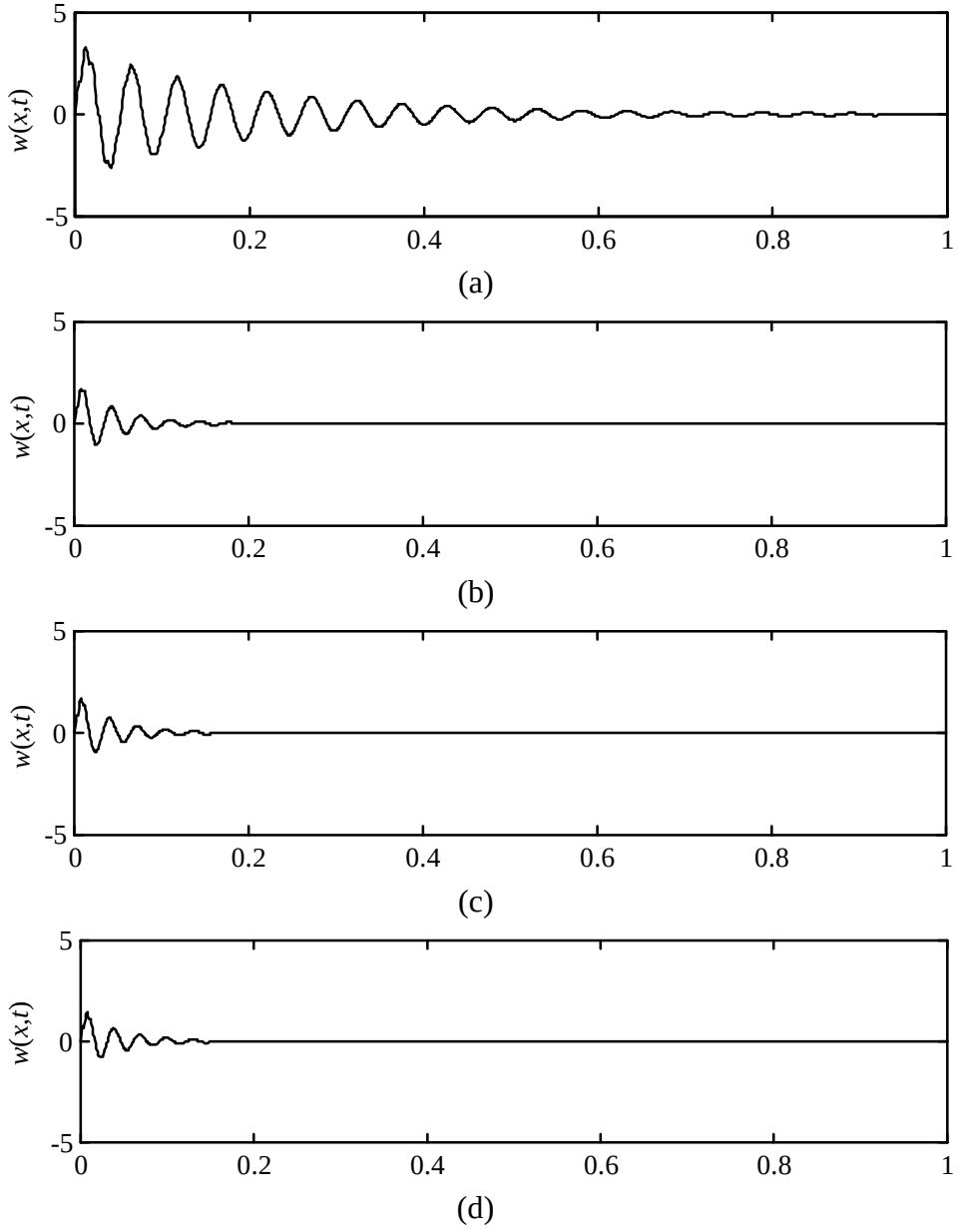

Figure 5. 12 Passive Tip Displacement (mm) vs Time (sec) for Optimal Control Force Overshoot: a) ACLD, b) PZT Same Side, c) PZT Opposite, e) PZT Under

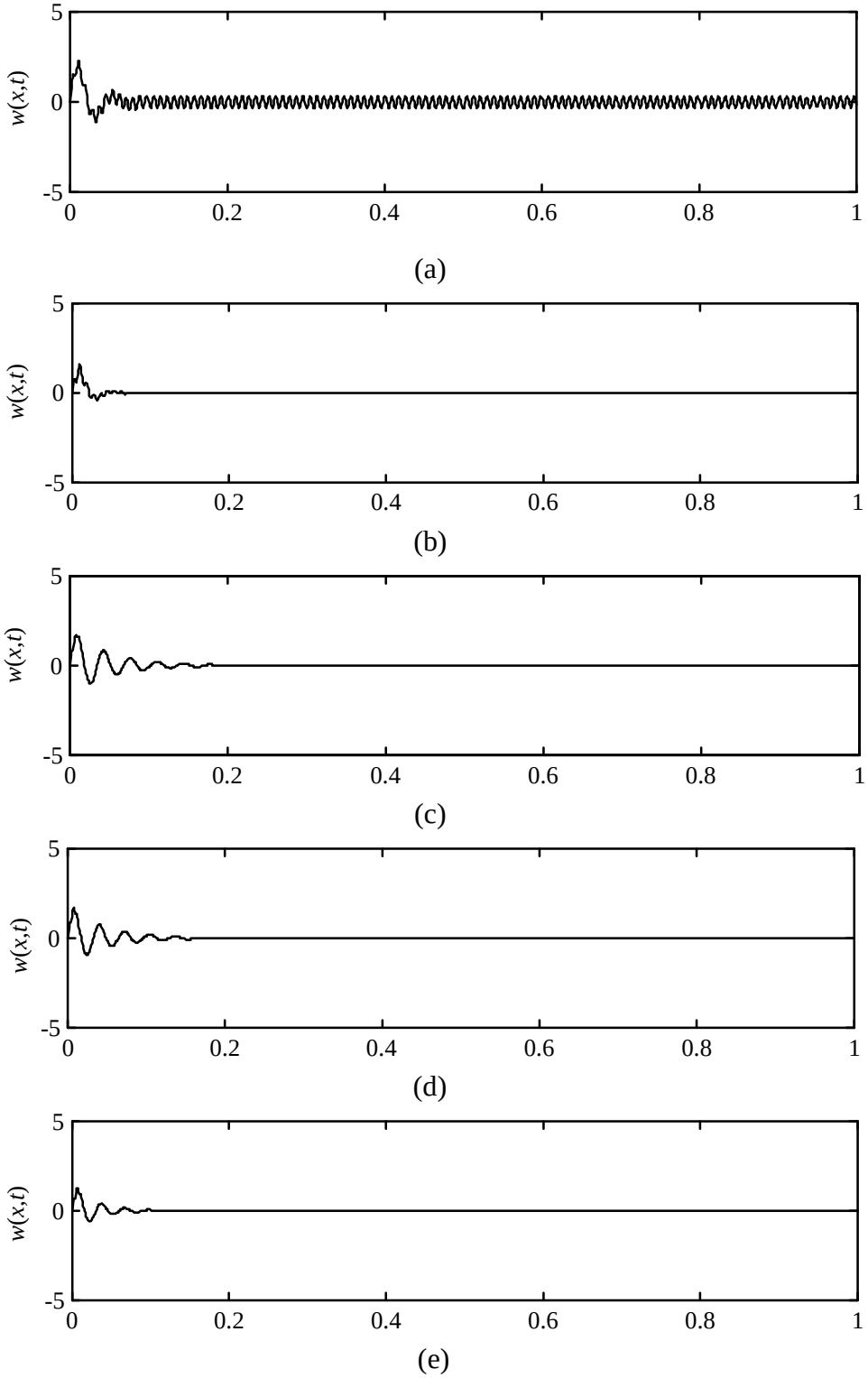

Figure 5. 13 Active Tip Displacement (mm) vs Time (sec) for Optimal Control Force Overshoot: a)PZT, b) ACLD, c) PZT Same, d) PZT Opposite, e) PZT Under

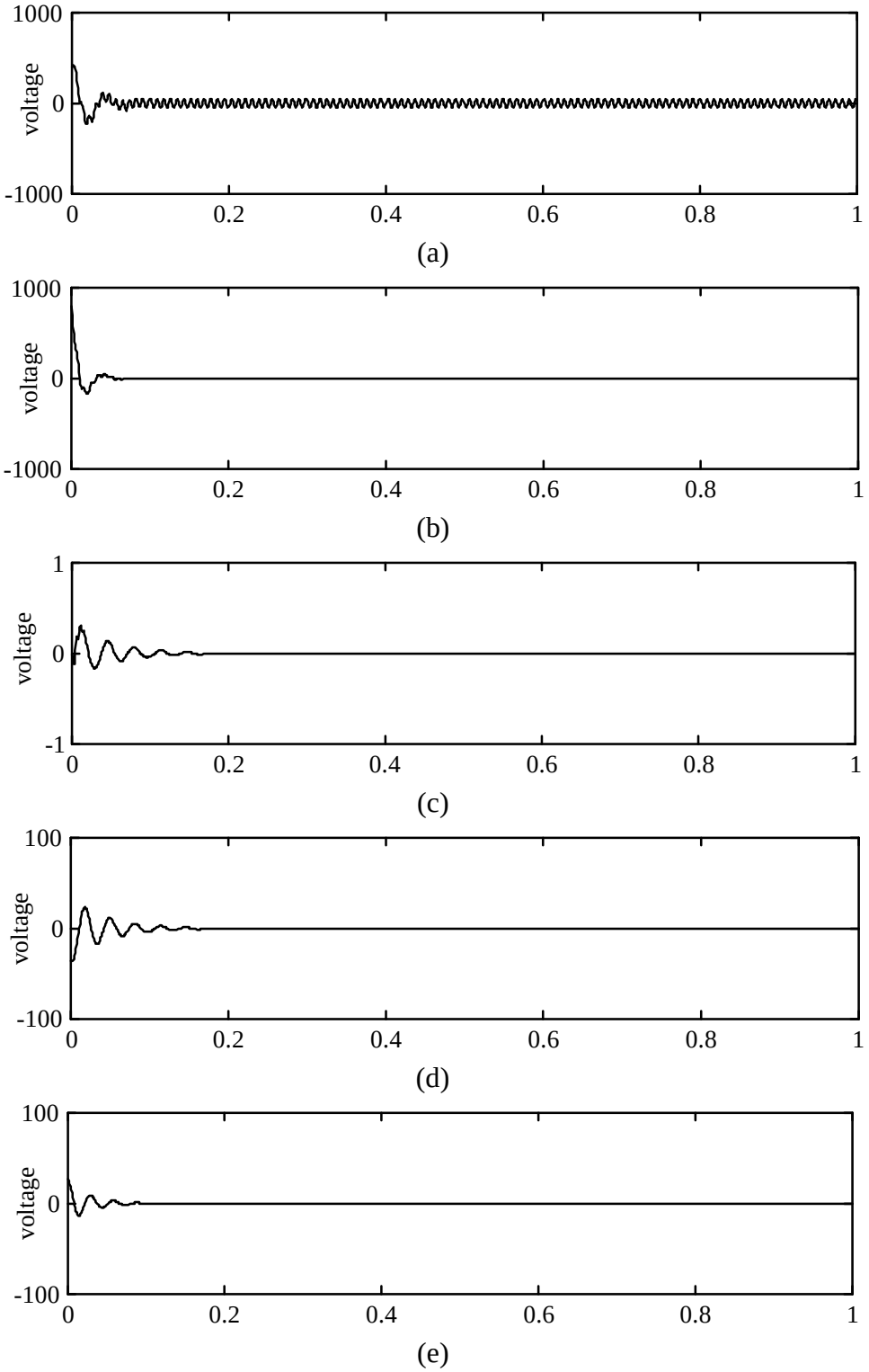

Figure 5. 14 Control Force (V) vs Time for Optimal Control Force Overshoot: a) PZT, b) ACLD, c) PZT Same Side, d) PZT Opposite Side, e) PZT Under

5.3.7 Minimum Passive Vibration Suppression Index

The optimal values for the length and placement of treatment, as well as the passive vibration suppression index are given in Table 5.8. A lower value for the vibration suppression index signifies more vibration suppression. The passive tip displacement for a cantilevered aluminum beam is given in Fig. 5.15. Since PZT does not have frequency dependent damping, it is not optimized for a passive response.

The optimal length for PCLD is 27.2 cm, with a minimum passive vibration suppression index of 3.57e-8. Figure 5.15(a) shows the passive tip displacement for this configuration. ACLD has an optimal length of 27 cm with an index of 5.29e-7. The passive tip displacement is shown in Fig. 5.15(b). As was seen in all previous sections, this high passive vibration suppression index is due to the lack of stiffness when using a PZT as constraining layer. Placing the PZT and PCLD the same side of the beam gives an optimal index of 3.62e-8. The length of treatment is 1 cm for the PZT and 26.8 cm for the PCLD. The PCLD is placed at the root, and the PZT is placed 27 cm from the root. The time history is shown in Fig. 5.15(c). Note that this configuration is again trying to simulate PCLD by minimizing the length of the PZT, as was the case for passive response settling time and overshoot. In fact, the vibration suppression index is higher since the PZT adds stiffness to the structure. By placing the PZT on the opposite side of the beam, the passive vibration suppression index is lowered to 2.48e-8, where the optimal PZT length is 26.4 cm and the optimal PCLD length is 27.2 cm. Figure 5.15(d) shows the tip displacement of this configuration. The optimal passive vibration suppression index is achieved by placing the PZT underneath the PCLD, where the cost function becomes 2.40e-8 and the length of treatment is 26.9 cm. This optimal configuration has a time response as shown in Fig. 5.15(e).

Table 5. 8 Minimum Values for Passive Vibration Suppression Index for Different Treatments

	L_{pzt} (m)	Loc_{pzt} (m)	L_{pcld} (m)	Loc_{pcld} (m)	$J_{passive}$
PCLD			0.272	0.001	3.5698e-8
ACLD	0.270	0.001	0.270	0.001	5.2944e-7
PZT/PCLD same side	0.010	0.270	0.268	0.001	3.6277e-8
PZT/PCLD opposite	0.264	0.001	0.272	0.001	2.4800e-8
PZT under PCLD	0.269	0.001	0.269	0.001	2.3979e-8

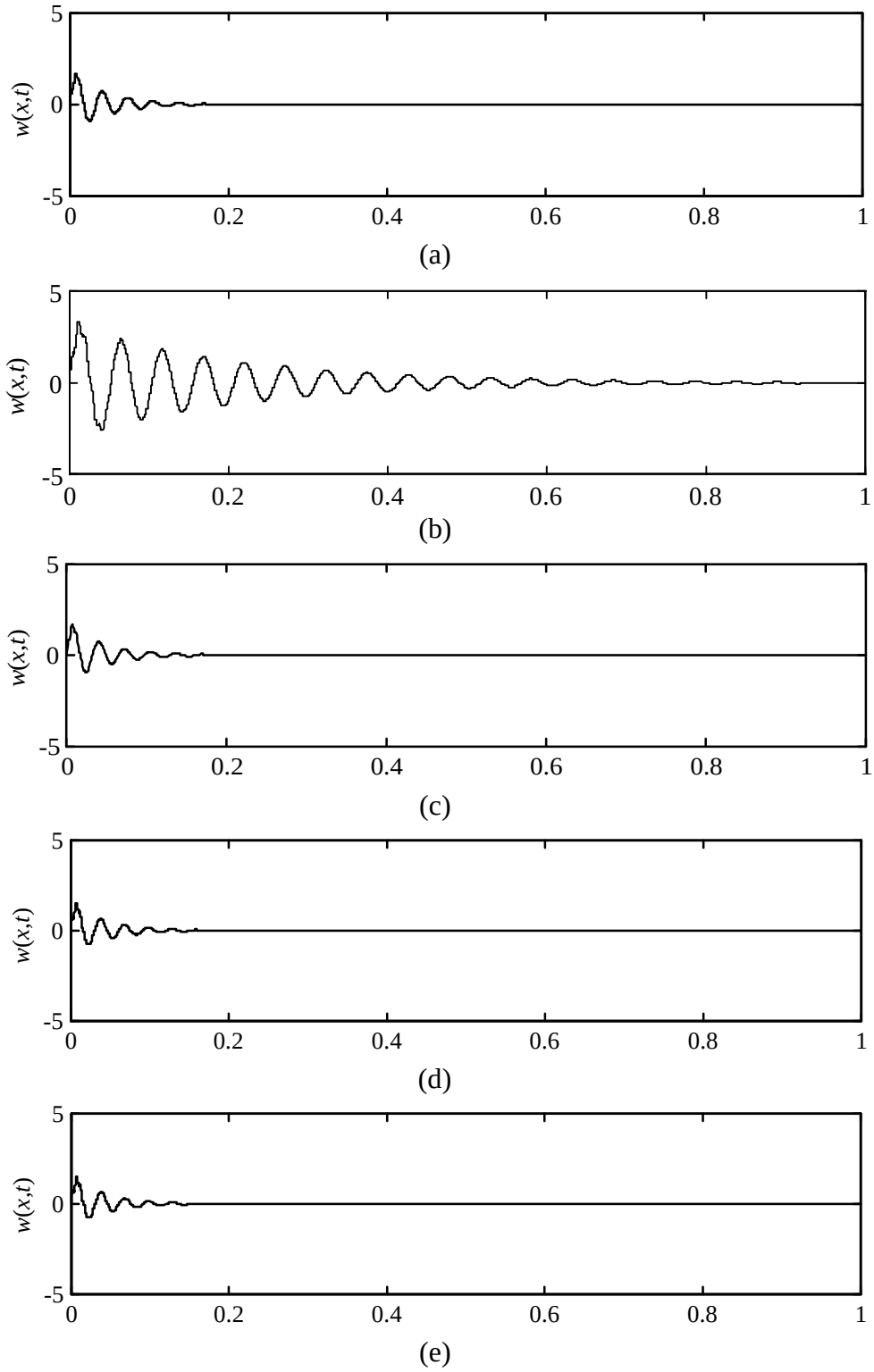

Figure 5. 15 Tip Displacement (mm) vs Time (sec) for Optimal Passive Vibration Index: a) PCLD, b) ACLD, c) PZT Same Side, d) PZT Opposite Side, e) PZT Under

5.3.8 Minimum Active Vibration Suppression Index

The passive and active tip displacements for optimal active vibration suppression are shown in Fig. 5.16-17, respectively. Figure 5.18 shows the control force associated with the active tip displacement. The optimal lengths and placement of treatment as well as the minimum active vibration suppression index are given in Table 5.9. Only the active response and control force for a PZT are reported, since there is no frequency dependent damping associated with a PZT.

The optimal active vibration suppression index for a PZT is 3.63e-8, where the PZT is 28.3 cm long. For ACLD, the treatment must be 28.5 cm long to achieve an active vibration suppression index of 1.71e-8. When placing the PZT and PCLD on the same side, the PZT must be 27.1 cm long and placed 1.1 cm from the root. The PCLD must be 1 cm long, placed at the root. The corresponding active vibration suppression index is 2.02e-8. The optimal active vibration suppression index occurs when a PZT is placed on the opposite side of the beam. The active vibration suppression index is found to be 8.70e-9, where the length of the PZT is 27.5 cm and the length of the PCLD is 27.1 cm. Both are placed at the base of the beam. When placing the PZT underneath the PCLD, an active vibration suppression index of 1.50e-8 is obtained, where the treatment length is set to 26.7 cm placed at the root.

Using only a PZT gives the worst active vibration suppression index. This is shown in Fig. 5.17(a): the active tip displacement. The control force necessary to obtain the optimal active vibration suppression index is shown in Fig. 5.18(a). Using ACLD, the active response is shown in Fig. 5.17(b) and the control force in Fig. 5.18(b). Again, the passive tip displacement does not settle quickly, as seen in Fig. 5.16(a). When placing the PZT and PCLD on the same side of the beam, the treatment tries to optimize to PZT coverage. This is shown by the fact that the length of the PCLD is at the minimum value, while the PZT is long. The passive response is shown in Fig. 5.16(a). While the PCLD is

Table 5. 9 Minimum Values for Active Vibration Suppression Index for Different Treatments

	L_{pzt} (m)	Loc_{pzt} (m)	L_{pcld} (m)	Loc_{pcld} (m)	J_{VS}
PZT	0.283	0.001			3.6312e-8
ACLD	0.285	0.001	0.285	0.001	1.7056e-8
PZT/PCLD same side	0.271	0.012	0.010	0.001	2.0159e-8
PZT/PCLD opposite	0.275	0.001	0.271	0.001	8.7024e-9
PZT under PCLD	0.267	0.001	0.267	0.001	1.4964e-8

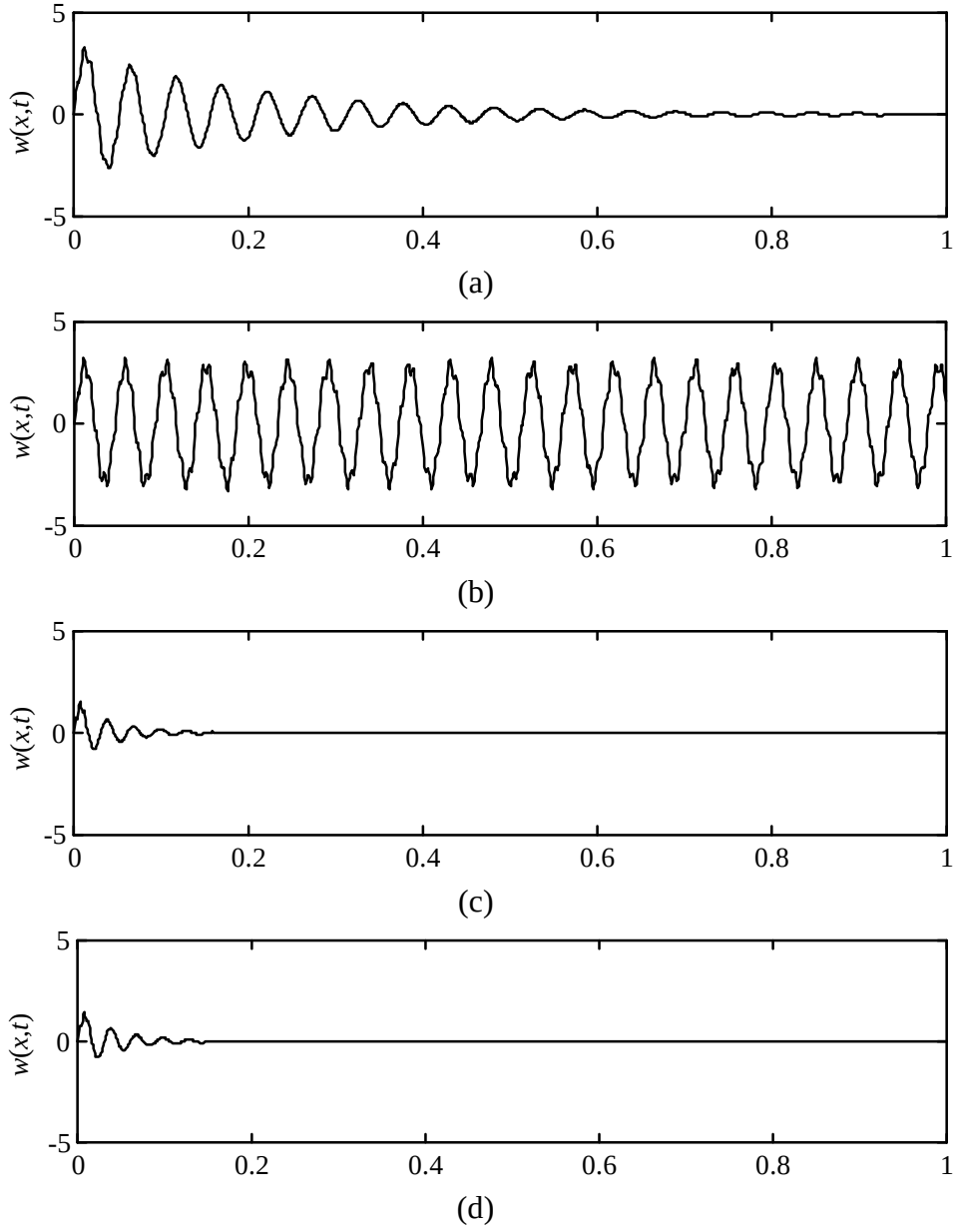

Figure 5. 16 Passive Tip Displacement (mm) vs Time (sec) for Optimal Active Vibration Index: a) ACLD, b) PZT Same Side, c) PZT Opposite Side, d) PZT Under

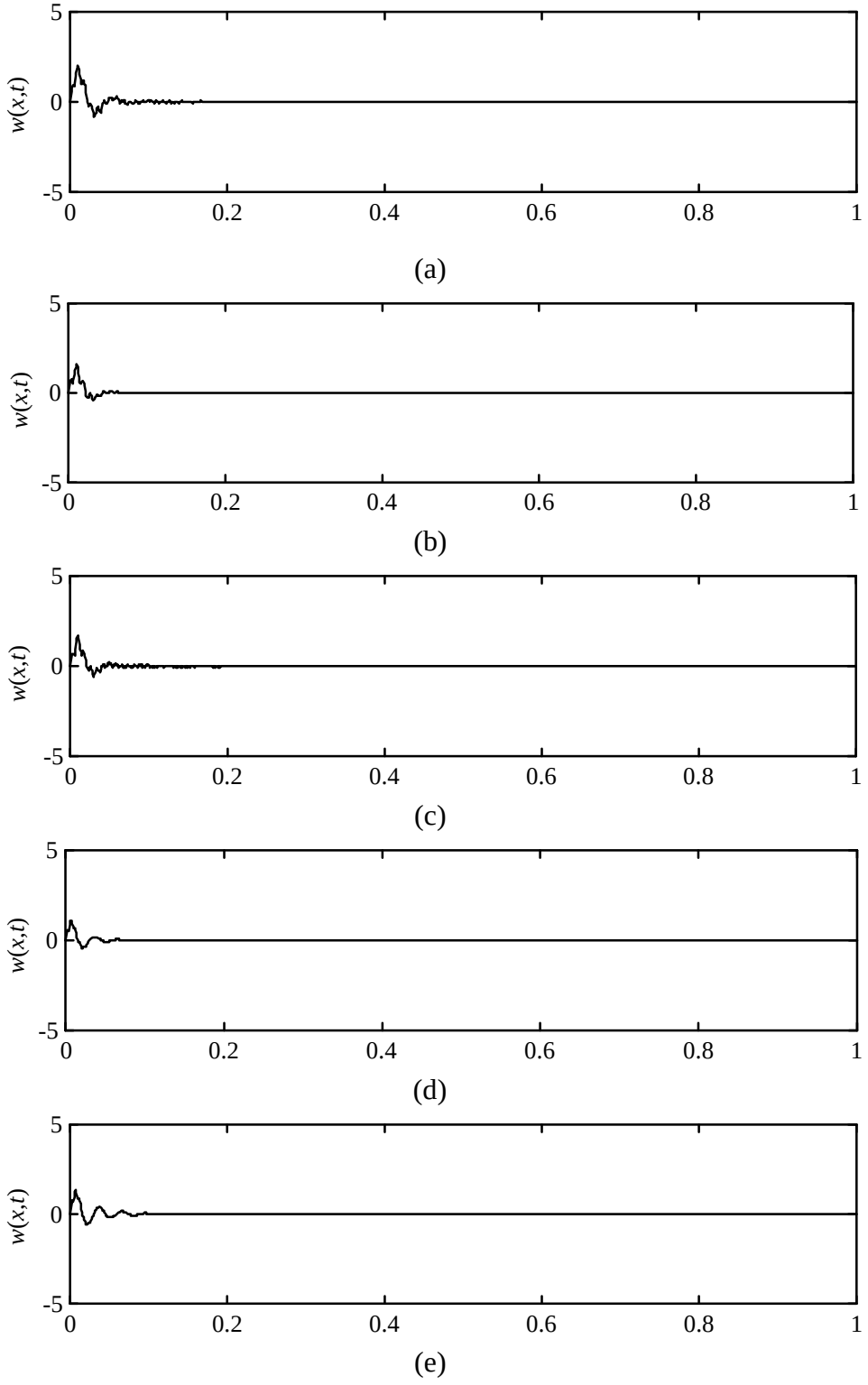

Figure 5. 17 Active Tip Displace. (mm) vs Time (sec) for Optimal Active Vibration Index: a) PZT, b) ACLD, c) PZT Same Side, d) PZT Opposite Side, e) PZT Under

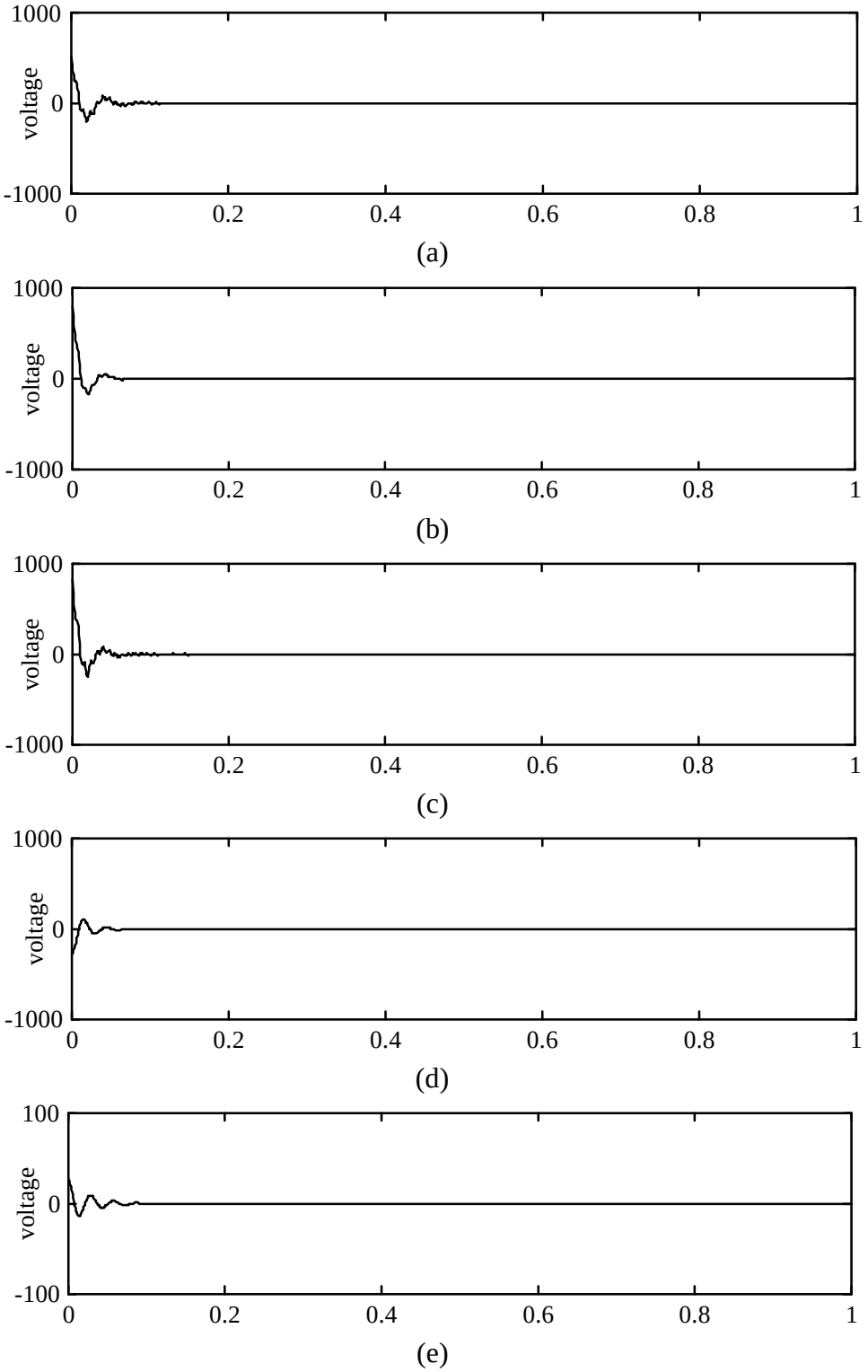

Figure 5. 18 Control Force (V) vs Time (sec) for Optimal Active Vibration Index: a) PZT only, b) ACLD, c) PZT Same Side, d) PZT Opposite Side, e) PZT Under

placed at the root, it is too short to add much vibration suppression. Therefore, to use this configuration does not add in the fail-safe benefit of passive damping. The active tip displacement and control force can be seen in Fig. 5.17(c) and 5.18(c), respectively. Adding the PZT on the opposite side of the beam gives the optimal configuration. As can be seen in Fig. 5.6(c), the passive tip displacement damps out quickly. The active tip displacement is shown in Fig. 5.17(d), and the control force in Fig. 5.18(d). If the opposite surface is not available for treatment, it is still advantageous to place the PZT under PCLD. In this case, the passive treatment damps quickly, as seen in Fig. 5.16(d). The active response is still good as seen in Fig. 5.17(e). One advantage is the reduced control force, as seen in Fig. 5.18(e). Note the difference in axis.

5.3.9 Minimum Control Effort

The control effort is investigated in this section. A lower control effort index indicates less control force used to control vibration. The minimum values for the control effort along with the length and placement of treatment are reported in Table 5.10. The passive and active tip displacements are shown in Fig. 5.19-20, respectively. Figure 5.21 shows the control force time history. Only active control is investigated for a PZT, due to a lack of frequency dependent damping.

The optimal length of a PZT is 27.7 cm, which gives a control effort of 1130. The active tip displacement is shown in Fig. 5.20(a) and the control force in Fig. 5.21(a). ACLD has a higher control effort at 2200 due to the actuation of the PZT through the VEM. The optimal treatment length is 27.2 cm. This high control effort can be seen when comparing the control force of the PZT, Fig. 5.21(a), to the control force of ACLD, Fig. 5.21(b). However, the active response has lower overshoot and settles more quickly, as seen in Fig. 5.20(b). Again, the passive tip displacement is not as effective as the other hybrid treatments, due to the lack of stiffness of the PZT when used as a constraining layer. Placing the PZT and PCLD on opposite sides of the beam, gives a control effort of

Table 5. 10 Minimum Values of Control Effort for Different Treatments

	L_{pzt} (m)	Loc_{pzt} (m)	L_{pcld} (m)	Loc_{pcld} (m)	J_{CE}
PZT	0.277	0.001			1.128e3
ACLD	0.272	0.001	0.272	0.001	2.197e3
PZT/PCLD same side	0.010	0.304	0.302	0.001	0.0012
PZT/PCLD opposite	0.010	0.001	0.274	0.001	15.650
PZT under PCLD	0.267	0.001	0.267	0.001	277.16

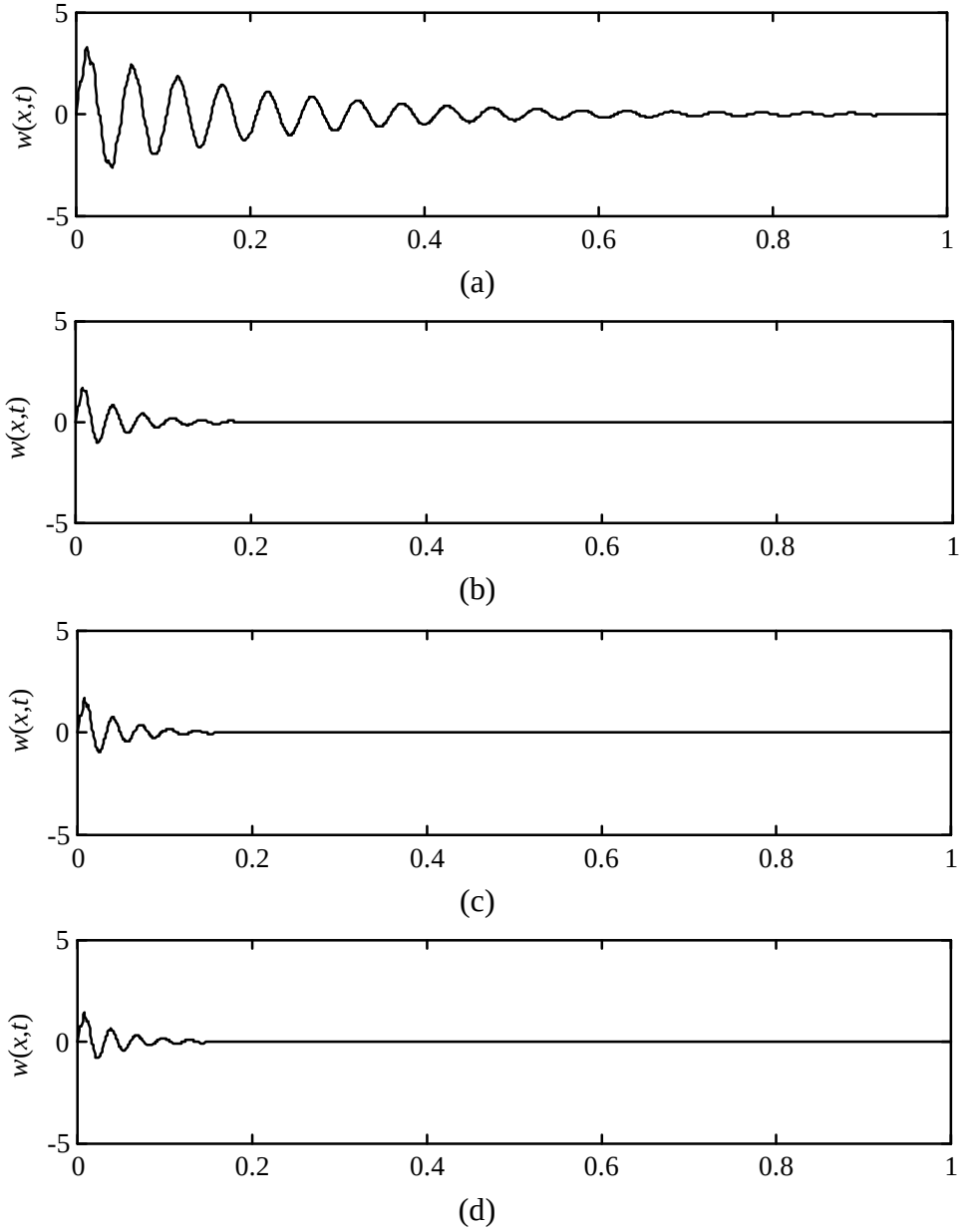

Figure 5. 19 Passive Tip Displacement (mm) vs Time (sec) for Optimal Control Effort: a) ACLD, b) PZT Same Side, c) PZT Opposite Side, d) PZT Under

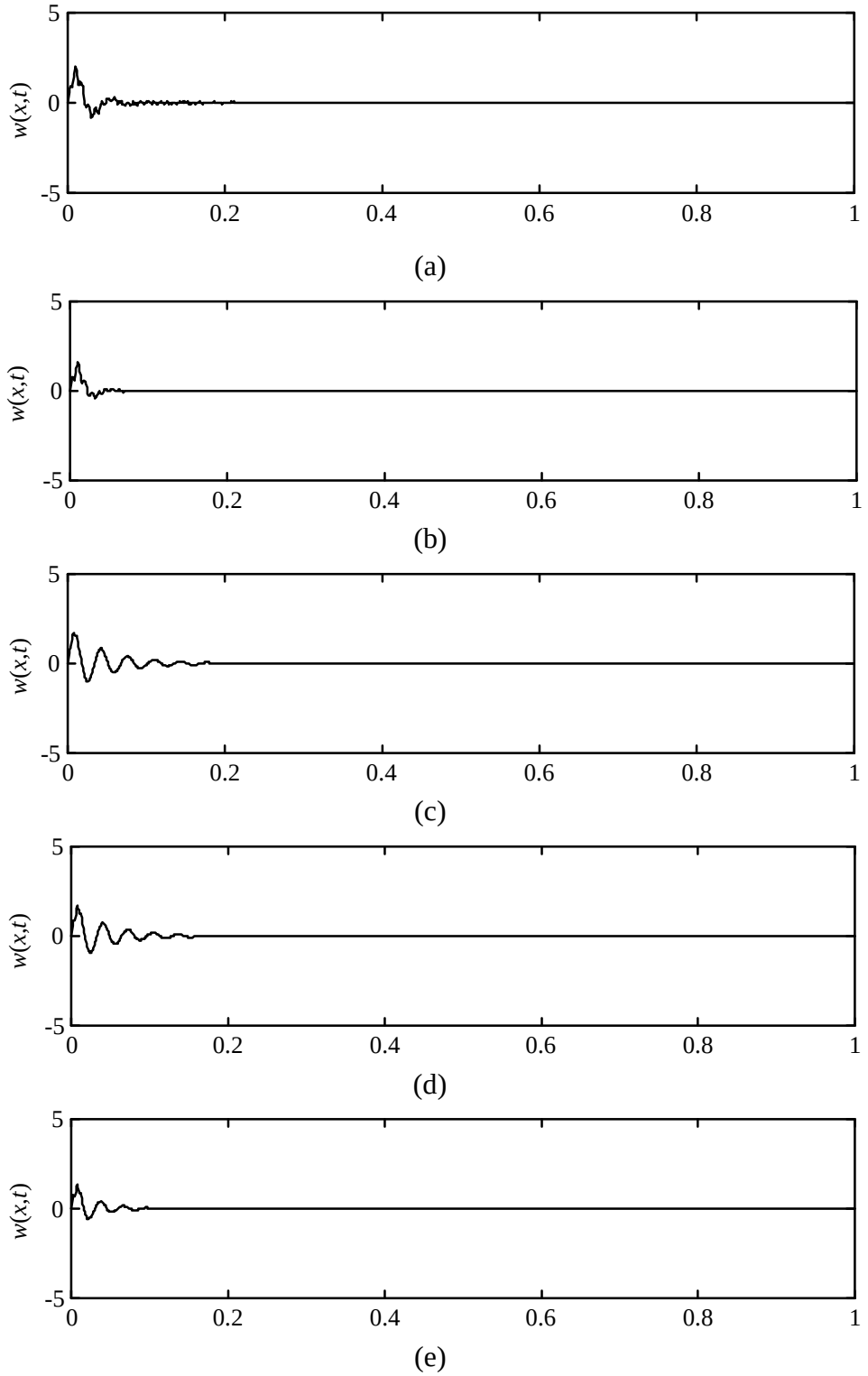

Figure 5. 20 Active Tip Displacement (mm) vs Time (sec) for Optimal Control Effort: a) PZT, b) ACLD, c) PZT Same Side, d) PZT Opposite, e) PZT Under

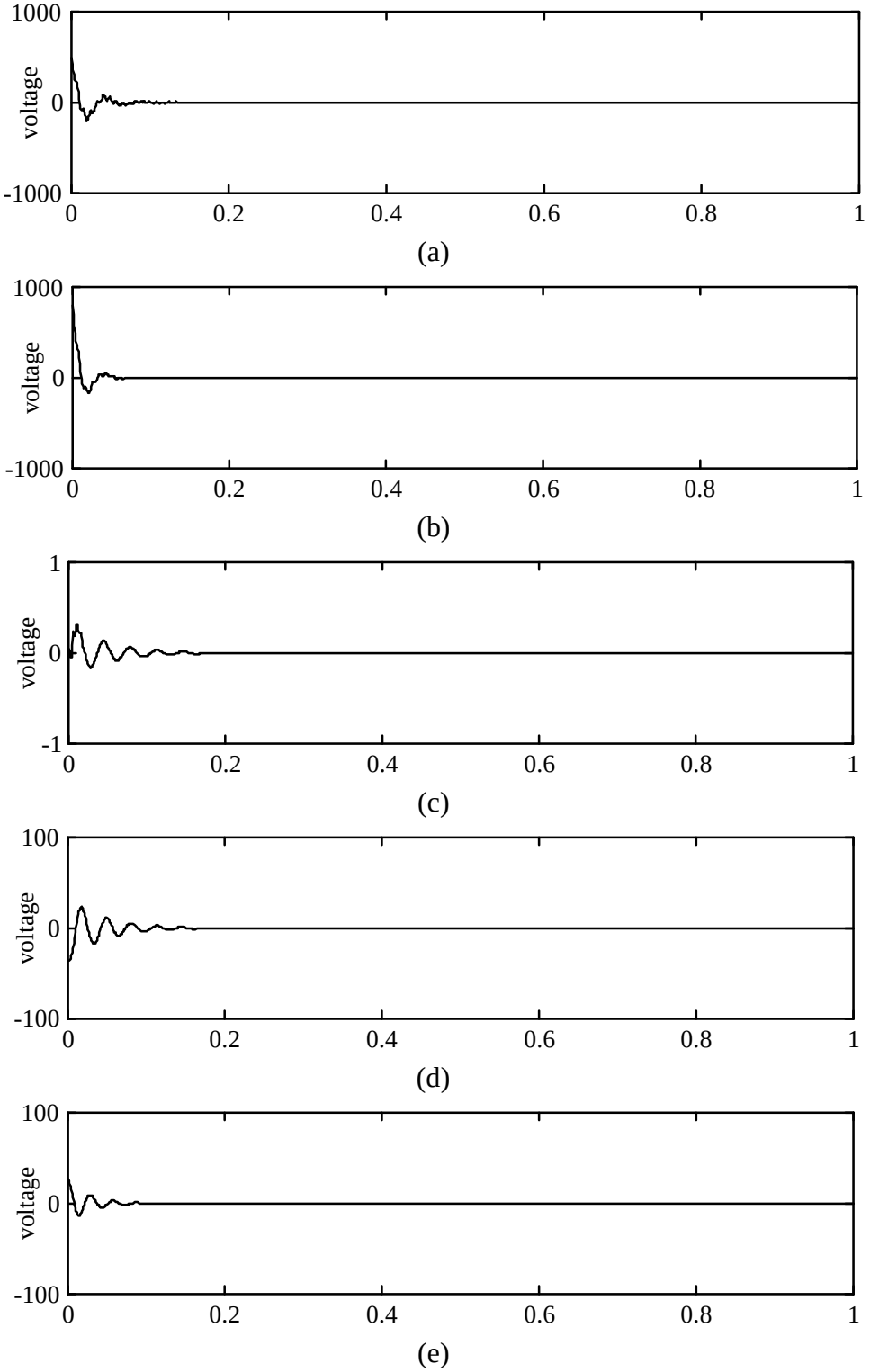

Figure 5. 21 Control Force (V) vs Time (sec) for Optimal Control Effort: a) PZT, b) ACLD, c) PZT Same Side, d) PZT Opposite Side, e) PZT Under

0.001. This is achieved by placing a 30.2 cm PCLD at the root, and a 1 cm PZT directly after. This configuration has such a long control effort because it tries to optimize to PCLD. This can be seen in Fig. 5.19(b) (passive tip displacement) and 5.20(c) (active tip displacement), since there is no improvement due to active control. Figure 5.21(c) shows the control force. This configuration is therefore not a valid control effort index optimization. A similar circumstance occurs when the PZT is placed on the opposite side. The optimal control index is 15.7 where the PZT and PCLD are 1 cm 27.4 cm, respectively. Again, when comparing the passive tip displacement, Fig. 5.19(c), with the active tip displacement, Fig. 5.20(d), there is no improvement in response. The control force is shown in Fig. 5.21(d). The treatment tries to optimize to PCLD, and is not valid. Placing the PZT underneath the PCLD gives the optimal control effort index at 277. The optimal treatment length is 26.7 cm. The corresponding control force is shown in Fig. 5.21(e). The passive and active tip displacements are shown in Fig. 5.19(e) and 5.20(e), respectively.

5.3.10 Minimum LQR Cost Function

This section investigates the value of the LQR cost function as different hybrid treatments are applied. Table 5.11 lists the optimal lengths and placements of the treatments along with the minimum LQR cost function. The passive, active and control force time histories of the hybrid treatments at the optimal lengths can be found in Fig. 5.22-24, respectively. Only the active time histories for the PZT are reported.

When the PZT is 28.1 cm long, the LQR cost function becomes 4762. For ACLD, the optimal length is 28 cm, with a value of 3919 for the LQR cost function. Both treatments are placed at the base of the beam. When placing the PZT and PCLD on the same side of the beam, the length of the PCLD is 26.9 cm, placed at the root, and the length of the PZT is 1 cm, placed 27.1 cm from the root. The LQR cost function is 3623. By allowing the PZT to be placed on opposite side of the beam, the cost function becomes 1244. This

Table 5. 11 Minimum Values for LQR Cost Function for Different Treatments

	L_{pzt} (m)	Loc_{pzt} (m)	L_{pcld} (m)	Loc_{pcld} (m)	J_{total}
PZT	0.281	0.001			4.762e3
ACLD	0.280	0.001	0.280	0.001	3.919e3
PZT/PCLD same side	0.010	0.271	0.269	0.001	3.623e3
PZT/PCLD opposite	0.270	0.001	0.270	0.001	1.244e3
PZT under PCLD	0.267	0.001	0.267	0.001	1.774e3

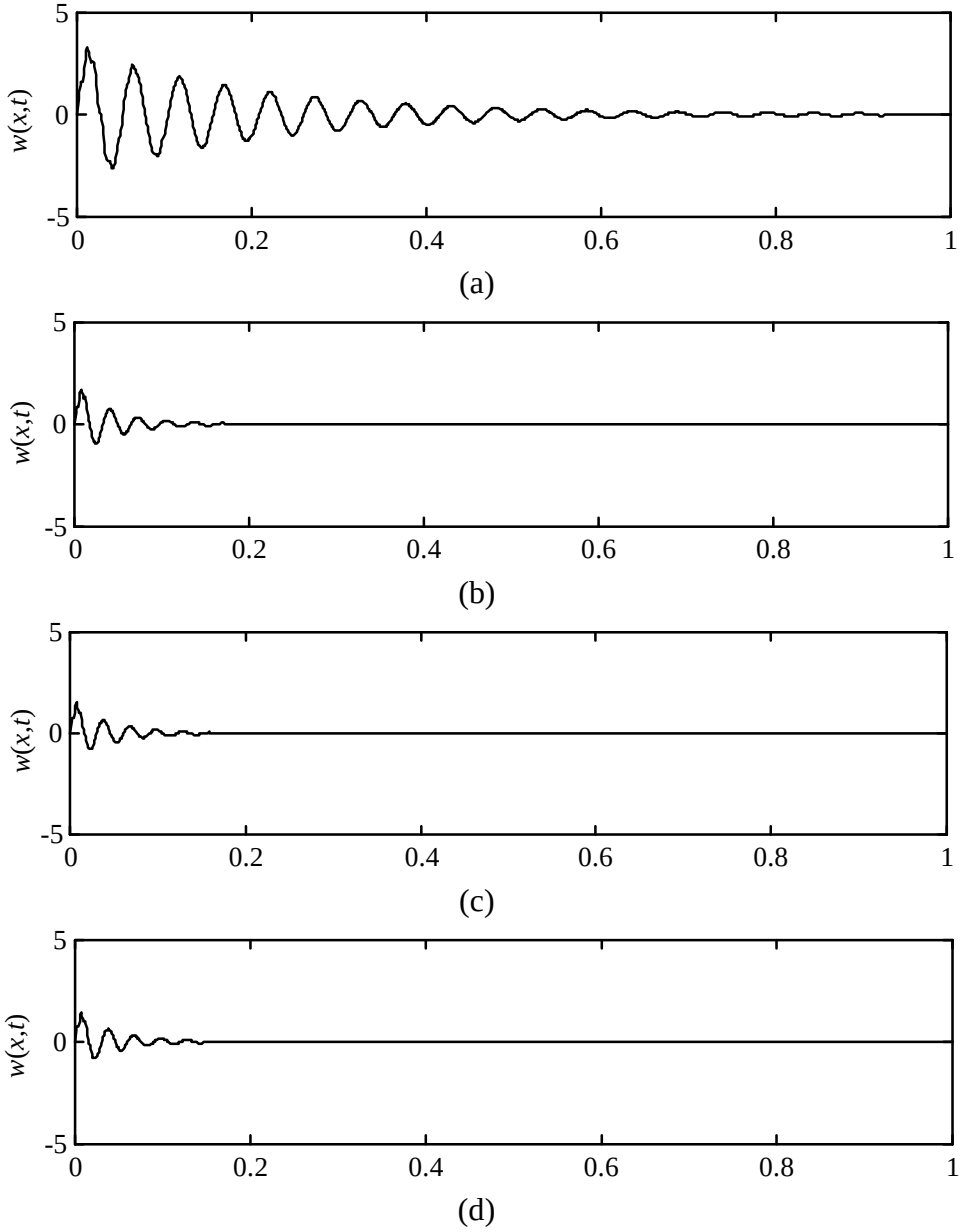

Figure 5. 22 Passive Tip Displacement (mm) vs Time (sec) for Optimal LQR Cost Function: a) ACLD, b) PZT Same Side, c) PZT Opposite Side, d) PZT Under

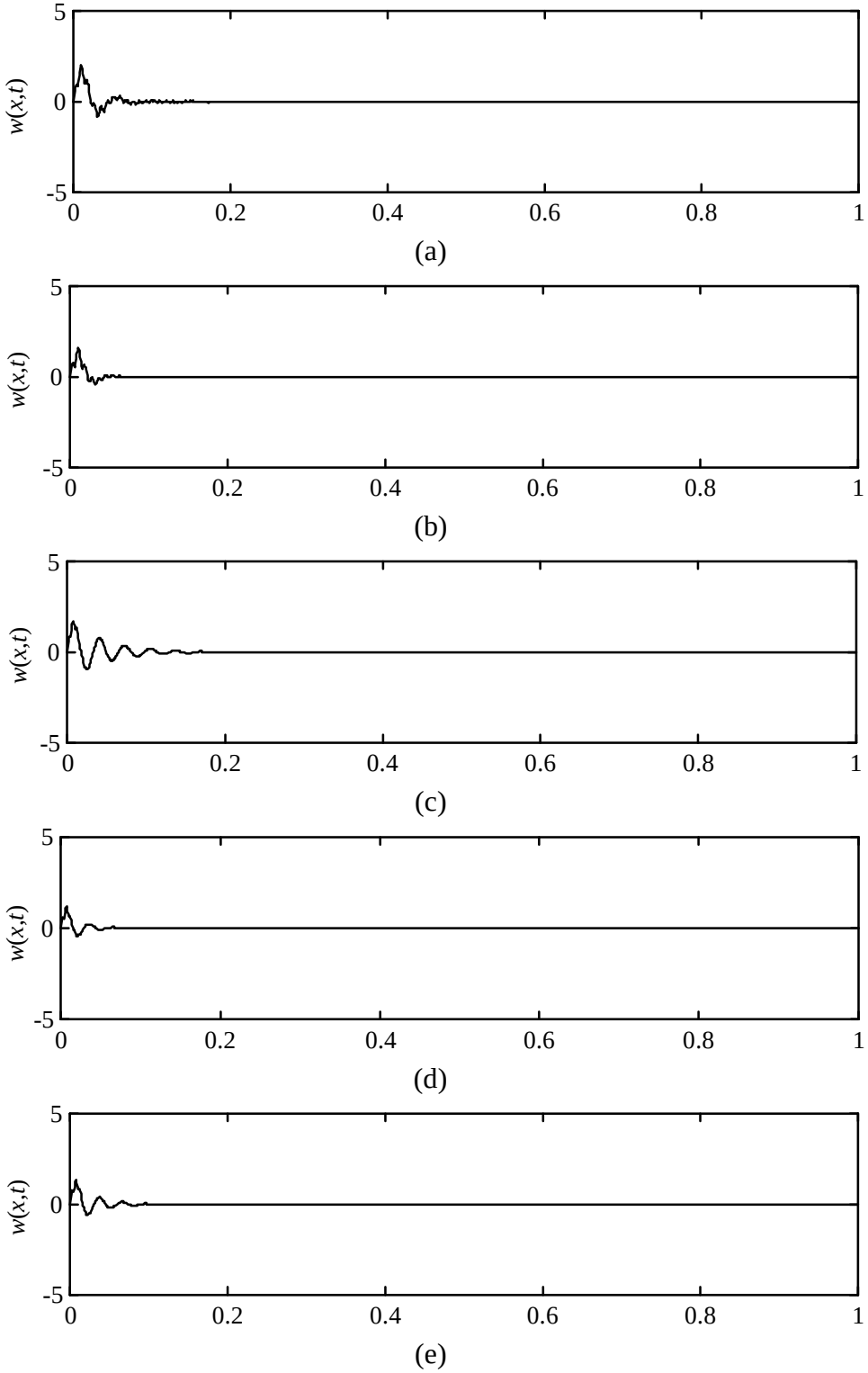

Figure 5. 23 Active Tip Displacement (mm) vs Time (sec) for Optimal LQR Cost Function: a) PZT, b) ACLD, c) PZT Same Side, d) PZT Opposite, e) PZT Under

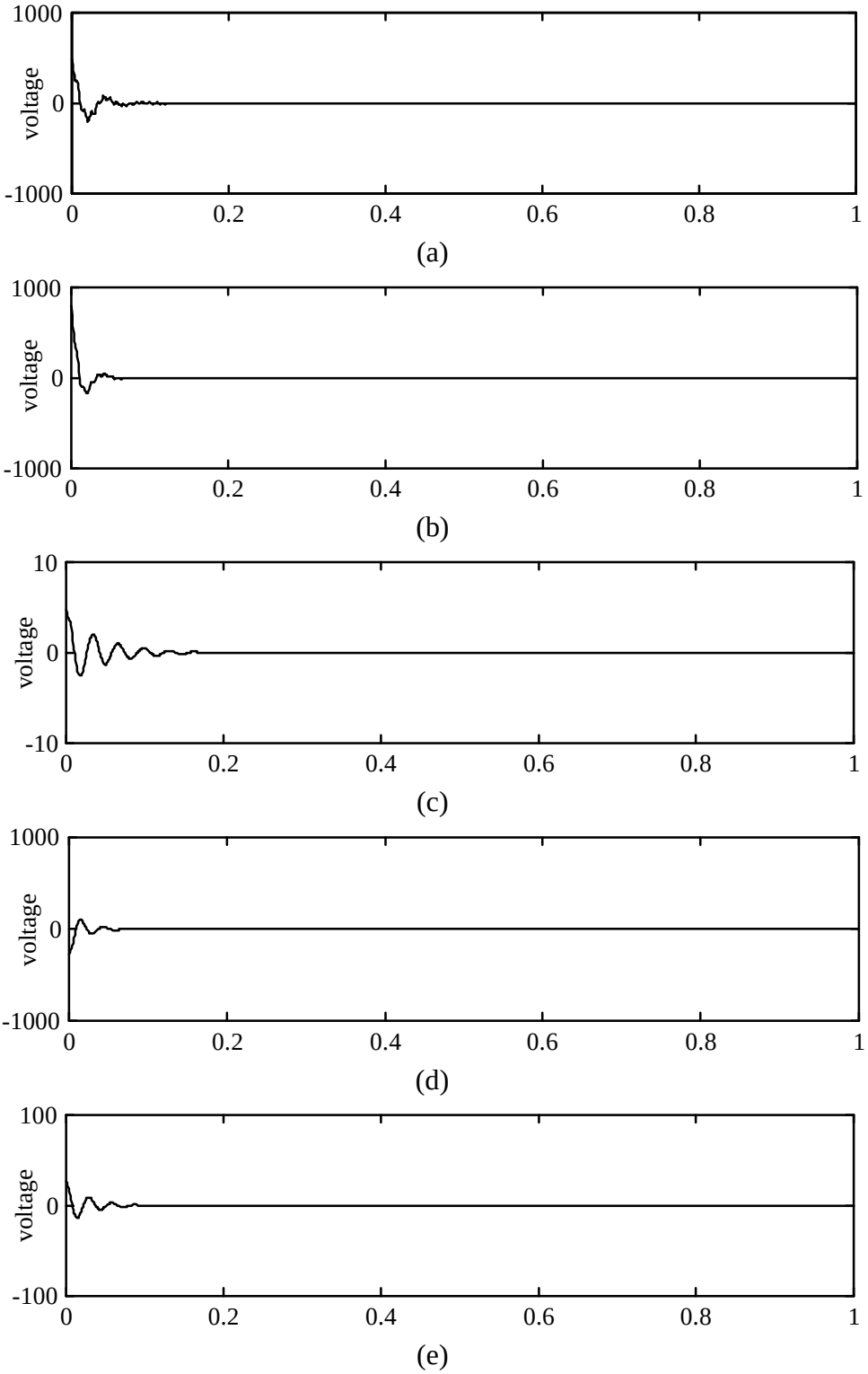

Figure 5. 24 Control Force (V) vs Time (sec) for Optimal LQR Cost Function: a) PZT only, b) ACLD, c) PZT Same Side, d) PZT Opposite Side, e) PZT Under

occurs when the PZT and the PCLD are 27 cm long. Placing the PZT underneath the PCLD gives a cost function of 1774 when the treatment length is 26.7 cm. The active tip displacement for a PZT is shown in Fig. 5.23(a) and the corresponding control force is shown in Fig. 5.24(a). The passive tip displacement for ACLD is shown in Fig. 5.22(a). Due to the lack of stiffness in the PZT constraining layer, the ACLD is not as effective as other hybrid treatments in suppressing passive vibration. However, it is still more advantageous to use ACLD than PZT, as can be seen by the lower cost function, the active tip displacement (Fig. 5.23(b)), and the control force (Fig. 5.24(b)). The cost function can be lowered yet again when placing the PZT and PCLD on the same side. As before, the treatment tries to optimize toward PCLD, since the PZT length is the lower limit and placed 27.1 cm from the root. This can be seen in the passive and active tip displacement, Fig. 5.22(b) and 5.23(c), respectively. Note there is no improvement in when the controller is active. The control force is shown in Fig. 5.24(c). The optimal solution allows the PZT to be placed on the other side of the beam. The passive tip displacement is shown in Fig. 5.23(c). The active response, seen in Fig. 5.23(d) settles quickly, with little overshoot. The control force is shown in Fig. 5.24(d). If it is not possible to place the PZT on the other side of the beam, a good alternative is to place the PZT underneath the PCLD. It takes less control force than the previous treatment, as seen in Fig. 5.24(e). Although the active tip displacement, Fig. 5.23(e), has more vibration, the passive tip displacement damps quickly, as seen in Fig. 5.22(e).

5.4 Output Feedback

The control used so far has assumed full state feedback. However, it is unlikely that all states are available for feedback control. In this section, output feedback will be explored. Equations 4.7-10 define output feedback and the output feedback gain matrix. It is assumed that only the transverse displacement, measured at the tip, is available for feedback.

Table 5. 12 Values of Indices for Different Treatments
(Treatment at Optimal Length to Minimize LQR Cost Function)

	$J_{passive}$	J_{VS}	J_{VSout}
PZT	∞	1.55e-7	∞
ACLD	9.06e-7	2.69e-8	8.62e-7
PZT/PCLD same side	1.53e-6	2.35e-8	1.17e-6
PZT/PCLD opposite	3.24e-8	1.04e-8	2.59e-8
PZT under PCLD	2.96e-8	1.81e-8	2.96e-8

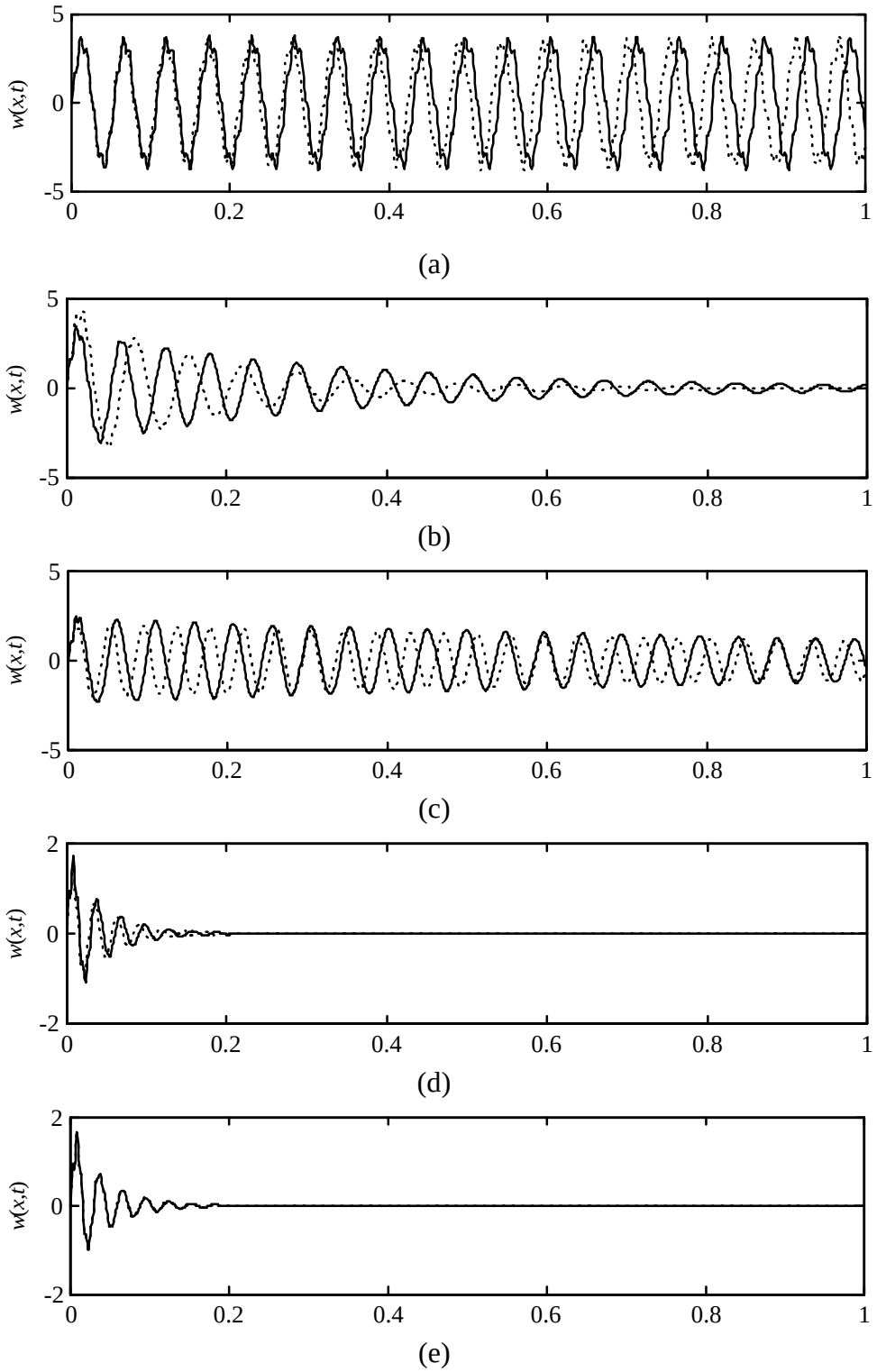

Figure 5. 25 Tip Displacement (mm) vs Time (sec) for Passive (solid) and Output Feedback (dotted): a) PZT, b) ACLD, c) PZT Same, d) PZT Opposite, e) PZT Under

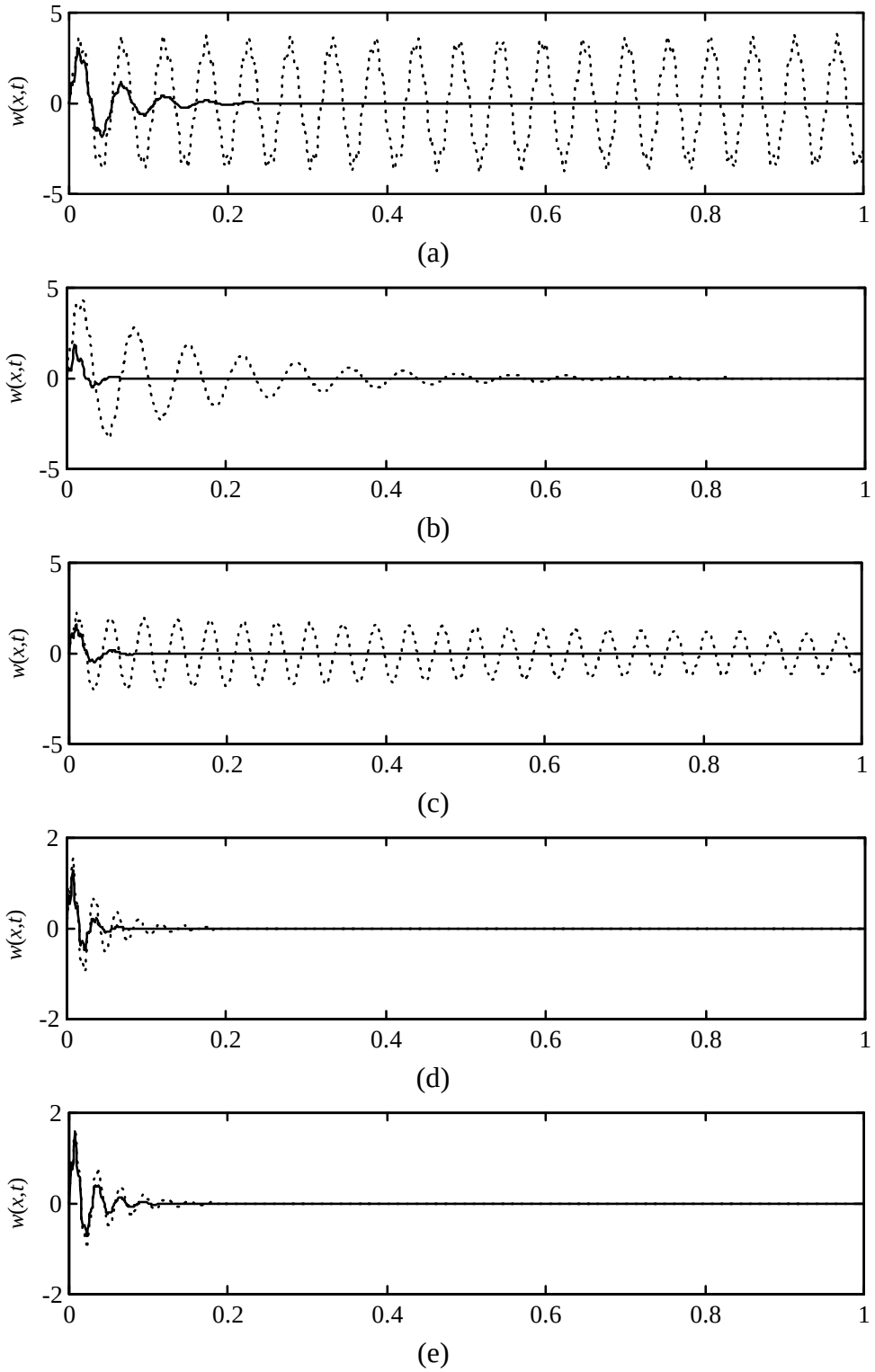

Figure 5. 26 Tip Displacement (mm) vs Time (sec) for Full State (solid) and Output Feedback (dotted): a) PZT, b) ACLD, c) PZT Same, d) PZT Opposite, e) PZT Under

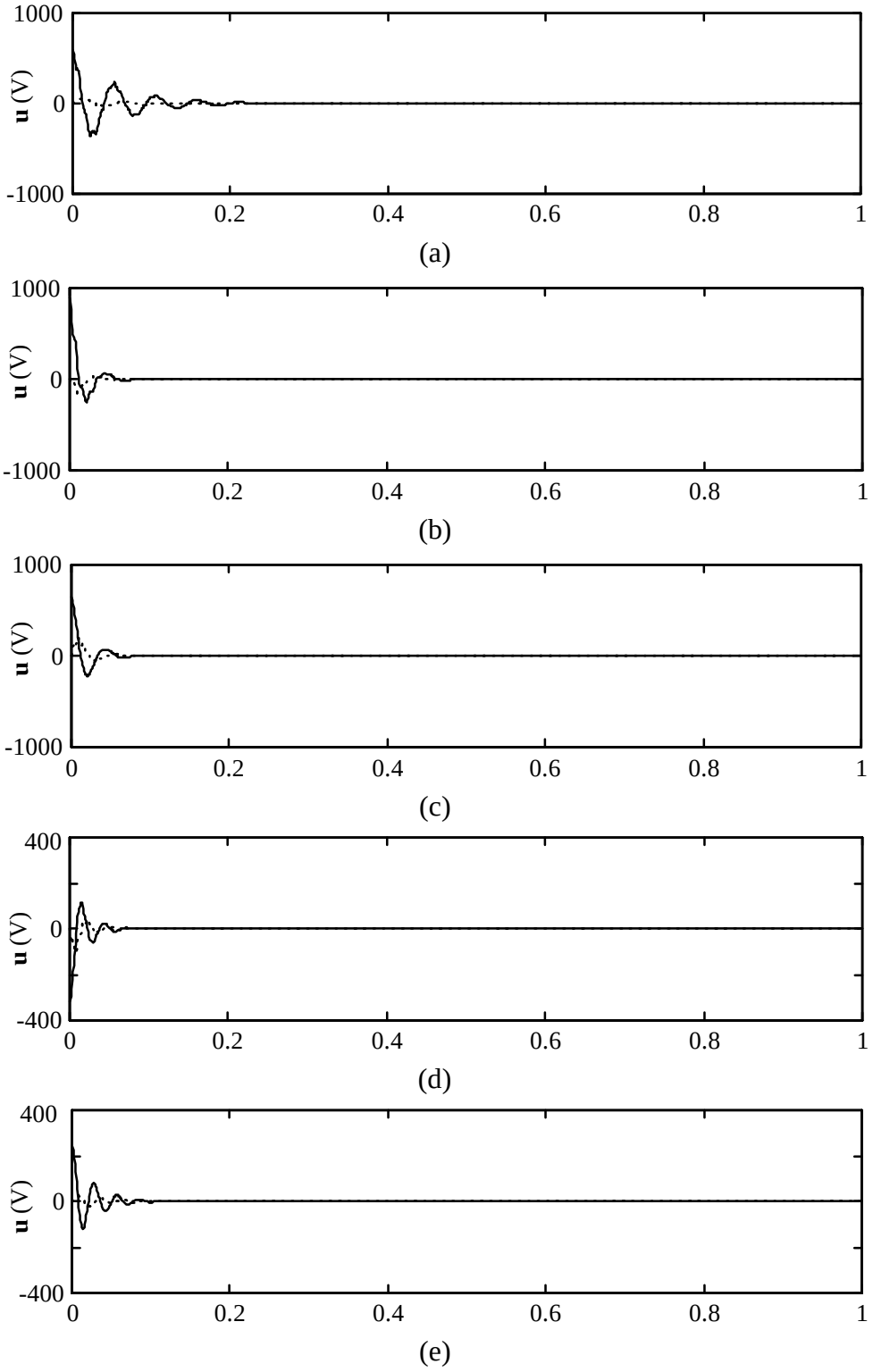

Figure 5. 27 Control Force (V) vs Time (sec) for Full State (solid) and Output Feedback (dotted): a) PZT, b) ACLD, c) PZT Same, d) PZT Opposite, e) PZT Under

The lengths of treatment are set to the optimal configuration active response settling time, as listed in Table 5.3. This criteria was chosen, since for all treatments the response improves when control is activated.

Table 5.12 lists the different vibration suppression and control effort indices. The passive and active vibration suppression indices for full state feedback are $J_{passive}$ and J_{VS}, respectively. The output vibration suppression index, $J_{VSoutput}$, denotes the active vibration suppression due to output feedback.

The time histories of the passive and active response comparing output feedback to full state feedback are shown in Fig. 5.25 and 5.26, respectively. The control force time histories are shown in Fig. 5.27. In Fig. 5.25-27 the dotted line represents output feedback and the solid line represents full state feedback.

Output feedback, where only the tip displacement is available, does not effectively damp vibration for a PZT only. The passive response is shown in Fig. 5.25(a), the active response in Fig. 5.26(a), and the control force in Fig. 5.27(a). Note that output feedback only changes the natural frequency of the passive response, but is not able to damp the vibration. This is shown by the value for the passive vibration index for output control, which is infinity. For ACLD, output feedback does not damp as effectively as full state feedback, as seen in Fig. 5.26(b). The corresponding control forces are shown in Fig. 5.27(b). It is more effective than the passive damping, as shown in Fig. 5.25(b). Comparing the vibration suppression indices from Table 5.12, $J_{passive}$ is 9.06e-7 while $J_{VSoutput}$ is 8.62-7. However, full state feedback has a vibration suppression index of 2.69e-8. Recall a lower vibration suppression index means more vibration suppression is present in the structure. When the PZT and PCLD are placed on the same side, the vibration suppression index of the passive response is 1.53e-6. The output vibration suppression index is 1.17e-6 and the LQR vibration suppression index is 2.35e-8. Therefore, output

feedback is better than a purely passive system, as seen in Fig. 5.25(c), but full state feedback is the most effective method to damp vibration, as seen in Fig. 5.26(c). The corresponding control force is shown in Fig. 5.27(c). By placing the PZT on the opposite side, the passive vibration suppression index becomes 3.25e-8. Output feedback improves this to 2.59e-8, as seen in Fig. 5.25(d), but again full state feedback is most effective at 1.04e-8, as seen in Fig. 5.26(d). Figure 5.27(d) shows the corresponding control force. Placing the PZT underneath the PCLD does not allow the output feedback gain matrix to improve upon the passive response. Both passive and output feedback vibration suppression indices are 2.96e-8, and their responses coincide as seen in Fig. 5.25(e). Figure 5.26(e) shows the active response and Fig. 5.27(e) the control force necessary to achieve the active response. Note in all cases output feedback was not able to put enough energy into the system, making it less effective than full state feedback.

For the graphs shown, the output for feedback was assumed to be the tip displacement. The tip displacement is a linear combination of the transverse modes. If more states are available, it is possible to improve the effectiveness of output feedback. If optimal output feedback is used instead of a least squares approach, it is also possible to improve the effectiveness.

5.5 Model Reduction

The Golla-Hughes-McTavish (GHM) model is used to model the frequency dependence of the viscoelastic materials. The general equations are derived in chapter 3. One problem with GHM is the addition of dissipation coordinates. The size of the final characteristic equation quickly increases as the number of mini-oscillators is increased. In this section, the internally balanced model reduction method is applied to the equations to revert the system back to its original order as explained in section 3.3.

The time histories of the passive and active response of the reduced systems are shown in Fig. 5.27-28. The solid line represents the time response of the reduced model, while the dotted line is the difference between in responses of the full order and reduced systems. The lengths and placements of treatment are given in Table 5.3.

Three modes are included in the modal expansion to obtain equations of motion. Because the equation of motion is obtained through the summation of modes, a numeric difficulty is encountered. The diagonal terms associated with the transverse displacement are orders of magnitude greater than the diagonal terms associated with the VEM. The difference in order of magnitude makes the system numerically uncontrollable and unobservable: two criteria that must be satisfied for model reduction. The problem is alleviated by non-dimensionalizing the system. Non-dimensional time and displacement are defined as

$$t_{nd} = \frac{t}{L^2}\sqrt{\frac{E_b I_b}{\rho_b A_b}}$$

$$x_{nd} = \frac{x}{L}$$

where E_b is Young's modulus, I_b is the moment of inertia, ρ_b the density, A_b the cross sectional area, and L the length of the aluminum beam.

The passive tip displacement is shown in Fig. 5.27. For ACLD, there is some error between the reduced model output and the actual output, as seen by the dotted line. However, this error quickly dies out and the reduced model is able to simulate the full order exactly by 0.3 sec. For the active reduced response, as shown in Fig. 5.28(a), there is some error until the vibration settles after 0.4 sec. Because the PZT is actuating through the VEM, the model reduction method is not able to completely simulate the

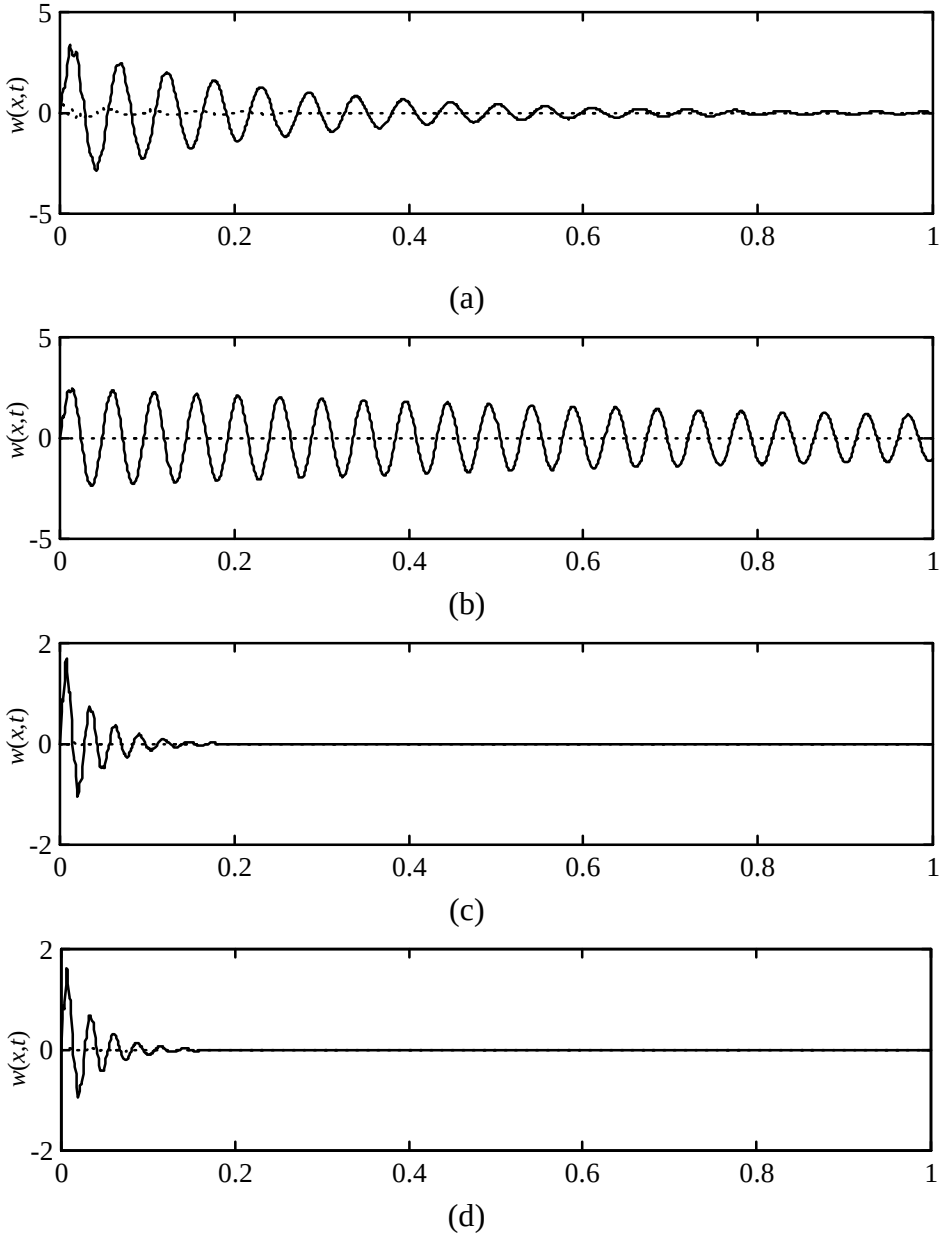

Figure 5. 28 Tip Displacement (mm) vs Time (sec) of Reduced Passive Response (solid) and Difference Between GHM and Reduced Passive Response (dotted):
a) ACLD, b) PZT/PCLD Same Side, c) PZT/PCLD Opposite, d) PZT Under

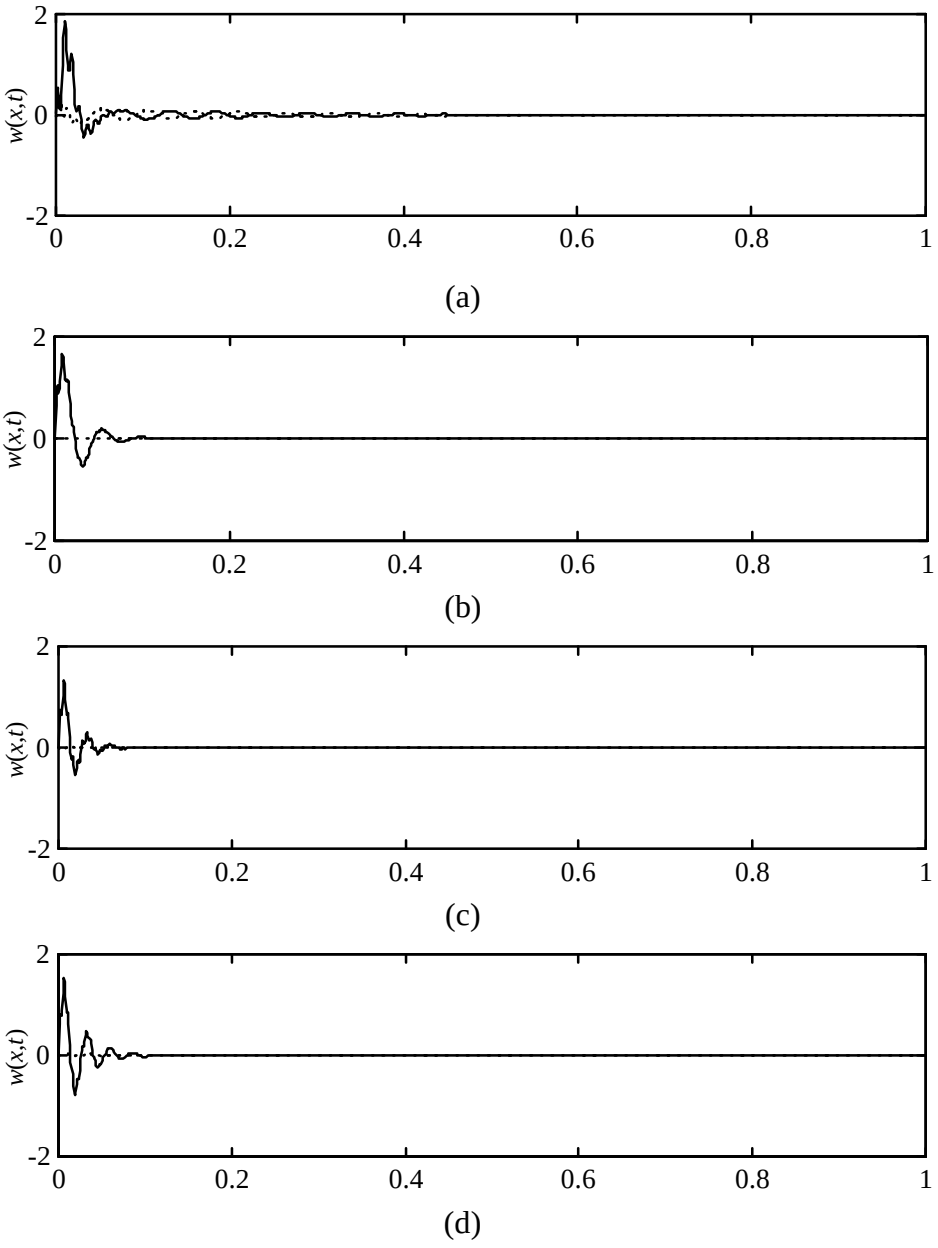

Figure 5. 29 Tip Displacement (mm) vs Time (sec) of Reduced Active Response (solid) and Difference Between GHM and Reduced Active Response (dotted):
a) ACLD, b) PZT/PCLD Same Side, c) PZT/PCLD Opposite, d) PZT Under

response. The remaining variations (PZT and PCLD on same side, PZT on the opposite side and PZT underneath the PCLD) the reduced model simulates passive response of the full order model exactly. This is shown by the straight dotted lines in Fig. 5.27(b)-(d). This holds true for the active response as well, as seen in Fig. 5.28(b)-(d).

CONCLUSIONS AND FUTURE WORK

New hybrid active/passive models are proposed to suppress vibration. The passive damping mechanism provides fail-safe damping and improves the stability and robustness of the system. Two new hybrid configurations are introduced by separating the passive and active elements. In the first variation, the active and passive element are constrained to the same side of the beam. The other variation allows one of the treatments to be placed on the opposite side of the beam.

The equations of motion are obtained using energy methods and Lagrange's equation. Assumed modes are used to discretize these equations. The frequency dependent damping is modeled using the Golla-Hughes-McTavish (GHM) method. An experiment is performed to verify the analytical model. It is shown that GHM accounts for the frequency dependent damping since there is good correlation between the experiment and the analytical model. Furthermore, GHM is able to account for increased damping associated with a thicker VEM layer.

The damping is modeled through the addition of fictitious dissipation states, which increase the size of the system. The internally balanced model reduction method is applied to reduce the equations of motion back to their original size. A numeric difficulty is encountered when trying to calculate the controllability and observability grammians. Since the assumed modes method is used to obtain the equations of motion, the diagonal terms in the mass and stiffness matrix are orders of magnitude different for the transverse displacement and shear angle. The controllability and observability test matrices are therefore numerically not full-rank, which in turn does not allow calculation of the controllability and observability grammians. This is alleviated by non-dimensionalizing the system and keeping fewer modes in the assumed modes method. Time histories of the

passive and active response show that the model reduction adequately models the behavior of the system.

A linear quadratic regulator (LQR) is used to actively control the vibration. LQR assumes all states are available for feedback, which is usually not possible. When only a few states are available, output feedback must be used to control vibration. While it is not as effective as full state feedback, it is more realistic. Here the assumption is made that only the tip displacement is available for feedback. The results are shown for output feedback using a least squares approach. The results can be improved if optimal output feedback is used.

Comparisons of passive and active tip displacements as well as control force time histories are made with pure active, passive constrained layer damping (PCLD), active constrained layer damping (ACLD), a variation which places the PZT underneath the PCLD and the new hybrid variations. Optimization of the length and placement of the treatment is applied using different criteria: minimizing the settling time, maximum overshoot, passive and active vibration suppression index, control effort and LQR cost function for the passive response, active response and control force.

For any optimization scheme, using a PZT is not the optimal solution. There is no damping, except structural, associated with a PZT, which means there is no fail-safe mechanism. Also, it takes large control forces to actuate the structure. When output feedback is applied, only the natural frequency of the output is changed. Therefore, output feedback of the tip displacement is not adequate to control vibration of the system since not enough energy is added to the system.

Good vibration suppression can be achieved using PCLD. The limitation of course is the lack of active control. PCLD is not able to damp vibrations as easily as most active

configurations. Therefore, it is more advantageous to choose a treatment that has similar passive damping characteristics as PCLD, and where active control enhances the passive vibration suppression further.

ACLD is a better alternative than PZT, due to its passive damping capabilities. However, it is clearly shown that PZT is not stiff enough to be used as constraining layer. The passive vibration does not settle quickly when compared to other hybrid treatments. While the active response is often better than PZT, it takes even larger voltages to achieve this vibration suppression. The PZT is actuating the system through a VEM, thereby increasing the needed control force. It is also shown that output feedback of the tip displacement increases the vibration suppression of the system. While it is not as good as full state feedback, there is an improvement over passive damping.

Placing the PZT and PCLD apart on the same side is not desirable. For most optimizations, the treatment tries to become either purely passive or purely active, and would therefore have the limitations mentioned before. When minimizing the active response settling time and overshoot, PZT and PCLD of similar lengths are placed on the beam. However, the passive response does not have enough vibration suppression associated with it since the passive treatment is placed too far from the root. Output feedback of the tip displacement is applied to the configuration which places a PZT and PCLD of similar length on the beam. It is not able to add much vibration suppression to the system, and is therefore not more effective than only passive control.

For all optimization schemes except for the passive vibration suppression index, the optimal case occurs when the PZT is placed on opposite side of the beam. Vibration suppression is effective for both the passive and active cases. The control forces associated with the active control were smaller than PZT or ACLD. When output feedback is applied, it is able to damp the vibration more quickly than passive damping.

While placing the PZT on the opposite side of the PCLD is usually preferable, it is not always possible and the best alternative is to place the PZT underneath the PCLD. In fact, it is the optimal solution when minimizing the passive vibration suppression index. It requires the least control force and has good passive vibration suppression. It is also shown that output feedback of the tip displacement is not able to put enough energy into the system. It therefore reacts the same as passive damping.

While the results in this work show great promise, there is still much work to be done. The internally balanced model reduction method does not work well with assumed modes method, since the diagonal terms are orders of magnitude different. It is therefore advantageous to seek another modeling method, such as finite elements, which does not introduce this numeric problem.

The structure used in this work is a cantilevered beam, which is a simple structure. Research must be done to see the effect of the hybrid damping on more complex structures, such as plates. It is possible that applying the PZT and PCLD separately on a plate will be more effective than it is on a beam.

Another issue to be studied is the temperature dependence of the VEM. The shear modulus is dependent on both temperature and frequency. The model presented in this work accounts for the frequency dependence, but does not address the temperature dependence.

REFERENCES

[1] Johnson, C. D., 1995. "Design of Passive Damping Systems," *Transactions of the ASME: Special 50th Anniversary Design Issue*, **117**, 171-176.

[2] Kerwin, Jr., E. M., 1959. "Damping of Flexural Waves by a Constrained Viscoelastic Layer," *Journal of the Acoustical Society of America*, **31**(7), 952-962.

[3] DiTaranto, R. A., 1965. "Theory of Vibratory Bending for Elastic and Viscoelastic Layered Finite-Length Beams," *Journal of Applied Mechanics*, 881-886.

[4] Mead, D. J., and Markus, S., 1969. "The Forced Vibration of a Three-Layer, Damped Sandwich Beam with Arbitrary Boundary Conditions," *Journal of Sound and Vibration*, **10**(2), 163-175.

[5] Douglas, B. E., and Yang, J. C. S., 1978. "Transverse Compressional Damping in the Vibratory Response of Elastic-Viscoelastic-Elastic Beams," *AIAA Journal*, **16**(9), 925-930.

[6] Torvik, P. J., ed., 1980. "The Analysis and Design of Constrained Layer Damping Treatments," *ASME Damping Applications for Vibration Control*, AMD **38**, 85-112.

[7] Rao, D. K., 1978. "Frequency and Loss Factors of Sandwich Beams Under Various Boundary Conditions," *Journal Mechanical Engineering Science*, **20**(5), 271-282.

[8] Ravi, S. S. A., Kundra, T. K., and Nakra, B. C., 1994. "Eigenvalue Reanalysis of Sandwich Beams with Viscoelastic Core Using Perturbation Method," *International Journal of Analytical Experimental Modal Analysis*, **9**(3), 203-217.

[9] Bai, J. M., and Sun, C. T., 1995, "The Effect of Viscoelastic Adhesive Layers on Structural Damping of Sandwich Beams," *Mechanical Structures and Machines*, **23**(1), 1-16.

[10] Bhimaraddi, A., 1995. "Sandwich Beam Theory and the Analysis of Constrained Layer Damping," *Journal of Sound and Vibration*, **179**(4), 591-602.

[11] Lifshitz, J. M., and Leibowitz, M., 1987. "Optimal Sandwich Beam Design for Maximum Viscoelastic Damping," *International Journal of Solids and Structures*, **23**(7), 1027-1034.

[12] Lekszycki, T., and Olhoff, N., 1982. "Optimal Design of Viscoelastic Structures under Forced Steady-State Vibration," *Journal Structural Mechanics*, **9**(4), 363-387.

[13] Plunkett, R., and Lee, C. T., 1970. "Length Optimization for Constrained Viscoelastic Layer Damping," *Journal of the Acoustical Society of America*, **48**(1)-part 2, 150-161.

[14] Kerwin Jr., E. M., and Smith Jr., P. W., 1984. "Segmenting and Mechanical Attachment of Constrained Viscoelastic Layer Damping Treatments for Flexural and Extensional Waves," *Damping '84*, kk1-kk24.

[15] Roy, P. K., and Ganesan, N., 1993. "A Vibration and Damping Analysis of Circular Plates With Constrained Damping Layer Treatment," *Computers and Structures*, **49**(2), 269-274.

[16] Tomlinson, G. R., 1990. "The Use of Constrained Layer Damping in Vibration Control," *International Journal of Mechanical Sciences*, **32**(3), 233-242.

[17] Sun, C. T., Sankar, B. V., and Rao, V. S., 1990. "Damping and Vibration Control of Unidirectional Composite Laminates Using Add-On Viscoelastic Materials," *Composites Damping and Vibration Control*, Academic Press, Ltd., 277-287.

[18] Rao, M. D., and He, S., 1993. "Dynamic Analysis and Design of Laminated Composite Beams with Multiple Damping Layers," *AIAA Journal*, **31**(4), 736-745.

[19] Hetnarski, R. B., West, R. A., and Torok, J. S., 1993. "Damping of Vibrations of Layered Elastic-Viscoelastic Beams," *Applied Mechanics Review*, **46(**11), Part 2, S305-S311.

[20] McTavish, D. J., and Hughes, P. C., 1993. "Modeling of Linear Viscoelastic Space Structures," *Journal of Vibration and Acoustics*, **115**, 103-110.

[21] Olson, H. F., 1956. "Electronic Control of Mechanical Noise, Vibration Reverberations," *The Journal of the Acoustical Society of America*, **28**(5), 966-972.

[22] Rao, S. S., and Sunar, M., 1994. "Piezoelectricity and its Use in Disturbance Sensing and Control of Flexible Structures: A Survey," *ASME Journal of Applied Mechanics Review*, **47**(4), 113-121.

[23] Crawley, E. F., and de Luis, J., 1987. "Use of Piezoelectric Actuators as Elements of Intelligent Structures," *AIAA Journal*, **25**(10), 1373-1385.

[24] Hagood, N. W., Chung, W. H., and von Flotow, A., 1990. "Modelling of Piezoeletric Actuator Dynamics For Active Structural Control," *Journal of Intelligent Materials, Systems, and Structures*, **1**(3), 327-354.

[25] Dosch, J. J., Inman, D. J., and Garcia, E., 1992. "A Self-Sensing Peizoelectric Actuator for Collocated Control," *Journal of Intelligent Material Systems and Structures*, **3**, 166-185.

[26] Cole, D. G., Saunders, W. R., and Robershaw, H. H., 1992. "Modal Parameter Estimation for Piezostructures," ONR Grant No. N00014-92-J-1170.

[27] Kim, S. J., and Jones, J. D., 1991. "Optimization of Piezo-Actuator/Substructure Coupling for Active Noise and Vibration Control," *Proceedings of the Conference on Recent Advances in Active Control of Sound and Vibration*, 78-94.

[28] Masters, A. R., and Jones, J. D., 1991. "Optimal Design of Piezo-Actuators in a Layered Composite Structure for Active Noise and Vibration Control," *ASME Smart Structures and Materials, AMD*, **123**, 123-129.

[29] Devasia, S., Meressi, T., Paden, B., and Bayo, E., 1993. "Piezoelectric Actuator Design for Vibration Suppression: Placement and Sizing," *Journal of Guidance, Control and Dynamics*, **16**(5), 859-864.

[30] Agnes, G., and Napolitano, K., 1993. "Active Constrained Layer Viscoelastic Damping," *AIAA Journal*, 3499-3506.

[31] Baz, A. M., 1993. "Active Constrained Layer Damping," *Proceedings for Damping '93*, **3**, IBB-1 - IBB-23.

[32] Shen, I. Y., 1994. "Stability and Controllability of Euler-Bernoulli Beams with Intelligent Constrained Layer Treatments," *ASME Journal of Vibration and Acoustics*, DE-**75**, 169-178.

[33] Baz, A. M., and Ro, J.-J., 1995. "Optimum Design and Control of Active Constrained Layer Damping," *Transactions of the ASME: Special 50th Anniversary Design Issue*, **117**, 135-144.

[34] Liao, W. H., and Wang, K. W., 1996. "On the Active-Passive Hybrid Control Actions of Structures with Active Constrained Layer Treatments," *ASME Journal of Vibration and Acoustics*, in review.

[35] Azvine, B., Tomlinson, G. R., and Wynne, R. J., 1995. "Use of Active Constrained-Layer Damping for Controlling Resonant Vibration," *Smart Materials and Structures*, **4**, 1-6.

[36] Huang, S. C., Inman, D. J., and Austin, E. M., 1996. "Some Design Considerations for Active/Passive Constrained Layer Damping Treatments," *Smart Materials and Structures*, **5**, 301-313.

[37] Baz, A. M., and Ro, J.-J., 1993. "Partial Treatment of Flexible Beams With Active Constrained Layer Damping," *AMD Recent Developments in Stalility, Vibration and Control in Structural Systems*, **167,** 61-80.

[38] Baz, A. M., and Ro, J.-J., 1993. "Finite Element Modeling and Performance of Active Constrained Layer Damping," *Ninth Conference on Dynamics & Control of Large Structures*, 345-358.

[39] Baz, A. M., and Ro, J.-J., 1996. "Vibration Control of Plates with Active Constrained Layer Damping," *Smart Materials and Structures*, **5**, 272-280.

[40] Shen, I. Y., 1994. "Hybrid Damping Through Intelligent Constrained Layer Treatments," *ASME Journal of Vibration and Acoustics*, **116**(3), 341-349.

[41] Shen, I. Y., 1994. "Bending-Vibration Control of Composite and Isotropic Plates Through Intelligent Constrained-Layer Treatments," *Smart Materials and Structures*, **3**, 59-70.

[42] Shen, I. Y., 1995. "Bending and Torsional Vibration Control of Composite Beams Through Intelligent Constrained-Layer Damping Treatments," *Smart Material Structures*, **4**, 340-355.

[43] Shen, I. Y., Guo, W., and Pao, Y. C., 1994. "Torsional Vibration Control of a Shaft Through Intelligent Constrained Layer Damping Treatments," *Journal of Vibration and Acoustics*, in print.

[44] Shen, I. Y., 1995. "A Variational Formulation, A Work-Energy Relation and Damping Mechanisms of Active Constrained Layer Treatments," *Design Engineering Technical Conference*, **3**(C), 149-160.

[45] Yellin, J. M., and Shen, I. Y., 1997. "An Experimental Investigation of a Self-Sensing Active Constrained Layer Damping Treatment," *SPIE: Passive Damping and Isolation*, ed. L. P. Davis, **3045**, paper #34.

[46] Rongong, J. A., Wright, J. R., Wynne, R. J., and Tomlinson, G. R., 1997. "Modelling of a Hybrid Constrained Layer/Piezoceramic Approach to Active Damping," *Transactions of the ASME*, **119**, 120-130.

[47] Veley, D. E., and Roa, S. S., 1996. "A Comparison of Active, Passive and Hybrid Damping Treatments in Structural Design," *SPIE North American Conference on Smart Structures and Materials*, **2720**, 184-195.

[48] Crassidis, J., Baz, A., and Wereley, N., 1997. "H_∞ Control of Active Constrained Layer Damping," *Eleventh Symposium on Structural Dynamics & Control*, in print.

[49] Van Nostrand, W. C., 1994. "Active Constrained Layer Damping Using PZT Actuators," Ph. D. Thesis, State University of New York at Buffalo.

[50] Van Nostrand, W. C., and Inman, D. J., 1995. "Finite Element Model for Active Constrained Layer Damping," *SPIE North American Conference on Smart Structures and Materials*, **2427**, 124-1139.

[51] Saunders, W. R., Inman, D. J., and Robertshaw, H. H., 1994. "Pole-Zero Modeling for Smart Viscoelastic Structures," *International Conference on Intelligent Materials*, 1044-1054.

[52] Liao, W. H., and Wang, K. W., "A New Active Constrained Layer Configuration with Enhanced Boundary Actions," *Smart Materials and Structures*, **5**, 638-648.

[53] Lesieutre, G. A., and Lee, U., 1996. "A Finite Element for Beams Having Segmented Active Constrained Layers with Frequency-Dependent Viscoelastics," *Smart Materials and Structures*, **5**, 615-627.

[54] Ray, M. C., and Baz, A., 1996. "Optimization of Energy Dissipation of Active Constrained Layer Damping Treatments of Plates," *Journal of Vibration and Acoustics*, in review.

[55] Inman, D. J., and Lam, M. J., 1997. "Active Constrained Layer Damping Treatments," *Key note address at the 6th Recent Advances in Structural Dynamics Conference*, Great Britain.

[56] Bagley, R. L., and Torvik, P. J., 1983. "Fractional Calculus – A Different Approach to the Analysis of Viscoelastically Damped Structures," *AIAA Journal*, **21**, 741-748.

[57] Slater, J. C., 1991. "Modeling of Non-proportional Frequency Dependent Viscoelastic Damping in Space Structures," Master's Thesis, SUNY at Buffalo.

[58] McTavish, D. J., and Hughes, P. C., 1985. "Dynamics of Viscoelastic Structures - A Time-Domain, Finite Element Formulation," *Journal of Applied Mechanics*, **52**, 897-906.

[59] Lam, M. J., Saunders, W. R., and Inman, D. J., 1995. "Modeling Active Constrained Layer Damping Using Golla-Hughes-McTavish Approach," *SPIE North American Conference on Smart Structures and Materials*, **2445**, 86-97.

[60] Liao, W. H., and Wang, K. W., 1995. "On the Active-Passive Hybrid Vibration Control Actions of Structures with Active Constrained Layer Treatments," *ASME Design Engineering Technical Conferences*, DE-**84**(3), 125-141.

[61] Meitzler, AH, Tiersten, HF, Warner, A. W., Berlincourt, D., Coquin, G. A., and Welsh, III, F. S., 1987. "IEEE Standard on Piezoelectricity," *ANSI/IEEE Std*. 17-1987.

[62] Shames, I. H., and Cozzarelli, F. A., 1992. *Elastic and Inelastic Stress Analysis*, Prentice-Hall, Englewood Cliffs, 1st edition.

[63] Meirovitch, L., 1980. *Computational Methods In Structural Dynamics*, Sijthoff & Noordhoff International Publishers, Alphen aan den Rijn.

[64] Christensen, R. M., 1982. *Theory of Viscoelasticity: An Introduction*, Academic Press, Inc., New York, 2nd edition.

[65] Friswell, M. I., Inman, D. J., and Lam, M. J., 1997. "On the Realisation of GHM Models in Viscoelasticity," *Journal of Intelligent Material Systems and Structures*, in review.

[66] Yae, K. H., and Inman, D. J., 1992. "Model Reduction in a Subset of the Original States," *Journal of Sound and Vibration*, **155**(1), 165-176.

[67] Laub, A. J., 1980. "Computation of Balancing Transformation," *Proceedings of the 1980 JACC*, San Francisco, session FA8-E.

[68] 3M: Scotchdamp™ Vibration Control Systems, 1993. *Product Information and Performance Data*, St. Paul.

[69] Allemang, R. J., Brown, D. L., and Rost, R. W., 1987. *Experimental Modal Analysis and Dynamic Component Synthesis*, **2**, AFWAL-TR-87-3069.

[70] Nashif, A., Jones, D., and Henderson, J., 1985. Vibration Damping, John Wiley & Sons, New York.

[71] Kirk, D. E., 1970. *Optimal Control Theory*: *an Introduction*, Prentice-Hall, Inc., Englewood Cliffs, 12th edition.

[72] Chen, C.-T., 1984. *Linear Systems Theory and Design*, Holt, Rinehart and Winston, Inc., New York, 1st edition.

[73] "Piezo Systems, Inc. Product Catalog," Piezo Systems, Inc., Cambridge Massachusetts.

[74] Inman, D. J., 1994. *Engineering Vibration*, Prentice-Hall, Inc., Englewood Cliffs, 1st edition.

[75] MATLAB Reference Guide, 1992. The Mathworks Inc., Natick, MA.

[76] Garcia, E., and Inman, D. J., 1990, "Control Formulations for Vibration Suppression of an Active Structure in Slewing Motions," *ASME 1990 Winter Meeting*, 1-5.

VITA

Margaretha Johanna Lam was born on November 10, 1968 in Amsterdam, The Netherlands. Her family moved to the United States in 1981, and she became a naturalized citizen in 1990. She attended the State University of New York at Buffalo, where she received a Bachelor of Science degree in Mechanical Engineering in June, 1991. During her undergraduate studies, she spent the summer between junior and senior year working for Dr. Inman in the Mechanical Systems Laboratory.

She officially joined the Mechanical System Laboratory as a graduate student in 1991, and received her Masters of Science in Mechanical Engineering on November 15, 1994. When Dr. Inman became the Samuel Herrick professor in the Engineering Science and Mechanics Department at Virginia Polytechnic Institute and State University, in Blacksburg, Virginia, she followed her advisor and transferred to the Mechanical Engineering Department.

She stayed in Virginia for one year, before moving to New York City, New York. There she works as an adjunct professor in the Mechanical Engineering Department at the Cooper Union for Advancement of Science and Art. She has taught feedback control systems, control systems design, mechanical vibrations, heat transfer and freshman guided design.